

**CATENARY BEHAVIOR OF STEEL GIRDERS UNDER
PROGRESSIVE COLLAPSE-TYPE LOADS**

by

Thomas J. Cotter

A thesis submitted to the Faculty of the University of Delaware in partial fulfillment
of the requirements for the degree of Master of Civil Engineering

Spring 2013

© 2013 Thomas J. Cotter
All Rights Reserved

**CATENARY BEHAVIOR OF STEEL GIRDERS UNDER
PROGRESSIVE COLLAPSE-TYPE LOADS**

by

Thomas J. Cotter

Approved: _____
Jennifer E. Righman McConnell, Ph.D.
Professor in charge of thesis on behalf of the Advisory Committee

Approved: _____
Harry W. Shenton III, Ph.D.
Chair of the Department of Civil and Environmental Engineering

Approved: _____
Babatunde A. Ogunnaike, Ph.D.
Interim Dean of the College of Engineering

Approved: _____
James G. Richards, Ph.D.
Vice Provost for Graduate and Professional Education

ACKNOWLEDGMENTS

I would first like to thank my advisor, Dr. Jennifer Righman McConnell, for her patience, encouragement and wisdom throughout this process. I would especially like to thank my wife, parents and siblings for giving me the strength and confidence to push forward when the going got tough. I would also like to thank all of my friends who made the graduate school experience so enjoyable and memorable. Finally, I would like to thank the University of Delaware, not only for their support of this project, but also for giving me a great education and some of the best years of my life.

TABLE OF CONTENTS

| | |
|-----------------------|------|
| LIST OF TABLES | vii |
| LIST OF FIGURES | viii |
| ABSTRACT | xiv |

Chapter

| | | |
|-------|---|----|
| 1 | INTRODUCTION | 1 |
| 1.1 | Introduction to Progressive Collapse..... | 1 |
| 1.2 | Early History of Progressive Collapse and Initial Observations | 2 |
| 1.3 | Need for Current Research | 3 |
| 1.4 | Objectives of Research | 4 |
| 1.5 | Scope of Research | 5 |
| 2 | LITERATURE REVIEW | 8 |
| 2.1 | Introduction to Current State of Practice and Relevant Research | 8 |
| 2.2 | Current Progressive Collapse Guidelines | 8 |
| 2.2.1 | UFC Guidelines | 9 |
| 2.2.2 | GSA Guidelines..... | 16 |
| 2.3 | Behavior of Steel-Framed Structures during Progressive Collapse Events | 17 |
| 2.4 | Current Research Relating to Alternate Load Path Method | 19 |
| 2.5 | Catenary Behavior of Steel Beams under Progressive Collapse Events | 24 |
| 2.6 | Connection Performance during Progressive Collapse Events | 48 |
| 2.6.1 | Research into Performance of Non-Proprietary Steel Connections | 49 |
| 2.6.2 | SidePlate™ Connection..... | 72 |
| 2.7 | Summary..... | 73 |
| 3 | METHODOLOGY | 80 |
| 3.1 | Geometric Properties of Steel Components | 81 |

| | | |
|-------|--|-----|
| 3.2 | Methods of Analysis in Previous Related FEA Research | 83 |
| 3.3 | Methodology of Design of Girder and Beams | 90 |
| 3.4 | Finite Element Analysis | 92 |
| 3.4.1 | FEA Programs Utilized | 93 |
| 3.4.2 | Assumptions and Modeling Techniques | 93 |
| 3.5 | Quantification of Data to be Acquired from FEA Analysis | 104 |
| 3.5.1 | Selection of Cross-section Cuts..... | 105 |
| 3.5.2 | Tension Depth Analysis | 105 |
| 3.5.3 | Beam Rotation Calculations | 106 |
| 3.5.4 | Axial Girder Connection Forces..... | 107 |
| 3.6 | Verification of Results..... | 107 |
| 3.7 | Summary..... | 110 |
| 4 | PARAMETRIC STUDY | 111 |
| 4.1 | Parametric Values..... | 112 |
| 4.1.1 | Beam Dimensions..... | 115 |
| 4.1.2 | Lateral Bracing | 116 |
| 4.1.3 | Loads | 117 |
| 4.1.4 | Support Conditions..... | 118 |
| 4.1.5 | Residual Stresses | 119 |
| 4.1.6 | Geometric Imperfections | 120 |
| 4.2 | Connection Rotation Results | 120 |
| 4.3 | Percentage of Web Depth in Tension Results | 130 |
| 4.3.1 | Results of Cross-section at 28 Inches: Model 1-1 through Model 1-3 | 134 |
| 4.3.2 | Results of Cross-section at 224 Inches: Model 1-1 through Model 1-3 | 138 |
| 4.3.3 | Results of Cross-section at 324 Inches: Model 1-1 through Model 1-3 | 141 |
| 4.3.4 | Results of Cross-section at 28 Inches: Model 1-3 and Model 2-3..... | 146 |
| 4.3.5 | Results of Cross-section at 324 Inches: Model 1-3 and Model 2-3..... | 149 |
| 4.4 | Connection Force Results..... | 153 |

| | | |
|-------|--|-----|
| 4.4.1 | Connection Force Results: Model 1-1 through Model 1-3..... | 154 |
| 4.4.2 | Connection Force Results: Model 1-3 and Model 2-3 | 159 |
| 4.5 | Summary..... | 165 |
| 5 | CONCLUSION | 169 |
| 5.1 | Summary of Results | 170 |
| 5.2 | Need for Further Research..... | 174 |
| | REFERENCES | 178 |
| | Appendix | |
| | REPRINT PERMISSION LETTERS..... | 182 |

LIST OF TABLES

| | | |
|-------------------|--|-----|
| Table 2.1. | Summary of data of required rotation for catenary action | 76 |
| Table 2.2. | Summary of FEA data of available rotation for different connections | 77 |
| Table 2.3. | Summary of experimental data of available rotation for different connections | 78 |
| Table 3.1. | AISC Z_x table with limiting braced lengths (table from AISC 2005).... | 83 |
| Table 4.1. | Parametric combinations used for analyzed models | 114 |
| Table 4.2. | Summary of model results | 166 |

LIST OF FIGURES

| | | |
|---------------------|--|----|
| Figure 2.1. | Types of ties in TFM (figure from UFC 4-023-03, DoD 2010)..... | 10 |
| Figure 2.2. | Force vs. deformation graphs (figure from UFC 4-023-03, DoD 2010) | 11 |
| Figure 2.3. | Classification of governing action for structural steel buildings (figure from UFC 4-023-03, DoD 2010) | 12 |
| Figure 2.4. | Method for column removal (figure from UFC 4-023-03, DoD 2010) | 13 |
| Figure 2.5. | Deformation-controlled acceptance criteria for steel connections, non-linear procedure (figure from UFC 4-023-03, DoD 2010)..... | 14 |
| Figure 2.6. | Deformation-controlled acceptance criteria for steel connections, linear procedure (figure from UFC 4-023-03, DoD 2010) | 15 |
| Figure 2.7. | Actual versus assumed steel behavior (figure from Byfield 2004) | 18 |
| Figure 2.8. | Plan view of three-story structure (figure from Hoffman and Fahnestock 2011) | 20 |
| Figure 2.9. | Plan view of ten-story structure (figure from Hoffman and Fahnestock 2011) | 21 |
| Figure 2.10. | Results of FE analyses (data from Hoffman and Fahnestock 2011) | 22 |
| Figure 2.11. | Column removal locations (figure from Liu 2011) | 23 |
| Figure 2.12. | Comparison of member sizes for various levels of design (data from Liu 2011)..... | 24 |
| Figure 2.13. | Catenary action in multi-story building (figure from Khandelwal and El-Tawil 2007) | 25 |
| Figure 2.14. | Double-span beam model setup (Lee et al. 2009) | 26 |
| Figure 2.15. | Input and measured parameters (Lee et al. 2009) | 26 |

| | |
|--|----|
| Figure 2.16. Typical moment-axial tension interaction curve (Lee et al. 2009)..... | 27 |
| Figure 2.17. Normalized axial load vs. chord rotation (Lee et al. 2009)..... | 29 |
| Figure 2.18. Sub-assembly structure of two beams deformed after removal of column (Kim and An 2009) | 30 |
| Figure 2.19. Types of buildings modeled and analyzed (Kim and An 2009)..... | 30 |
| Figure 2.20. Material model for beam analysis (Kim and An 2009)..... | 32 |
| Figure 2.21. Push-down analysis results of the sub-assembly model (Kim and An 2009) | 33 |
| Figure 2.22. Load factor vs. rotation for moment frames (Kim and An 2009) | 34 |
| Figure 2.23. Normalized forces vs. rotation for moment frames (Kim and An 2009) | 35 |
| Figure 2.24. Model with missing column and no lateral beam support (Khandelwal and El-Tawil 2007)..... | 37 |
| Figure 2.25. Model with missing column and lateral beam support (Khandelwal and El-Tawil 2007) | 38 |
| Figure 2.26. Measured parameters (Khandelwal and El-Tawil 2007)..... | 39 |
| Figure 2.27. Beam catenary forces vs. displacement for non-RBS beams (figure from Khandelwal and El-Tawil 2007) | 40 |
| Figure 2.28. Beam catenary forces vs. displacement for RBS beams (figure from Khandelwal and El-Tawil 2007)..... | 41 |
| Figure 2.29. Steel frame used for FEM analysis (figure from Liu and Mei 2012)..... | 42 |
| Figure 2.30. Location of column removal for FEM analysis (figure from Liu and Mei 2012)..... | 43 |
| Figure 2.31. Overload factor versus vertical displacement (figure from Liu and Mei 2012)..... | 44 |
| Figure 2.32. Bending moment and axial tension in beam versus vertical displacement (adapted from Liu and Mei 2012)..... | 44 |
| Figure 2.33. Test setup (figure from Sadek et al. 2011) | 45 |

| | |
|---|----|
| Figure 2.34. Vertical load vs. center column displacement (figure from Sadek et al. 2011) | 47 |
| Figure 2.35. Beam axial force vs. center column displacement (figure from Sadek et al. 2011) | 47 |
| Figure 2.36. Connection geometry and measured parameters (figure from Munoz-Garcia et al. 2005)..... | 50 |
| Figure 2.37. Rate of loading vs. strength (figure from Munoz-Garcia et al. 2005).... | 51 |
| Figure 2.38. Vertical displacement vs. elapsed time for 3-story model in moderate seismic region (figure from Kim and Kim 2009) | 53 |
| Figure 2.39. Plastic hinge rotation vs. elapsed time for 3-story model in moderate seismic region (figure from Kim and Kim 2009) | 54 |
| Figure 2.40. Beam rotation vs. cyclic loading for: (a) flanges and web welded to column; (b) RBS with both flanges and web welded to column; (c) bolted T-stub (figures from Popov and Tsai 1989)..... | 55 |
| Figure 2.41. Parameters of test connections (adapted from Schneider and Teeraparbwong 2002) | 56 |
| Figure 2.42. Example connection geometry (figure from Schneider and Teeraparbwong 2002) | 57 |
| Figure 2.43. Testing apparatus (figure from Schneider and Teeraparbwong 2002)... | 57 |
| Figure 2.44. Moment vs. plastic rotation hysteretic graph (figures from Schneider and Teeraparbwong 2002) | 58 |
| Figure 2.45. Primary yield mechanisms of bolted T-stub connection (adapted from FEMA 2000) | 60 |
| Figure 2.46. Common failure mechanisms of bolted T-stub connection (figure from FEMA 2000) | 61 |
| Figure 2.47. Typical moment-rotation curve for T-stub connection and W24 beam (figure from FEMA 2000)..... | 61 |
| Figure 2.48. Specimen 1 (figure from Popov and Takhirov 2002)..... | 63 |
| Figure 2.49. Specimen 2 (figure from Popov and Takhirov 2002)..... | 64 |

| | |
|---|-----|
| Figure 2.50. Experimental test setup (figure from Popov and Takhirov 2002)..... | 65 |
| Figure 2.51. Finite element model (figure from Yang and Tan 2012) | 66 |
| Figure 2.52. Flush end plate connection (figure from Yang and Tan 2012) | 66 |
| Figure 2.53. Total and flexural reaction forces vs. connection rotation (figure from Yang and Tan 2012)..... | 67 |
| Figure 2.54. Tying force vs. connection stiffness (figure from Liu et al. 2005) | 68 |
| Figure 2.55. Vertical displacement and rotation at “missing” column vs. applied load (figure from Karns et al. 2009) | 70 |
| Figure 2.56. Axial tension vs. moment (figure from Karns et al. 2009)..... | 71 |
| Figure 2.57. Typical SidePlate™ Moment Connection Configuration (figure from SidePlate™ 2012) | 73 |
| Figure 3.1. Coordinate system, boundary conditions, and mesh of shell analysis (figure from Takhirov and Popov 2002)..... | 85 |
| Figure 3.2. Deformed shape of global shell analysis model (figure from Takhirov and Popov 2002) | 86 |
| Figure 3.3. Quarter model and mesh of solid T-stub connection analysis (figure from Takhirov and Popov 2002)..... | 88 |
| Figure 3.4. Deformed shapes of T-stub connection and bolts for solid element analysis (figure from Takhirov and Popov 2002) | 89 |
| Figure 3.5. Framing plan for member design | 91 |
| Figure 3.6. Flange out-of-squareness (figure from AISC)..... | 95 |
| Figure 3.7. Sweep for W-shapes (figure from AISC)..... | 95 |
| Figure 3.8. Text file input for Imperfection.FOR..... | 96 |
| Figure 3.9. Residual stress pattern (figure from Galambos and Ketter 1959)..... | 97 |
| Figure 3.10. Discretized residual stress pattern | 98 |
| Figure 3.11. Plastic command line used in analyses..... | 102 |

| | |
|--|-----|
| Figure 3.12. Steel material plastic input data..... | 102 |
| Figure 3.13. Geometry of experimentally tested steel plate girder..... | 108 |
| Figure 3.14. Comparison of verification girder FE with Righman data | 109 |
| Figure 4.1. Lateral bracing preventing LTB at flexural capacity | 117 |
| Figure 4.2. Load vs. rotation comparison for Model 1-1 | 122 |
| Figure 4.3. Load vs. connection rotation for Model 1-1, Model 1-2 & Model 1-3..... | 123 |
| Figure 4.4. Fixed support girder prior to flexural capacity..... | 124 |
| Figure 4.5. Fixed support girder after flexural capacity | 125 |
| Figure 4.6. Load vs. connection rotation for Model 1-3 & Model 2-3..... | 127 |
| Figure 4.7. Model 1-1 stress distribution prior to flexural capacity | 131 |
| Figure 4.8. Model 1-2 stress distribution prior to flexural capacity | 132 |
| Figure 4.9. Model 1-3 stress distribution prior to flexural capacity | 132 |
| Figure 4.10. Load vs. web tension depth at 28 and 224 inches for Model 2-3..... | 134 |
| Figure 4.11. Load vs. web tension depth at 28 inches for Model 1-1, Model 1-2 & Model 1-3..... | 136 |
| Figure 4.12. Load vs. web tension depth at 224 inches for Model 1-1, Model 1-2 & Model 1-3 | 140 |
| Figure 4.13. Load vs. web tension depth at 324 inches for Model 1-1, Model 1-2 & Model 1-3..... | 143 |
| Figure 4.14. Catenary comparison of Model 1-3 and Model 2-3 at 28 inches | 147 |
| Figure 4.15. Model 2-3 at flexural capacity..... | 148 |
| Figure 4.16. Catenary comparison of Model 1-3 and Model 2-3 at 324 inches | 150 |
| Figure 4.17. Fixed support beam at failure rotation | 153 |

| | |
|---|-----|
| Figure 4.18. Axial connection force vs. rotation comparison of Model 1-1, Model 1-2 & Model 1-3 | 155 |
| Figure 4.19. Axial connection force vs. applied load comparison of Model 1-1, Model 1-2 & Model 1-3 | 158 |
| Figure 4.20. Axial connection force vs. rotation comparison of Model 1-3 & Model 2-3 | 160 |
| Figure 4.21. Axial connection force vs. applied load comparison of Model 1-3 & Model 2-3 | 164 |

ABSTRACT

Progressive collapse occurs when local failure(s) of one or a limited number of structural components propagate to cause failure of a significant portion of the structure that is disproportionate to the original damage. Interest in mitigation of progressive collapse began after the full or partial collapses of structures such as the Ronan Point Apartments and Alfred P. Murrah Building. Current design guidelines exist for improving the progressive collapse resistance of structures, but these guidelines do not consider the potential catenary action of structural members under extreme deformation, which can potentially increase the load-resisting capacity of beams and girders compared to flexural capacity alone. By evaluating the potential catenary response, the actual behavior under extreme events can be more accurately considered and designed for and improved economy may also result.

In this thesis, a broad literature review was first performed to understand the prior work in this area and assess the practical limitations for developing catenary action. Then finite element analyses (FEA) were utilized, using ABAQUS, to determine and quantify the behavior of steel girders under a representative design scenario for the alternate path method of progressive collapse design, where a single column is removed from the structure. Several models were created to investigate the effects of: residual stresses; geometric imperfections; and support conditions, on the behavior of the steel girders under extreme load. Girder rotation, percentage of web depth in tension, and quantification of connection forces were all measured to analyze the girder behavior.

The results of the analyses revealed that girders with fixed supports were able to resist 80% more applied load after the flexural capacity of the girder was reached, regardless of the presence or absence of geometric imperfections and residual stresses. This compared to the shear support girder resisting only 30% more applied load after flexural capacity. All fixed support girders showed a constant increase in percentage of web depth in tension after the flexural capacity was reached up to a prescribed failure rotation of 0.05 radians, confirming catenary behavior is being utilized under additional applied load. At the failure rotation of 0.05 radians (a value selected based on review of past research), axial connection forces for the fixed support girders were between 350 kips and 372 kips. These results show that steel girders are able to utilize catenary behavior to resist additional applied load past their flexural capacity, which results in very large axial connection forces. It is suggested that consideration of these forces be incorporated in future efforts aimed to reduce the probability of progressive collapse.

Chapter 1

INTRODUCTION

1.1 Introduction to Progressive Collapse

Extreme loading events can potentially result in the progressive collapse of engineered structures. Progressive collapse occurs when local failures of one or a limited number of structural components propagate to cause failure of a significant portion of the structure that is disproportionate to the original damage. Interest in mitigation of progressive collapse began after a gas explosion at the Ronan Point Apartments triggered extensive damage to substantial portion of the 22-story precast concrete structure in 1968. More recently, the threat of global terrorist attacks, using destructive explosives, has fueled the need for effective measures in protecting structures against progressive collapse. The collapse of the Alfred P. Murrah Federal Building in Oklahoma City in 1995 was an example of progressive collapse due to the deliberate detonation of a vehicular bomb. Hamburger (2006), writes regarding the Murrah building that “extreme damage to columns at the first story of the 9-story building, led to progressive collapse of much of the structure.”

More dramatically, the World Trade Center (WTC) terrorist attacks of 2001 showcased how damage to multiple load-bearing members can lead to progressive collapse. It should be noted, however, that while the WTC collapse was due to progressive collapse, the failure was not disproportionate. The damage which occurred when large passenger jets crashed into the WTC was not localized and was severe enough that the failure of the buildings was not disproportionate.

Effective guidelines for the mitigation of progressive collapse are necessary to ensure life-safety in structures subject to blast loading. While the probability of progressive collapse of a structure due to extreme loads is low, the impact of potential loss of life and economic damage has led to the demand for more resilient structural designs. A study by Leyendecker and Burnett (1976) found that 15 to 20% of all building failures are due to progressive collapse. This relatively high percentage underscores the need for effective standards governing the design of structures to resist progressive collapse.

1.2 Early History of Progressive Collapse and Initial Observations

Byfield and Paramasivam (2007) detailed some of the early history and studies into the effects of extreme blast loading on buildings. During World War II, the city of London was subjected to large-scale bombing by Nazi Germany. Data on the effects of the bombing on civil structures was subsequently collected, including 60,000 basic reports on the bomb damage in addition to 5,000 detailed reports on individual damaged structures. This data helped to lay the groundwork for structural behavior subject to blast loading.

Lord J. F. Baker's observations during World War II were included in the review by Byfield and Paramasivam (2007). He concluded that of the roughly 50 steel framed buildings he surveyed, the vast majority of collapses were due to inadequate connections between perimeter columns and beams. Baker noted that even near-miss bomb blasts created enough blast pressure to cause widespread failure of the steel connections. Baker's observations led to his recommendation that both floor-to-wall and beam-to-column connections be strengthened. He noted that the steel connections

typically failed from either prying action of the bolted sections, an insufficient ability to sustain large end rotations, or excessive tensile loading.

In subsequent decades, terrorist attacks by the Provisional Irish Republican Army (PIRA) in the British Isles allowed for more study and observation of structures subject to blast (Byfield 2006). Beam-to-column joints in reinforced concrete frames were typically found to fracture at the location of steel reinforcement lapping. Dislocation of these joints can dislodge concrete members from their supports causing collapse of some or all of the building. The attacks by the PIRA on British structures displayed the necessity of effectively tying all components of a structure together (Byfield 2006). All of these examples of progressive collapse show the need to understand structural behavior of members and connections under extreme load so as to best design them to mitigate progressive collapse.

1.3 Need for Current Research

Current progressive collapse codes require structural members to be designed for the forces generated in the event of a removed column. Force and deformation criteria affect the sizes of these members. Beams are designed to the point of plastic hinge formation, at which point their load-carrying capacity is not assumed to increase. However, a structural phenomenon referred to as catenary action may allow beams to resist loads in a tensile or cable-like manner past their flexural capacity. Utilization of catenary action can potentially increase the load-resisting capacity of beams and girders compared to flexural capacity alone.

While progressive collapse has been a major research concern since the collapse of the Ronan Point Apartments in 1968, specific research into the utilization of catenary action has only recently been considered. The objective of this thesis will

be to provide quantitative data to help better understand the extent to which catenary action can be utilized in steel beams under extreme loads relative to the limits of typical modern connections. Current codes such as the GSA *Progressive Collapse Analysis and Design Guidelines* (2003) and UFC 4-023-03 *Design of Buildings to Resist Progressive Collapse* (2010) have no explicit guidelines for design of beams utilizing catenary action. Research is needed to quantify the forces and rotations generated in both the beam and connections during catenary action. Quantifying the additional applied load which a given structural member can resist past its flexural capacity is also of great importance. The influence of geometric imperfections and residual stresses on these results is a unique feature of the present work, having not been considered in prior research on this topic.

Aside from quantification of the catenary load capacity of specific flexural members, behavior of beam-column connections and the columns themselves must be understood so that they can be properly designed to resist the potentially extreme tensile loads developed during a “missing” column scenario. Crippling of column panel zones, fracture of connections, and prying of bolts are all areas of concern when considering a “missing” column scenario. The focus of this thesis will be the forces, rotations, and catenary behavior of a steel girder and its connections during extreme loading. Analysis of the effects of catenary action on the behavior of columns is left to future research.

1.4 Objectives of Research

The research presented in this thesis has several objectives relating to catenary behavior of girders and their connections during a ‘missing’ column loading event. The primary objectives of the research presented in this thesis are:

- To determine whether the assumption of catenary action is valid in steel girders under a ‘missing’ column load
- To quantify the extent to which catenary action can be developed in a steel girder if the assumption is valid
- To quantify the additional applied load which can be resisted by catenary action after flexural capacity of a steel girder is surpassed
- To quantify the rotation behavior of a steel girder during a ‘missing’ column load
- To quantify the connection forces as a result of catenary action
- To determine the effects, if any, of residual stresses and geometric imperfections on the catenary behavior of steel girders

The finite element analysis (FEA) software ABAQUS (Dassault Systemes 2011) was utilized to accomplish these objectives through models of a representative steel girder with differing support conditions and with the presence and absence of residual stresses and geometric imperfections. Chapter 3 of this thesis extensively details the setup and methodology used in the FEA models.

1.5 Scope of Research

The primary focus of this research is to quantify the forces, rotations, displacements, and stresses that occur during and are necessary to utilize catenary action on a steel beam with a “missing” column at mid-span. Although the column is removed, the beam-to-column continuity is assumed to remain intact. This scenario removes the common column supporting two adjacent beams, thus creating a single span out of two beams.

Four models were created to investigate the effects of geometric imperfections, residual stresses, and support conditions on the load-carrying capacity of the girder. The constants in each model were: beam size, a W21x55 steel beam; web stiffeners; lateral bracing; and load location and magnitude. Web stiffeners were located at mid-span of the beam as well as at the support locations. Beam elements were used at discrete locations to represent lateral bracing members. Finite Element Analysis (FEA) models beams were analyzed using the FEA software ABAQUS. The Riks algorithm was used to apply extreme levels of loading and the stress distribution, displacements, and total rotation of the beams was calculated. The Riks method applies incrementally increasing loads to the member in order to obtain a more accurate analysis of beam behavior at many different loads. Static loads representing forces transferred from adjacent beams in the simulated framing plan were applied along the length of the girder. An increasing Riks load was applied at mid-span of the girder representing the “missing” column load transferred from the above floors of the structure.

Among the results are graphs that were constructed to quantify the extent of the beam cross-section in tension versus the applied load. The percentage of the total beam cross-section in tension was used as a metric to measure its catenary behavior. Since total rotation of a steel flexural member is an important metric for determining ductility and potential failure of the member, graphs were also constructed plotting total rotation and connection forces vs. applied load.

This thesis is organized into five chapters: Chapter 1 – Introduction; Chapter 2 – Literature Review; Chapter 3 – Methodology; Chapter 4 – Parametric Study; and Chapter 5 – Conclusions. In Chapter 2, the data and results of several previous

research studies will be presented and discussed. A significant outcome of this review is the determination of appropriate limiting values for connection performance which are used to establish realistic limits on the girder response that is shown in Chapter 4. Chapter 3 will present the method of analysis used in this thesis as well as verification of the analysis method. Chapter 4 presents the data and results from the models analyzed in this thesis. Lastly, Chapter 5 will summarize the findings of this thesis as well as discuss recommended future research in this area.

Chapter 2

LITERATURE REVIEW

2.1 Introduction to Current State of Practice and Relevant Research

In the United States, both the Unified Facilities Criteria publication UFC 4-023-03, *Design of Buildings to Resist Progressive Collapse* (DoD 2010), and the General Services Administration publication, *Progressive Collapse Analysis and Design Guidelines* (GSA 2003), primarily govern the design of structures to prevent progressive collapse. These codes outline several current analysis methods used to ascertain whether a design is adequate for resisting progressive collapse.

These guidelines use fundamental structural mechanics, such as beam bending behavior, to generate acceptable progressive collapse designs. However, a phenomenon known as catenary action may offer the potential to greatly increase the load-carrying capacity of a beam past its flexural capacity. Catenary action occurs after a sufficient number of plastic hinges are formed and applied load is carried through axial tension in the beam.

This chapter will detail the current state of practice and research in progressive collapse design. The current findings relating to the development of catenary action as well as behavior of connections in these situations are also primary foci.

2.2 Current Progressive Collapse Guidelines

The analysis procedures for the two previously mentioned guidelines (DoD 2010, GSA 2003) have similar approaches; however the limiting criteria for structural

members differ between the two. ASCE 41-06 *Seismic Rehabilitation of Existing Buildings* (ASCE 2007) specifies methods to strengthen structures against progressive collapse; however no quantitative guidelines are specified. Both the UFC and GSA guidelines are further discussed in the following two subsections, respectively.

2.2.1 UFC Guidelines

The UFC guidelines allow for two distinct design methods: Indirect and Direct Design. Indirect design is accomplished through implicit consideration by specifying minimum forces to be resisted and/or providing a prescribed level of continuity and ductility. Direct design uses explicit considerations of the forces generated when a portion of the structure is damaged.

In indirect design, the Tie-Force Method (TFM) is utilized to provide adequate ductility, continuity, and structural redundancy by requiring the structure to resist minimum tensile forces. In the TFM, the floor and roof systems are used to horizontally transfer loads from the damaged portion of the structure to the undamaged portion. Columns or other vertically-oriented members may serve as vertical ties. These types of load transfer may be accomplished through the design of peripheral, longitudinal, transverse, and vertical ties in the manner shown in Figure 2.1.

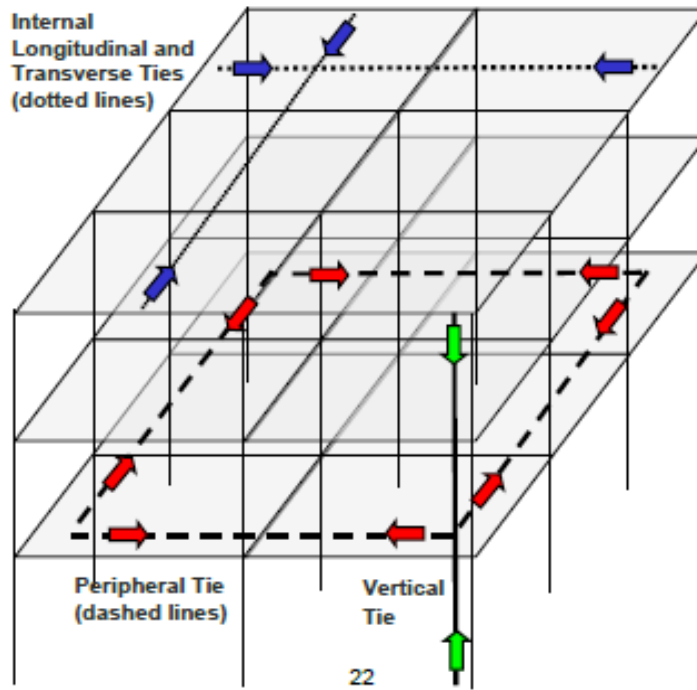


Figure 2.1. Types of ties in TFM (figure from UFC 4-023-03, DoD 2010)

In the UFC, direct design methods include the Alternate Path Method (APM) and the Specific Local Resistance Method (SLRM). The APM requires analysis and design of the structure for the case of removed column. The structure must be capable of bridging over the damaged column and arrest further damage of the structure. The SLRM requires that all or a portion of the building be designed to provide adequate strength for a specific load. Structural design using the SLRM requires strengthening the perimeter load-bearing walls and columns for increased flexure and shear. The amount of strength increase required is dictated by the occupancy of the structure.

The APM is a redundant design method in that it requires the engineer to design the structural members and connections for the loads generated during the removal of a column at any location. Three analysis procedures are available in the

APM. In increasing order of computation effort and accuracy, they are: Linear static, nonlinear static and nonlinear dynamic. Design of structural components using the APM uses the Load and Resistance Factor (LRFD) design method combined with incorporating an over-strength factor for deformation-controlled actions, which are actions defined in the following paragraph.

When using the APM, shear, flexural, and axial forces are classified as either force-controlled or deformation-controlled for all structural components. Figure 2.2 shows the force vs. deformation graphs in UFC, which are used to determine whether an action is force-controlled or deformation-controlled. A primary structural component with a Type 1 or 2 curve and ' $e' \geq 2g$ ' (Fig. 2.2) is classified as having a deformation-controlled action. Otherwise, the action is defined as force-controlled, including all actions with force vs. deformation curves similar to a Type 3 curve (Fig. 2.2). In this thesis, beam flexure and connection rotation will be classified as deformation-controlled due to the large plastic rotations incurred during progressive collapse situations in steel-framed buildings. This assumption is also justified in part by Figure 2.3, which is reproduced from UFC 4-023-03.

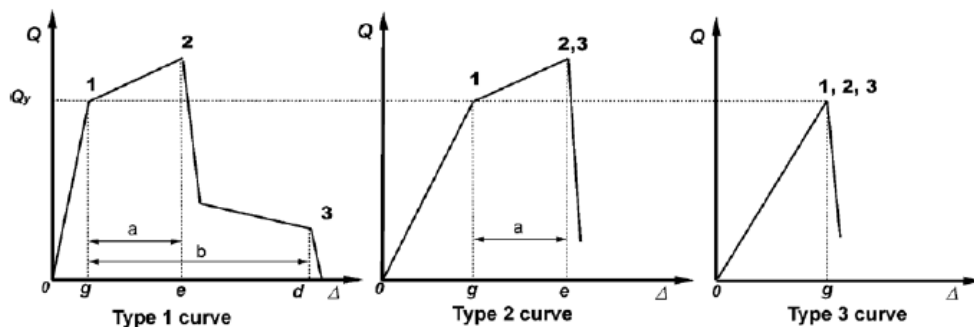


Figure 2.2. Force vs. deformation graphs (figure from UFC 4-023-03, DoD 2010)

| Component | Deformation- Controlled Action | Force- Controlled Action |
|---|-----------------------------------|--|
| Moment Frames • Beams • Columns • Joints | Moment (M) M -- | Shear (V) Axial load (P), V V ¹ |
| Shear Walls | M, V | P |
| Braced Frames • Braces • Beams • Columns • Shear Link | P -- -- V | -- P P P, M |
| Connections | P, V, M ² | P, V, M |

1. Shear may be a deformation-controlled action in steel moment frame construction.

2. Axial, shear, and moment may be deformation-controlled actions for certain steel and wood connections.

Figure 2.3. Classification of governing action for structural steel buildings (figure from UFC 4-023-03, DoD 2010)

Analysis of a structure for progressive collapse is performed by removing a column or load-bearing wall at certain prescribed locations and designing the structural members to resist the applied forces. The beam-to-beam continuity is assumed to remain intact during column removal as shown by Figure 2.4. Thus, beam-to-beam continuity was assumed for the models presented in this thesis, allowing the utilization of catenary action. Once the column has been removed, members and connections are checked against acceptance criteria presented in UFC 4-023-03, which adopts much of the same criteria found in ASCE 41-06 (ASCE 2007). However, acceptance criteria for steel connections differs for UFC 4-023-03 and ASCE 41-06. Acceptance criteria in UFC 4-023-03 for the deformation-controlled actions of steel moment connections are shown in Figure 2.5. Members which provide

collapse resistance due to a column removal are designated as primary components. Therefore, the acceptable rotations for those members are those designated as primary. The values shown in Figure 2.5 are the maximum allowable per code. If the analysis of a structure yields values greater than those shown in Figure 2.5, members and/or connections must be re-designed to be within the acceptable range.

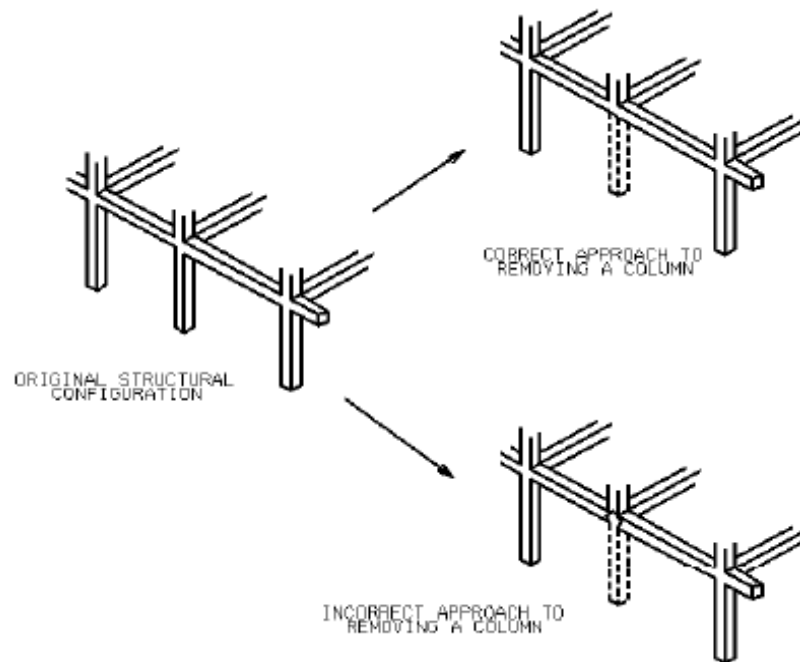


Figure 2.4. Method for column removal (figure from UFC 4-023-03, DoD 2010)

| Connection Type | Nonlinear Modeling Parameters ⁽¹⁾ | | | Nonlinear Acceptance Criteria | |
|---|---|-------------------------------|-------------------------|---------------------------------|--------------------------------|
| | Plastic Rotation Angle, radians | | Residual Strength Ratio | Plastic Rotation Angle, radians | |
| | a | b | | Primary ⁽²⁾ | Secondary ⁽²⁾ |
| Fully Restrained Moment Connections | | | | | |
| Improved WUF with Bolted Web | 0.021 - 0.0003d | 0.050 - 0.0006d | 0.2 | 0.021 - 0.0003d | 0.050 - 0.0006d |
| Reduced Beam Section (RBS) | 0.050 - 0.0003d | 0.070 - 0.0003d | 0.2 | 0.050 - 0.0003d | 0.070 - 0.0003d |
| WUF | 0.0284 - 0.0004d | 0.043 - 0.0006d | 0.2 | 0.0284 - 0.0004d | 0.043 - 0.0006d |
| SidePlate [®] | 0.089 - 0.0005d ⁽³⁾ | 0.169 - 0.0001d | 0.6 | 0.089 - 0.0005d | 0.169 - 0.0001d |
| Partially Restrained Moment Connections (Relatively Stiff) | | | | | |
| Double Split Tee | | | | | |
| a. Shear in Bolt | 0.036 | 0.048 | 0.2 | 0.03 | 0.040 |
| b. Tension in Bolt | 0.016 | 0.024 | 0.8 | 0.013 | 0.020 |
| c. Tension in Tee | 0.012 | 0.018 | 0.8 | 0.010 | 0.015 |
| d. Flexure in Tee | 0.042 | 0.084 | 0.2 | 0.035 | 0.070 |
| Partially Restrained Simple Connections (Flexible) | | | | | |
| Double Angles | | | | | |
| a. Shear in Bolt | 0.0502 - 0.0015d _{bg} ⁽⁴⁾ | 0.072 - 0.0022d _{bg} | 0.2 | 0.0502 - 0.0015d _{bg} | 0.0503 - 0.0011d _{bg} |
| b. Tension in Bolt | 0.0502 - 0.0015d _{bg} | 0.072 - 0.0022d _{bg} | 0.2 | 0.0502 - 0.0015d _{bg} | 0.0503 - 0.0011d _{bg} |
| c. Flexure in Angles | 0.1125 - 0.0027d _{bg} | 0.150 - 0.0036d _{bg} | 0.4 | 0.1125 - 0.0027d _{bg} | 0.150 - 0.0036d _{bg} |
| Simple Shear Tab | 0.0502 - 0.0015d _{bg} | 0.072 - 0.0022d _{bg} | 0.2 | 0.0502 - 0.0015d _{bg} | 0.1125 - 0.0027d _{bg} |

⁽¹⁾ Refer to Figure 3-6 for definition of nonlinear modeling parameters a, b, and c

⁽²⁾ Refer to Section 3-2.4 for determination of Primary and Secondary classification

⁽³⁾ d = depth of beam, inch

⁽⁴⁾ d_{bg} = depth of bolt group, inch

Figure 2.5. Deformation-controlled acceptance criteria for steel connections, non-linear procedure (figure from UFC 4-023-03, DoD 2010)

The linear static procedure defined in UFC 4-023-03 differs significantly from the nonlinear static procedure. Figure 2.6 shows the table which is used to calculate ‘m’ factors for various connections types. The ‘m’ factor is then used to satisfy the following equation, $\phi m Q_{CE} \geq Q_{UD}$. Q_{CE} is the expected strength of connection and Q_{UD} is deformation-controlled action from analysis.

| Connection Type | Linear Acceptance Criteria | |
|---|---|-----------------------------|
| | <i>m</i> -factors | |
| | Primary ⁽¹⁾ | Secondary ⁽¹⁾ |
| Fully Restrained Moment Connections | | |
| Improved WUF with Bolted Web | 2.3 – 0.021d | 4.9 – 0.048d |
| Reduced Beam Section (RBS) | 4.9 – 0.025d | 6.5 – 0.025d |
| WUF | 4.3 – 0.083d | 4.3 – 0.048d |
| SidePlate® | 6.7 – 0.039d ⁽²⁾ | 11.1 – 0.062d |
| Partially Restrained Moment Connections (Relatively Stiff) | | |
| Double Split Tee | | |
| a. Shear in Bolt | 4 | 6 |
| b. Tension in Bolt | 1.5 | 4 |
| c. Tension in Tee | 1.5 | 4 |
| d. Flexure in Tee | 5 | 7 |
| Partially Restrained Simple Connections (Flexible) | | |
| Double Angles | | |
| a. Shear in Bolt | 5.8 – 0.107d _{bg} ⁽³⁾ | 8.7 – 0.161d _{bg} |
| b. Tension in Bolt | 1.5 | 4 |
| c. Flexure in Angles | 8.9 – 0.193d _{bg} | 13.0 – 0.290d _{bg} |
| Simple Shear Tab | 5.8 – 0.107d _{bg} | 8.7 – 0.161d _{bg} |

⁽¹⁾ Refer to Section 3-2.4 for determination of Primary and Secondary classification

⁽²⁾ d = depth of beam, inch

⁽³⁾ d_{bg} = depth of bolt group, inch

Figure 2.6. Deformation-controlled acceptance criteria for steel connections, linear procedure (figure from UFC 4-023-03, DoD 2010)

Several experiments into connection rotation are detailed in Section 2.3 of this chapter. The large ductility of steel compared with other materials allows steel beams and connections to achieve large inelastic rotations and deformations. High plastic rotations will be shown to be necessary to utilize the catenary behavior of a steel beam, which is discussed in Section 2.5 of this chapter.

2.2.2 GSA Guidelines

There are many similarities between the GSA and UFC progressive collapse guidelines. GSA guidelines rely solely on the direct design, specifically the alternate load path method in the same manner as UFC guidelines, but also describe the necessity for beam-to-beam continuity to mitigate progressive collapse. Column removal is performed in the same manner as UFC guidelines as well. However, there are only two analysis procedures for structural analysis in GSA as opposed to three in the UFC. These are: linear static and dynamic linear-elastic.

The linear static analysis procedure begins with the analysis of structural components following the instantaneous removal of a support. After the analysis of the structure prior to column removal, members and connections are checked against criteria for Demand-to-Capacity Ratios (DCR). The DCR is prescribed by the following equation:

$$DCR = \frac{Q_{UD}}{Q_{CE}} \quad \text{(Equation 2.1)}$$

Q_{UD} is the acting force in the member or connection and Q_{CE} is the un-factored capacity of the member or component. The acceptance criteria for the DCR of steel structures are found in Chapter 5 of the GSA guidelines. It should be noted that the DCR for the flanges of T-stub connections is '3' while other moment connections have a flange DCR of '2'. This shows the greater ductility of T-stub connections in relation to other moment connections.

Under the GSA guidelines, a non-linear analysis procedure may be utilized in lieu of a linear procedure. The acceptance criteria for the nonlinear procedure are given in terms of ductility and/or rotation of structural components in Table 2.1 of the GSA guidelines. The limiting rotation for flange yielding of a T-stub connection is

0.025 radians in GSA guidelines. This is an intermediate value compared to those found in previous analytical and experimental data that will be reviewed in Section 2.3 of this chapter.

UFC 4-023-03 requires that all primary and secondary components exceed the acceptance criteria defined in the code. If any component does not meet the criteria, the structure must be redesigned until all components do meet the acceptance criteria. GSA guidelines require that all components meet or exceed the allowable demand-to-capacity ratio (DCR) in areas outside of the allowable collapse region in order for the structure to be defined as having a low potential for progressive collapse.

2.3 Behavior of Steel-Framed Structures during Progressive Collapse Events

As shown in the previous section, steel connections must be designed to be both strong and ductile enough to allow the framing components to achieve the large inelastic deformations needed to resist large forces. The majority of progressive collapses caused by explosions and other extreme loading events can be attributed to the weakness of the beam-to-column connections (Byfield 2006). In England during World War II, Lord J. F. Baker surveyed around 50 steel framed buildings that had at least partially collapsed as a result of direct or near-miss bomb explosions. He concluded that the vast majority of these collapses were due to inadequate beam-to-column connections, specifically due to brittle tensile failure (Byfield 2006).

Modern buildings were shown to be susceptible to progressive collapse as a result of an explosion during the terrorist attack on the Murrah Building in 1995. Lightweight curtain wall cladding, transfer girders, and a lack of structural internal partitions in many modern steel buildings reduce alternate paths for excessive forces during an extreme loading event. The Murrah Building collapse demonstrated the

need for building frames which can sustain large deformations in the event of an extreme loading event. More so than other building materials, steel framing is able to be adequately designed to be strong and ductile enough to resist extreme forces. Byfield (2004) concludes that, “the important factor in achieving robustness in buildings is the ability to absorb energy through ductile failures.”

Byfield (2006) describes how modern steel buildings typically utilize beams that can often resist double their design load. One reason for this is that the actual yield stress of steel members can be between 16% and 37% higher than the minimum specified yield stress (Byfield 2004). Another contributing factor is the assumed rigid-plastic behavior of steel above yielding versus the actual strain hardened behavior, shown in Figure 2.7, resulting in steel having strength greater than that assumed in design due to strain hardening.

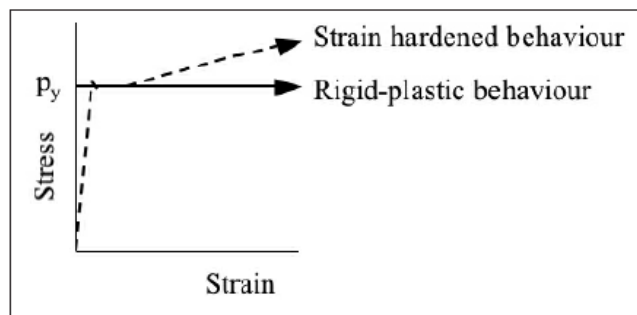


Figure 2.7. Actual versus assumed steel behavior (figure from Byfield 2004)

Beam overstrength can lead to non-ductile steel frames, due to the beam-to-column connections becoming the weakest link. Steel frames must exhibit substantial ductility to accommodate the large deformations required in an extreme loading event.

Therefore, it is necessary for connections to be strong enough to utilize the steel beam ductility and allow formation of plastic hinges. Byfield (2004) recommends that connections and columns in a building designed for progressive collapse be able to resist the upper-bound loads from beams which are based on realistic material strength and structural behavior. Catenary action in beams can be initiated only with sufficient ductility for enough plastic hinges to form to create a failure mechanism.

2.4 Current Research Relating to Alternate Load Path Method

As described in Section 2.2, APM is one of the code-prescribed methods for preventing progressive collapse. The alternate path method requires the structure to remain intact when selected load-bearing elements are removed. Specifically, the remaining members of the structure must be able to resist the internal forces generated in the event of a removed column. The three analysis options associated with APM are: linear static, nonlinear static, and nonlinear dynamic. The linear static method is the most conservative but least intensive method, while the nonlinear static and nonlinear dynamic methods involve more intensive modeling but produce more accurate results (Liu 2011).

Hoffman and Fahnestock (2011) used the FE program ABAQUS to analyze the behavior of multi-story steel buildings under a column loss scenario. They analyzed two building geometries, a three-story and ten-story structure. Both buildings consisted of simple shear connections in the interior of the structure with perimeter moment frames for lateral resistance as shown in Figure 2.8 and Figure 2.9. The floor system consisted of steel beams with a composite concrete deck. The beams, columns and girders all were modeled with both S3 and S4R shell elements. Nonlinear material behavior was accounted for using steel stress-strain properties from

experimental testing. Bolts for the connections were modeled using nonlinear springs and the flanges of beams in moment connections were rigidly connected to each other. Bolt tear-out was determined to be the governing limit state for the axial capacity of the connections. The bolt spring stiffness was determined from experimental data, and the spring was modeled to fail at the point of maximum strength (Hoffman and Fahnestock 2011). Figure 2.8 and Figure 2.9 show the plan view of the three-story and ten-story structure respectively.

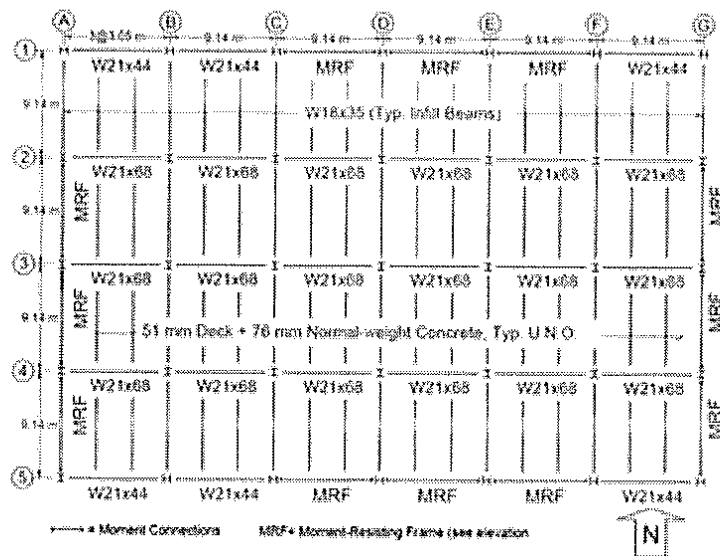


Figure 2.8. Plan view of three-story structure (figure from Hoffman and Fahnestock 2011)

Various interior, corner, and perimeter columns for each structure type were removed, one at a time, for the analyses. The floors were loaded with full dead load and 25% of the design live load. The models were then run for one second in order to reach the static loading condition. Next, the vertical boundary condition was turned

off at the removed column, and the model was run for one second. Displacement versus time plots show that the maximum displacement of the model is reached during the one second interval. Figure 2.10 details the results of the analyses in tabular form.

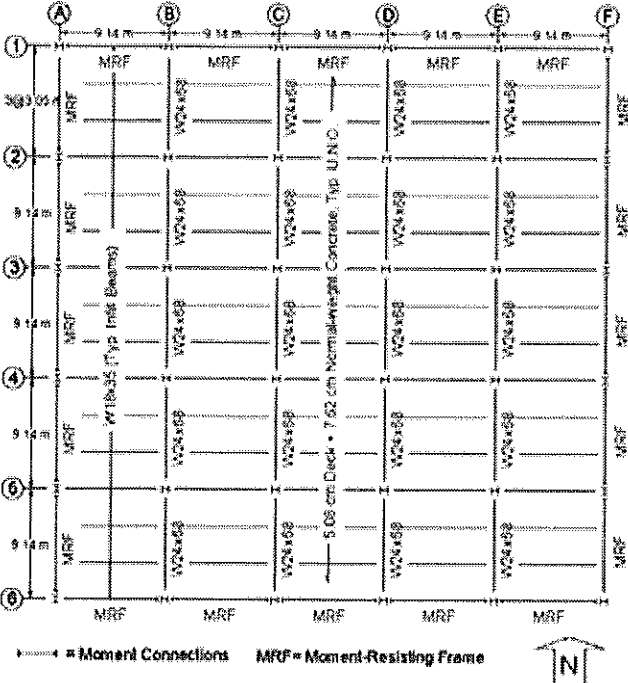


Figure 2.9. Plan view of ten-story structure (figure from Hoffman and Fahnestock 2011)

The results of the analyses show the ability of the structures to resist the applied loads and mitigate progressive collapse for most of the column removal scenarios. The steel structures have the strength and ductility to undergo vertical displacements between 120 mm (4.7 inches) and 610 mm (24 inches) at the location of the removed column. This deflection corresponds to a total, elastic plus plastic, beam end rotation of between 0.013 and 0.067 radians.

| Building height | Column location | Lost column | Displacement (mm) |
|-----------------|-----------------|-------------|-------------------|
| Three-story | Corner | A1 | NA - collapse |
| | | A5 | 320 |
| | Perimeter | A2 | 610 |
| | | A3 | 120 |
| | | A4 | 130 |
| | | B1 | NA - collapse |
| | | C1 | 380 |
| | Interior | D1 | 120 |
| | | B2 | 440 |
| | | B3 | 370 |
| C2 | | 350 | |
| Ten-story | Corner | C3 | 320 |
| | | A1 | 43 |
| | Perimeter | B1 | 41 |
| | | A2 | 53 |
| | Interior | B2 | 350 |

Figure 2.10. Results of FE analyses (data from Hoffman and Fahnestock 2011)

A recent publication by Liu (2011) details the application of the alternate path method through the use of design examples. Liu analyzed a nine-story, three-bay, intermediate moment frame steel building for progressive collapse using the three procedures allowed in UFC 4-023-03. For the linear static procedure, “an in-house linear elastic program is used.” The program, DRAIN-2DX, was used for the other two procedures (Liu 2011).

The example frame was designed to meet AISC seismic provisions for an intermediate moment frame (IMF), however progressive collapse was not accounted for. Figure 2.11 details the locations of column removal used by Liu in the progressive collapse analysis. The analyses performed by Liu are ended when a structural member reached the acceptable plastic rotation allowed by UFC. The data presented later in this thesis uses a similar approach to terminate the steel beam’s rotation at a predetermined value.

Liu then redesigned the steel frame to meet the progressive collapse criteria outlined in UFC. Figure 2.12 compares the structural members' sizes for seismic design and the three levels of analysis allowed by UFC.

From Figure 2.12, it can be seen that overall weights of structural members decrease for more refined levels of progressive collapse analysis. This is due to the fact that nonlinear behavior is taken into account for both the nonlinear static and nonlinear dynamic methods. Nonlinear behavior occurs after post-yield strength is reached but the member still has load-carrying capacity.

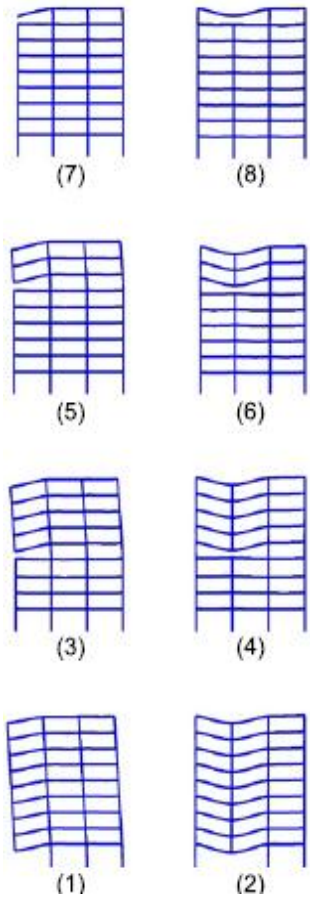


Figure 2.11. Column removal locations (figure from Liu 2011)

| Optimized designs through weight minimization | Steel weight | Member types | Member groups | | | |
|---|--|--------------|---------------|-------------|-------------|-------------|
| | | | 1–3 stories | 4–5 stories | 6–7 stories | 8–9 stories |
| Without considering progressive collapse (MWD) | 99.1 kips (440.6 kN) | Columns | W18 × 119 | W18 × 97 | W18 × 97 | W18 × 50 |
| | | Beams | W27 × 84 | W24 × 68 | W24 × 55 | W21 × 44 |
| Considering progressive collapse by different UFC analysis procedures | Nonlinear dynamic (PCND) 107.2 kips (476.8 kN) | Columns | W18 × 158 | W18 × 106 | W18 × 76 | W18 × 50 |
| | | Beams | W24 × 76 | W24 × 76 | W24 × 55 | W24 × 62 |
| | Nonlinear static (PCNS) 112.2 kips (498.9 kN) | Columns | W18 × 158 | W18 × 119 | W18 × 76 | W18 × 76 |
| Linear static (PCLS) 137.5 kips (611.6 kN) | 137.5 kips (611.6 kN) | Columns | W18 × 192 | W18 × 130 | W18 × 97 | W18 × 76 |
| | | Beams | W24 × 76 | W27 × 94 | W27 × 94 | W30 × 99 |

Figure 2.12. Comparison of member sizes for various levels of design (data from Liu 2011)

The design for progressive collapse uses standard design codes to determine the limit states and capacities of the steel members. Catenary action, which will be detailed in the next section, is not explicitly accounted for in progressive collapse design in either GSA or DoD guidelines. However, this is an area of research interest, as described in the following section. The potential for significantly increased load-carrying capacity due to utilizing catenary action will also be discussed in Chapter 4 of this thesis.

2.5 Catenary Behavior of Steel Beams under Progressive Collapse Events

In the Alternate Path Method (APM), discussed in Sections 2.2 and 2.4 of this thesis, the purpose of the structural analysis is to ensure that the structure can bridge over a damaged column. Since beam-to-beam continuity over a damaged column is assumed in UFC (DoD 2010) and GSA (2003) codes, the two beams on either side of a “missing column” are now analyzed as a single beam. Beams designed to traditional building codes would likely have insufficient flexural and/or shear capacity to bridge over a “missing” column and resist the additional loads. Catenary action may then occur and provide adequate load resistance after the flexural capacity of a beam is

reached and also a sufficient number of plastic hinges form to create a failure mechanism. Figure 2.13 shows a graphical representation of how catenary action is utilized in a structure.

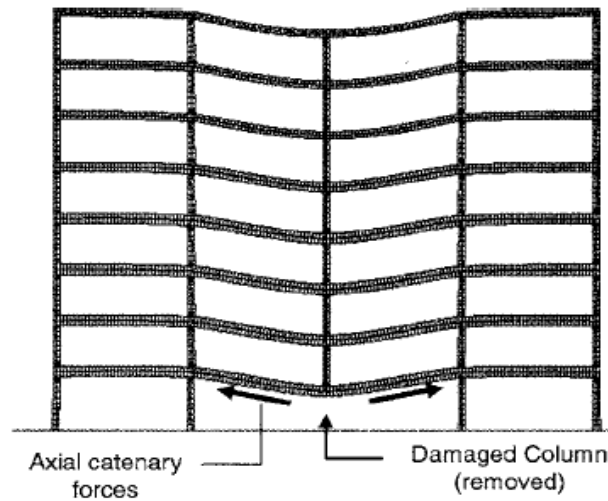


Figure 2.13. Catenary action in multi-story building (figure from Khandelwal and El-Tawil 2007)

Lee et al. (2009) researched the catenary behavior of welded steel moment frames using the finite element program ABAQUS to model double span wide flange beams of varying span-to-depth (L/D) ratios. Both the span, 'L', and the beam depth, 'D', were varied in the experiments, as shown by the fact that beams with varying depth were analyzed at the same span-to-depth ratio. The ends of the beams were laterally restrained. Lee et al. (2009) state that the model is constructed such that "the connections are stronger than the beams and have ample ductility." Also, "the panel zone is assumed to be sufficiently strong such that all inelastic action occurs in the beams", indicating that catenary action in the beams is possible. Review of Lee et

al.'s work also indicates that the beams are directly connected to the columns and continuity plates are modeled on the columns.

The primary parameter measured in the analyses was the beam chord rotation, θ , which is defined as the vertical beam deflection, u , divided by the clear span length, L , of the initial one-span beam. Figure 2.14 shows the setup of the model. Figure 2.15 depicts the input and measured variables in Lee et al.'s analyses.

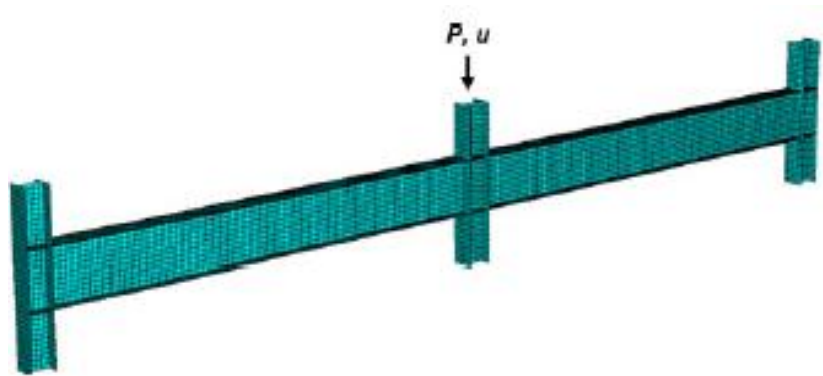


Figure 2.14. Double-span beam model setup (Lee et al. 2009)

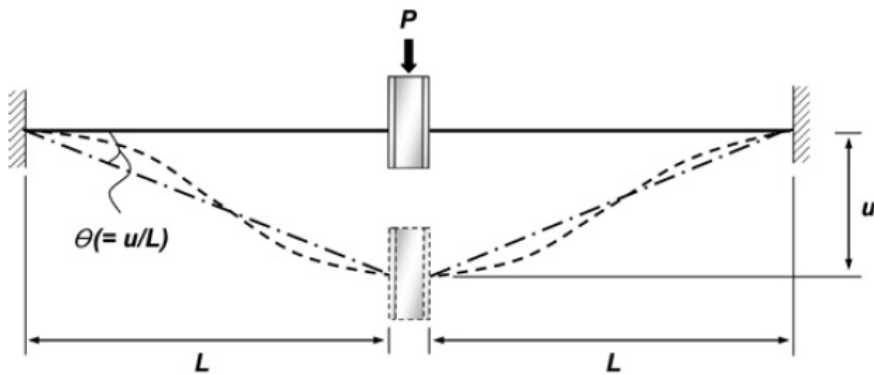


Figure 2.15. Input and measured parameters (Lee et al. 2009)

The moment and axial tension in the beam were normalized with respect to its plastic moment, M_p , and the tensile yield strength, T_y . Figure 2.16 shows a typical moment-axial tension interaction curve versus chord rotation for a beam with various span-to-depth ratios. In the analyses, both the beam length, L , and the beam depth, d , were varied to achieve the desired span-to-depth ratio. In Figure 2.16, the variable $L/2$ is the assumed distance to the inflection point, or mid-span of one of the single-span beams. Therefore, $2L$ is used to represent the total length of the double-span beam.

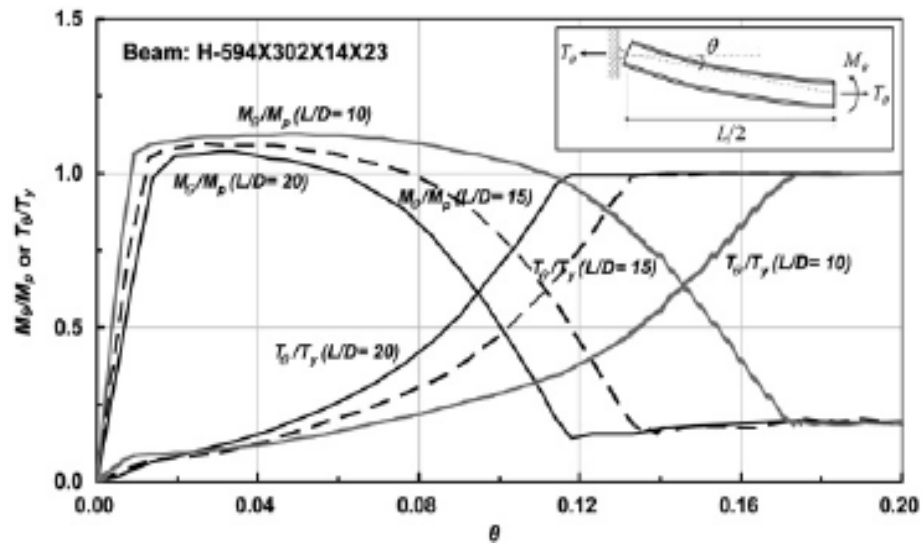


Figure 2.16. Typical moment-axial tension interaction curve (Lee et al. 2009)

This figure clearly shows the ability of a steel beam to utilize catenary behavior after the plastic moment has been reached, provided that the assumption of sufficient connection behavior can be achieved. The tensile force in the beam increases drastically while the internal beam moments decrease. However, large rotations are necessary to achieve substantial catenary capacity. Lee et al. (2009)

noted that “catenary action becomes dominant under very large chord rotations exceeding 0.1 radians”. Figure 2.16 also shows that this required total rotation increases with decreasing L/D ratio and becomes as high as 0.172 radians for an L/D ratio of 10, the lowest evaluated in this study. The limiting chord rotation is defined “as the rotation at the instant when the beam yields fully in tension” (Lee et al. 2009). Figure 2.16 shows significant catenary forces are developed in the beams prior to the limiting chord rotation being reached.

Another graph, shown in Figure 2.17, was constructed with the applied vertical load normalized with respect to the vertical load needed to create a plastic mechanism, P_p . Various beam sizes and span-to-depth ratios were analyzed. This figure depicts the potential load-carrying capacity of steel beams utilizing catenary action. If the beams are able to undergo large chord rotations, catenary action can potentially increase the capacity of a steel beam by as much as 500% for the parametric combinations investigated in the work of Lee et al. (2009). However, it is noted that the slope of the graphs in Figure 2.17 is fairly low once P/P_p first exceeds one, suggesting that for moderate amounts of total rotation permitted by typical connections, between 0.03 and 0.05 radians, the benefit resulting from catenary behavior is much more modest, being less than 20%. Their studies also indicated that the span-to-depth ratio of steel beams greatly affects the initiation and magnitude of catenary behavior. While this will not be investigated in this thesis, it is important to note that larger span-to-depth ratios lead to a greater post-flexural capacity.

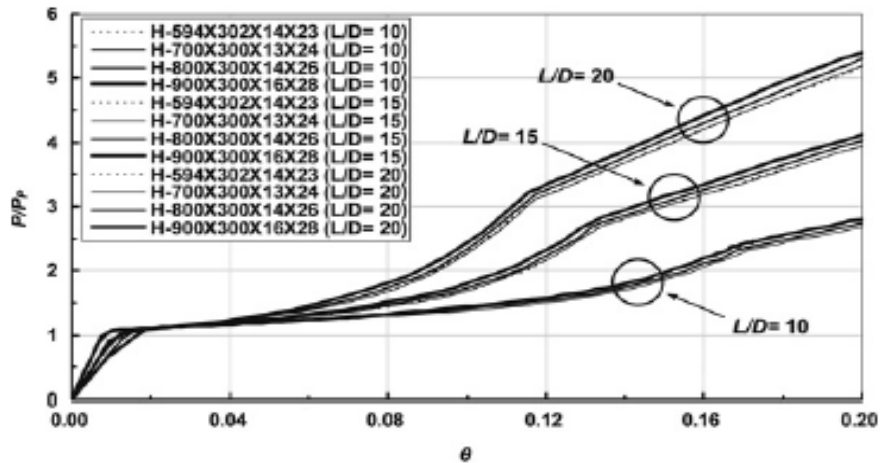


Figure 2.17. Normalized axial load vs. chord rotation (Lee et al. 2009)

Kim and An (2008) studied the “progressive collapse potential of steel moment frames designed per current design codes with and without considering catenary action”. They utilized a nonlinear analysis to investigate the potential for progressive collapse in structures. The behavior of structural members in a progressive collapse event is nonlinear; thereby making a nonlinear analysis a more accurate method than linear analysis. Kim and An (2009) analyzed a structure with a removed column and included geometric and material nonlinearity in their models. The cross-sections of both flanges and the web of the beam were divided into 50 fiber elements with each member modeled using four ‘nonlinearBeamColumn’ elements in the longitudinal direction. Two types of models were used for analysis using the program OpenSees, developed by the University of California at Berkeley (Mazzoni et al. 2006). The first considered an H 450x200x9x14 (W18x50) loaded with a concentrated load applied at mid-span, as shown in Figure 2.18. The modeled beams were fixed at both ends to resist moment. The second analysis type studied the effects of catenary behavior on

steel moment frames of varying number of bays and stories. Also, the effects of braced frames vs. no braced frames were examined. The structural members were designed “in accordance with the AISC Load Resistance Factor Design (2000)” (Kim and An 2009). Figure 2.19 shows the types of moment frames, with and without lateral bracing, used in the analysis.

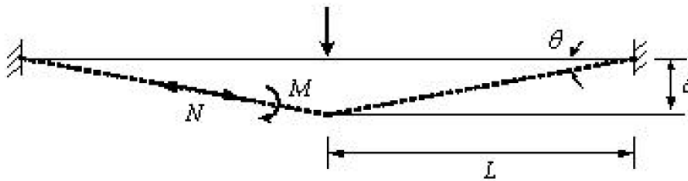


Figure 2.18. Sub-assembly structure of two beams deformed after removal of column (Kim and An 2009)

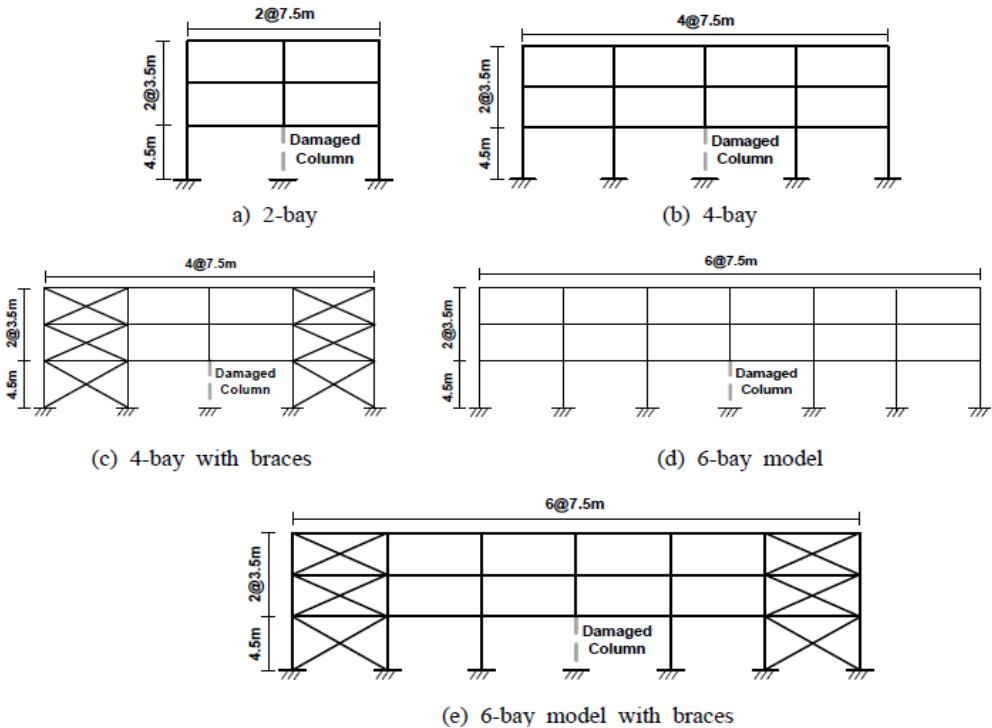


Figure 2.19. Types of buildings modeled and analyzed (Kim and An 2009)

Push-down analyses were conducted for both types of models to investigate the effects of catenary behavior. For the single member sub-assembly model, the push-down analysis consists of applying a concentrated load at mid-span of the beam. For the frame models, the “vertical displacement of the beam-column joint in which the lower story column is removed is gradually increased” (Kim and An 2009). Two cases, one with catenary action and one without catenary action, were analyzed in the study. For both cases, the cross-section of the flanges and web were divided into 50 fiber elements using non-linear beam column elements. In addition, “for the modeling of beam elements without considering catenary action (‘no-catenary action’ cases) the ‘linear’ geometric transformation option is used, whereas the ‘corotational’ geometric transformation is selected for beams analyzed considering catenary action.” (Kim and An 2009). This appeared to be the only difference between analysis of beams considering catenary action and not considering catenary action. The reason for this difference is unclear. The results utilizing catenary action are of interest to the present discussion, while the results neglecting catenary action are viewed with some skepticism since infinite member strength resulted from those analyses. In both cases, the post-yield stiffness of the beams was assumed to be 2% of the initial stiffness, and the model ‘ReinforcingSteel’, shown in Figure 2.20, was used to model the beams (Kim and An 2009). These nonlinear push-down analyses used the load combination set forth in the GSA guidelines, $2*(DL + .25*LL)$.

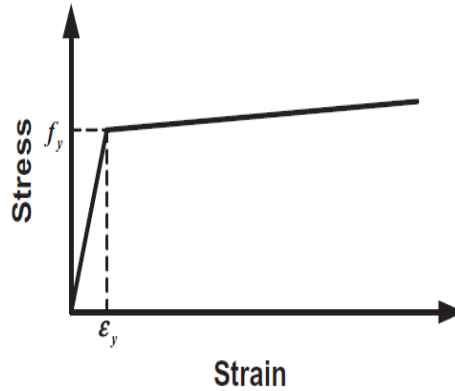


Figure 2.20. Material model for beam analysis (Kim and An 2009)

Results were represented with several graphs plotting moment, axial tensile force, and load factor vs. rotation. The rotation was calculated using the following equation, where the variables are defined in Figure 2.18 (Kim and An 2009):

$$\tan^{-1} = \delta/L \quad (\text{Equation 2.2})$$

The variable ‘L’ represents the single-span length of one of the beams. The moments were normalized using the plastic moment, while the axial tensile force was normalized with the tensile force causing yielding. The axis representing load factor measures the applied load divided by the GSA specified load. It is uncertain if the beams were sized to meet the GSA specified load. However, it appears that they may not have been designed to meet the GSA code which explains why beam yielding occurs at a load factor less than 1. Another possibility for explaining why yielding occurs at this level of load relates to the lateral bracing, as discussed below.

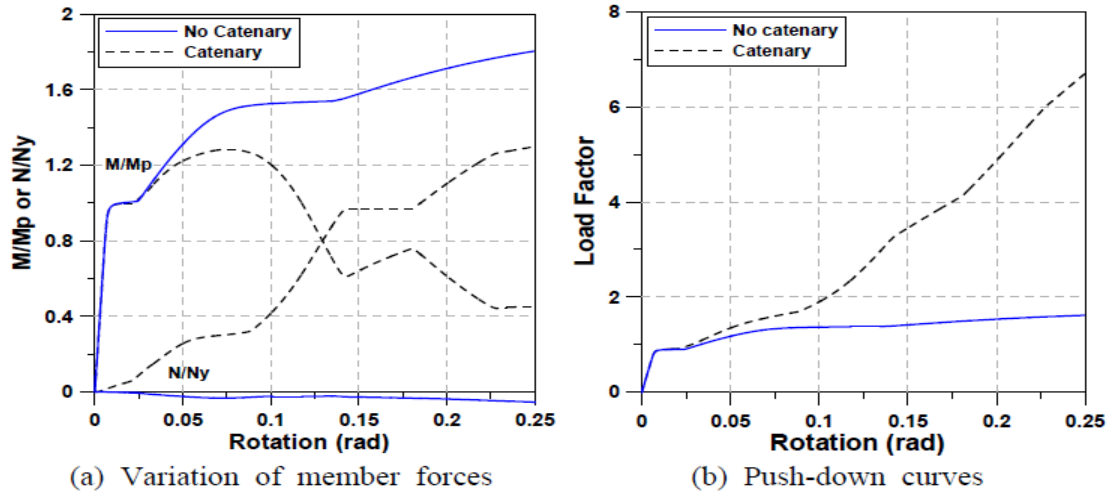


Figure 2.21. Push-down analysis results of the sub-assembly model (Kim and An 2009)

Figure 2.21 shows the results of the push-down analysis for the beam sub-assembly. It is observed from Figure 2.21 that the beams do not achieve their code-prescribed capacities at the end of the initial yield plateau, suggesting there may be some error in these results. Since there is no mention of lateral bracing of the beams, this could explain the reduced capacities. The graphs show that, as expected, when catenary action is assumed, the tensile force in the beam increases as the rotation angle increases. Catenary behavior of the beam drastically increases as the flexural capacity of the beam begins to decrease. At total rotations of about 0.05 radians, a rotation possible to achieve with existing connections, the load factor is approximately 1.2, a significant increase despite the beam only resisting approximately 25% of its tensile yield strength. However, the load factor when the member reaches its tensile yield strength is approximately 3 and the corresponding total rotation is 0.15. These results should be applied cautiously given that connection failure is not considered in the

analyses. The utilization of catenary action is shown to greatly increase the overall load-carrying capacity of the beam relative to code requirements.

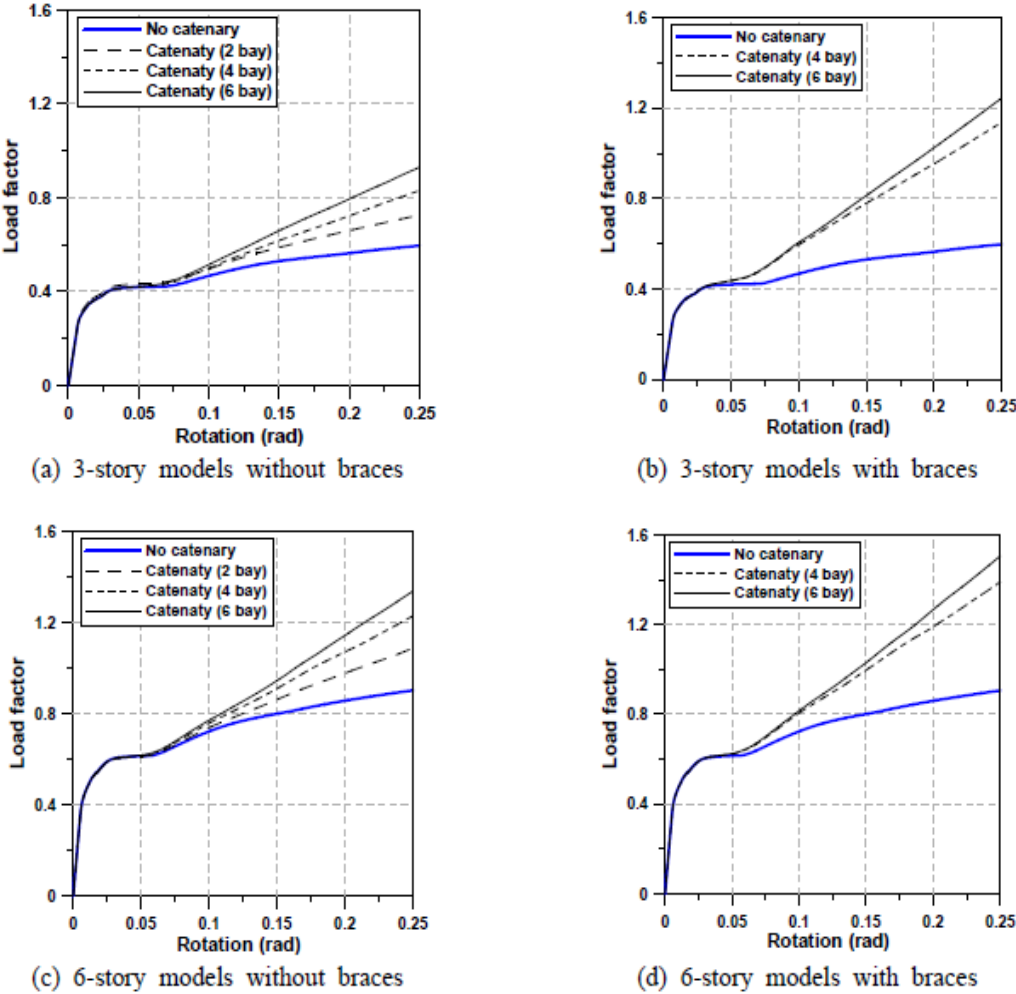


Figure 2.22. Load factor vs. rotation for moment frames (Kim and An 2009)

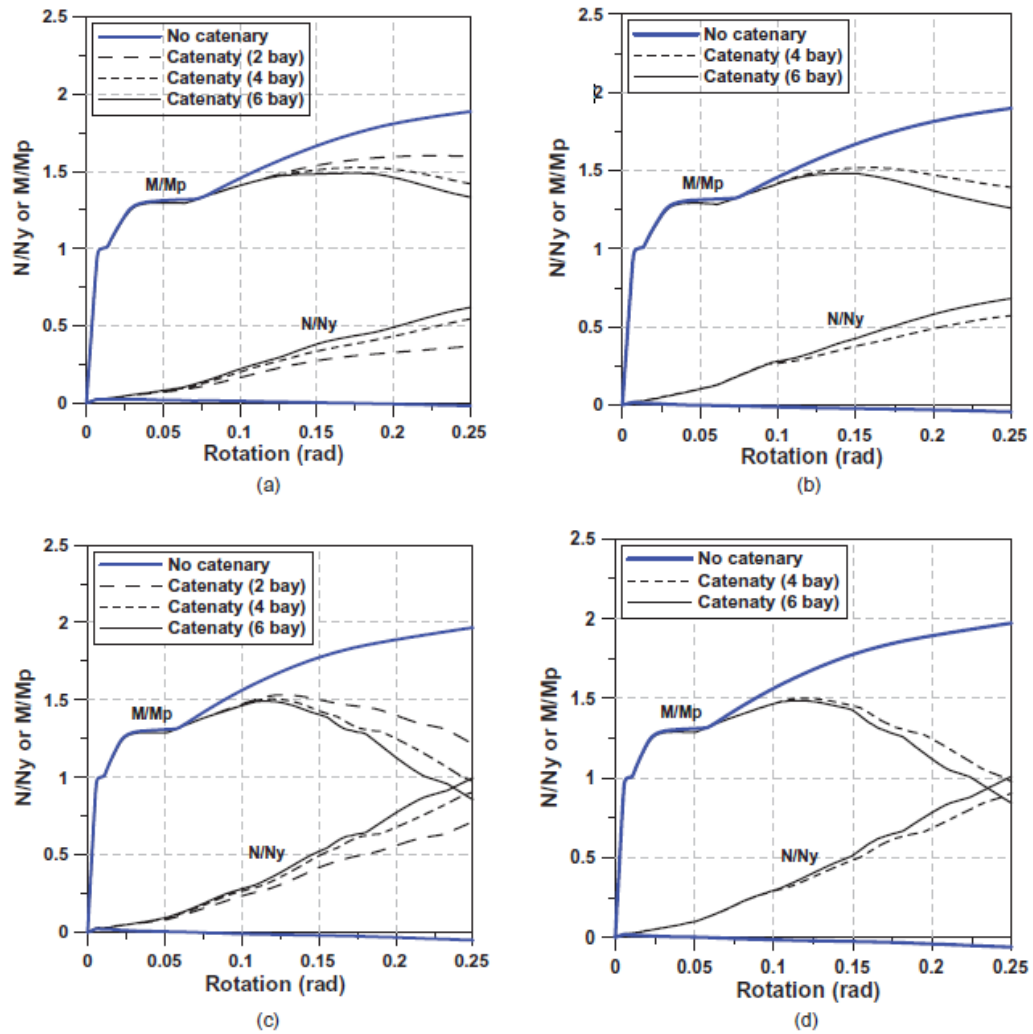


Figure 7. Variation of axial force and bending moment of model structures obtained from push-down analysis. (a) Three-story models without braces. (b) Three-story models with braces. (c) Six-story models without braces. (d) Six-story models with braces

Figure 2.23. Normalized forces vs. rotation for moment frames (Kim and An 2009)

Figures 2.22 and Figure 2.23 show the results of the push-down analysis for the various steel moment frames. As with the beam sub-assembly model, the load-carrying capacities of the frames are shown to greatly increase as rotation increases. Whether this can be attributed to catenary behavior in the analyses is uncertain given

that there is a constant slope to the load factor versus rotation curves for total rotations larger than 0.07 radians despite whether the moment resistance is increasing or decreasing. Kim and An (2009) noted that as “the number of bay and story increase the axial force in the beams increases, which implies that a large axial force or catenary action is induced when there exists a strong restraint at both sides of the structure against deformation towards the centre of the structure”. Most likely for the same reason, the laterally-braced frames have greater capacities when considering catenary action than the corresponding unbraced frames. Beam rotation capacity versus catenary behavior is a central focus in this thesis. The results of Kim and An (2009) indicate that, with proper lateral stiffness in a structure, total beam rotations greater than 0.075 radians result in large catenary forces as well as noticeable increases in the strength of a structure in a progressive collapse event. For a six-story building, the beam axial force is approximately 25% of its yield strength at a total rotation of 0.075 radians. The axial, or catenary force, in the beam increases to 100% of its yield strength at a rotation of about 0.25 radians.

Khandelwal and El-Tawil (2007) studied “key design variables that influence formation of catenary action in special moment resisting frame subassemblages”. For this to occur, large plastic deformations must develop in the beam which will then be able to resist additional loads in a “cable-like” manner. In other words, ductility in the system is necessary for the catenary forces to be developed.

Khandelwal and El-Tawil (2007) conducted an FEA on the behavior of a double-span steel frame with its middle column removed. They modeled a two-bay sub-assemblage of an eight story steel moment frame building having seismic detailing using MPP-DYNA, which is a finite element software program developed by

Livermore Software Technology Corporation. The two end columns in the sub-assembly were modeled with pinned-end connections (Fig. 2.24 and Fig. 2.25). The middle column was modeled with all movement restrained except vertical displacement, which was imposed at a rate of as 2.54 meters (8.33 feet) applied over a period of 2 seconds. The flanges of the beams were rigidly connected to the column nodes. A steel shear tab was modeled as being connected to the web of the beams. The yield stress of the steel used in the models was 345 MPa (50 ksi). To investigate the effects of a transverse gravity beam on the assembly, a W21x55 member was modeled in one configuration, and connected to the middle column with a shear connection. Figure 2.24 shows a model configuration without the transverse beam modeled, while Figure 2.25 shows the model with this member included. Reduced beam sections as well as full beam sections were modeled for the main girders, but not for the transverse bracing beam.

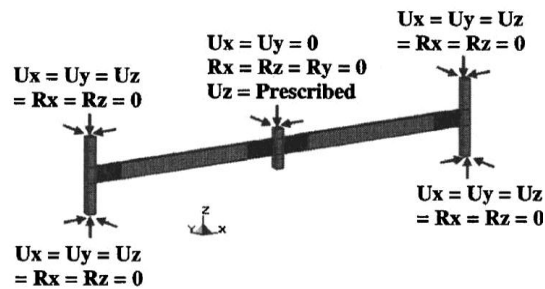


Figure 2.24. Model with missing column and no lateral beam support (Khandelwal and El-Tawil 2007)

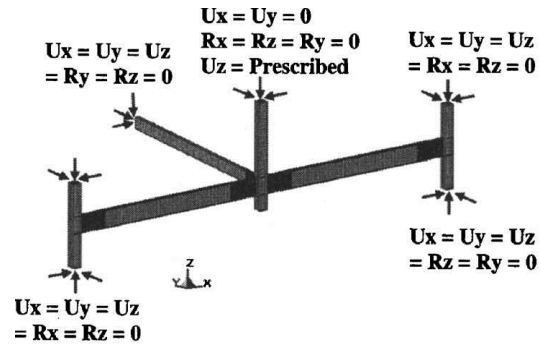


Figure 2.25. Model with missing column and lateral beam support (Khandelwal and El-Tawil 2007)

The failure load and displacement, as well as both the beam and column rotations were computed for the four beam and connection configurations, which were: Reduced beam section (RBS) with transverse bracing; reduced beam section (RBS) without transverse bracing; non-RBS with transverse bracing; and non-RBS without transverse bracing. Experimental data was utilized to obtain a realistic non-linear stress-strain behavior of the steel.

For all models, failure began as a fracture in the shear tab at the interface with the column. The crack then propagated to the beam flange causing final failure. Figure 2.26 shows several of the parameters measured during the analyses.

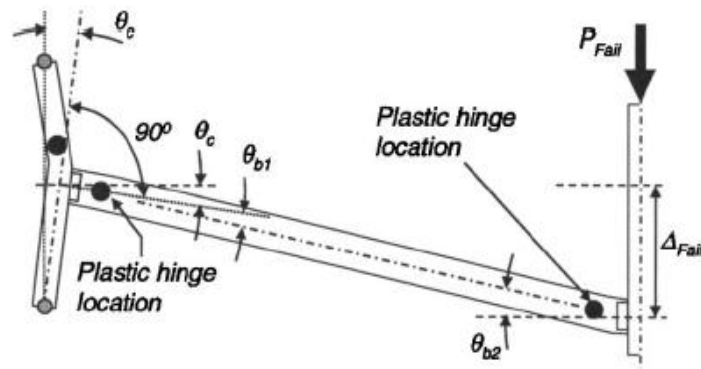


Figure 2.26. Measured parameters (Khandelwal and El-Tawil 2007)

The studies of Khandelwal and El-Tawil (2007) concluded that all sub-assembly models “deformed in a ductile manner and developed substantial catenary forces prior to failure”. The modeled first floor beams, W30x124, achieved the largest catenary forces. This summary will focus on the first floor beams, as they most closely represent the parametric studies performed in Chapter 4 of this thesis. The axial yield force for a W30x124 members with 50 ksi steel is approximately 8118 kN (1825 kips). The maximum catenary force for a W30x124 RBS beam was approximately 3400 kN (764 kips), or 42% of the axial yield force which occurred at a plastic beam end rotation of approximately 0.08 radians. The maximum catenary force for a W30x124 non-RBS beam was approximately 3500 kN (787 kips), or 43% of the axial yield force which occurred at a plastic beam end rotation of approximately 0.06 radians. This was due to the spread of inelasticity at the plastic hinges of the beams.

The failure load, P_{fail} , for a non-RBS beam with a transverse beam support was 1492 kN (335.4 kips); and the failure displacement was 0.58 meters (22.8 inches) (Khandelwal and El-Tawil 2007). Non-RBS beams were shown to be able to reach

total plastic rotations prior to failure, Θ_{b1} and Θ_{b2} , of 0.049 radians and 0.055 radians, respectively. The failure load, P_{fail} , for an RBS beam with transverse beam support was 1645 kN (369.8 kips); and the failure displacement was 0.76 meters (29.9 inches) (Khandelwal and El-Tawil 2007). RBS beams were shown to be able to reach total plastic rotations prior to failure, Θ_{b1} and Θ_{b2} , of 0.072 radians and 0.078 radians, respectively. These large inelastic beam rotations correlate to large deflections in the beam and are necessary to initiate catenary action. Figure 2.27 and Figure 2.28 plot the catenary forces developed in non-RBS and RBS beams versus the maximum beam deflection.

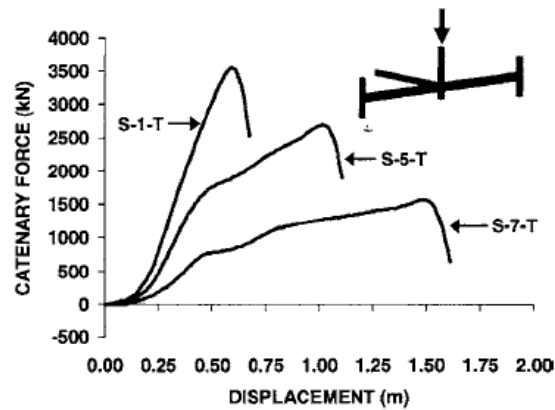


Figure 2.27. Beam catenary forces vs. displacement for non-RBS beams (figure from Khandelwal and El-Tawil 2007)

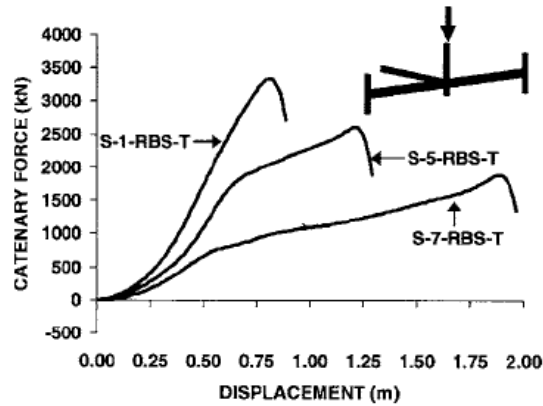


Figure 2.28. Beam catenary forces vs. displacement for RBS beams (figure from Khandelwal and El-Tawil 2007)

The numbers in the curve designations represent the floor location of the analyzed beam. As previously stated, only the results of the first floor models were investigated due to their similarity with the parametric studies presented in this thesis. Both figures above are for models with transverse beams modeled. However, Khandelwal and El-Tawil (2007) noted in their paper that the presence of a transverse beam had no significant effect on the model when compared to a model with no transverse beam, which is not surprising considering the boundary conditions used in these models mimic the effects of a transverse beam.

The models presented in this thesis were all of the non-RBS type. As shown by the analyses performed by Khandelwal and El-Tawil (2007), non-RBS steel beams have the ductility to achieve large inelastic rotations. These rotations allow for large catenary forces to be developed in the beam, which can help arrest progressive collapse in the event of a missing column.

Liu and Mei (2012) used finite element models (FEM) to investigate the behavior of a steel-framed structure under a column removal scenario. The

researchers used the program, ANSYS, to construct a “ten-story planar steel frame structure” designed according to Chinese seismic design code. They used beam-column elements which had the ability to model nonlinear structural behavior. Liu and Mei (2012) analyzed the structure for the cases of a middle column removal as well as an end column removal. Only the results of the middle column removal will be discussed here, since end column removal was not investigated in this thesis. However, the results for an end column removal showed about 86% less axial catenary force developed in the beam compared with a middle column removal. Figure 2.29 details the steel frame used in the analysis and Figure 2.30 shows the location of the column removal.

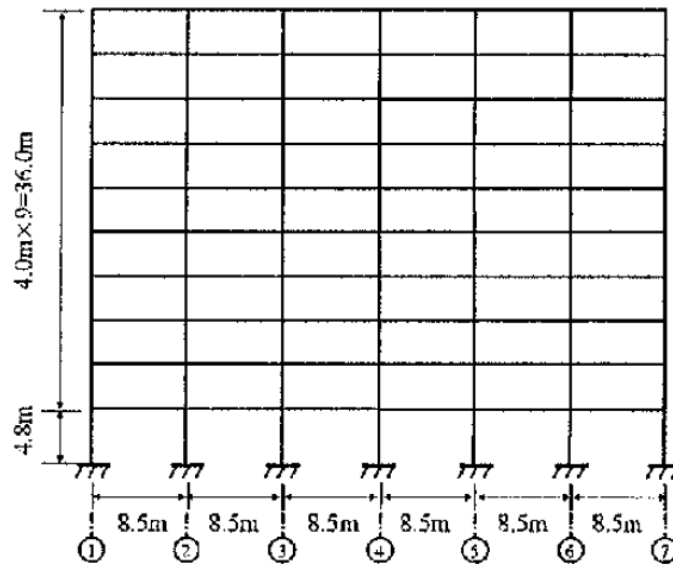


Figure 2.29. Steel frame used for FEM analysis (figure from Liu and Mei 2012)

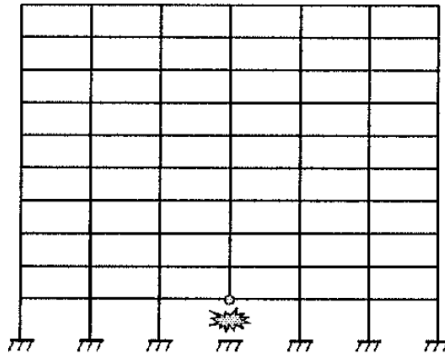


Figure 2.30. Location of column removal for FEM analysis (figure from Liu and Mei 2012)

Liu and Mei (2012) subjected the frame to a push-down analysis at the location of the missing column. “During the push-down analysis, gravity load is increased proportionally in the damaged bays, whereas the remaining part of the structure is subjected to nominal gravity loads” (Liu and Mei 2012). The nominal gravity load was given by the following equation (Liu and Mei 2012):

$$P_o = 1.0P_D + 0.25P_L \quad (\text{Equation 2.3})$$

P_D and P_L represent the dead and live loads respectively. The overload capacity of the steel structure is given by the following equation (Liu and Mei 2012):

$$P_{fac} = P_{actual} / P_o \quad (\text{Equation 2.4})$$

P_{actual} represents the load being resisted by the structure at a given displacement.

Liu and Mei (2012) plotted the vertical displacement, at the location of column removal, against the overload factor, P_{fac} , in Figure 2.31. The researchers also plotted both bending moment and axial tension in the beam versus vertical displacement in Figure 2.32. In Figure 2.31, ‘DoD2005’ represents the location of the graph where the rotation reaches the limit given in UFC-04-023-03. The term ‘Geometric unstable

system' represents the location where the authors assume catenary action becomes the dominant resistance mechanism.

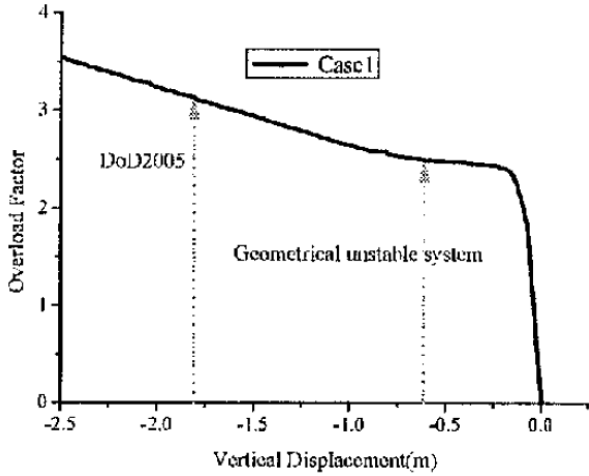


Figure 2.31. Overload factor versus vertical displacement (figure from Liu and Mei 2012)

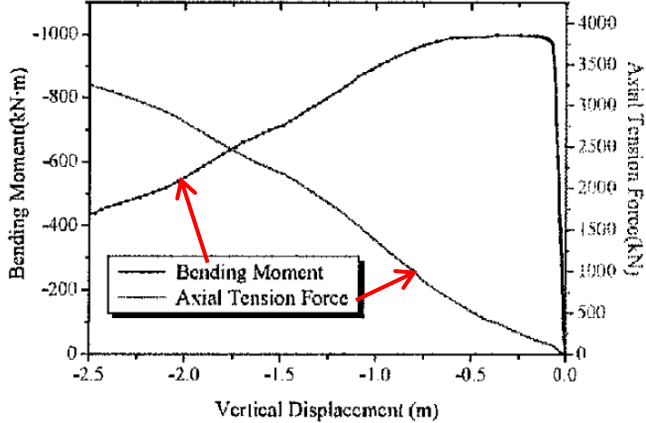


Figure 2.32. Bending moment and axial tension in beam versus vertical displacement (adapted from Liu and Mei 2012)

From the results of Liu and Mei (2012), it is shown that steel beams are able to undergo large displacement in a column removal scenario. The beam was also able to take more than three times the design load of the structure when a middle column was removed. Much of this additional capacity is shown to be due to the increase in axial tensile forces, catenary forces, in the beam under large displacements (Fig. 2.32).

Sadek et al. (2011) performed an experimental test and accompanying FEM analysis of an intermediate moment frame (IMF) assembly consisting of three W18x119 columns and two W21x73 beams. The two beams were connected to a column stub representing a removed column. The beam flanges were welded to the column flange with complete joint penetration welds and a shear tab was welded to the column and bolted to the beam. A monotonically increasing vertical displacement was applied to the column stub to simulate a missing column scenario (Sadek et al. 2011).

Figure 2.33 shows the test setup.

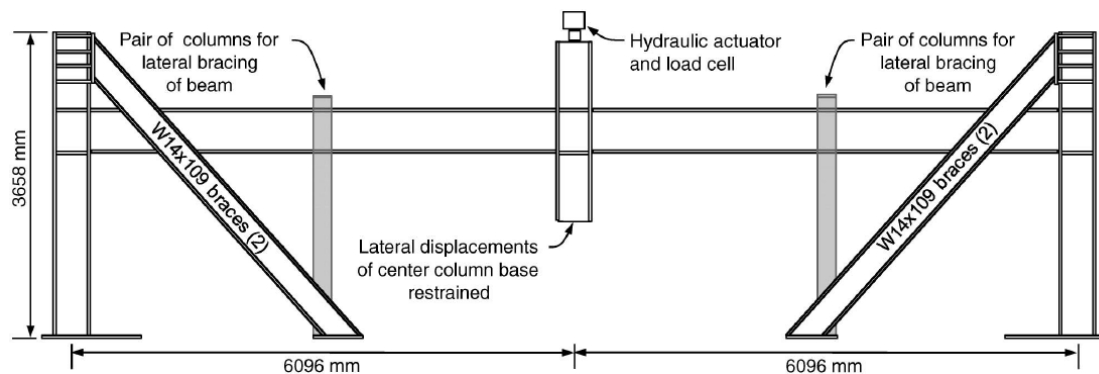


Figure 2.33. Test setup (figure from Sadek et al. 2011)

In the experimental test, the connection reached failure at a load of 890 kN (200 kip) and a vertical deflection at the missing column of 495 mm (19.5 inches) (Sadek et al. 2011). Failure occurred due to flange buckling and shearing of the bolts in the beam web at the center column. Sadek et al. (2011) built two FE models, using the program LS-DYNA, to compare to the results of the experimental test. One model, ‘detailed model’, was constructed of 300,000 “finely meshed solid elements representing the beams, columns, continuity plates, shear tabs, bolts and welds in the vicinity of the connection” and shell elements away from the connection (Sadek et al. 2011). The other model, ‘reduced model’, used beam elements with cross-section integration and a piecewise-linear plasticity model based on coupon test data (Sadek et al. 2011). For the ‘reduced model’, two cases considering pinned and fixed column bases were analyzed.

Figure 2.34 and Figure 2.35 plot the vertical load and beam axial force versus the vertical displacement of the middle column respectively. The experimental and FE data were plotted on the same graphs and show extremely good correlation between behavior of the beam. This shows the validity of both detailed and reduced models in accurately predicting experimental data. The initial negative values in Figure 2.35 indicate that “the behavior of the assembly was primarily flexural, with compressive axial forces in the beams” (Sadek et al. 2011). The drastic decrease in vertical load shown in both graphs occurs at the instant of failure in the specimen.

Sadek et al. (2011) noted that, “the assembly remained in the elastic range up to a vertical displacement of approximately 50 mm.” The researchers also noted that, “with increased vertical displacement of the center column, the response of the assembly was dominated by catenary action, as indicated by the development of axial

tension in the beams” (Sadek et al. 2011). The above show a maximum beam axial force of 667 kN (150 kips) achieved at a total rotation of approximately 0.082 radians, based on measuring the rotation at a reference point at the center of the column. The axial yield force of the analyzed beams is approximately 4782 kN (1075 kips). Therefore, the analyzed beams achieved about 14% of their maximum axial force.

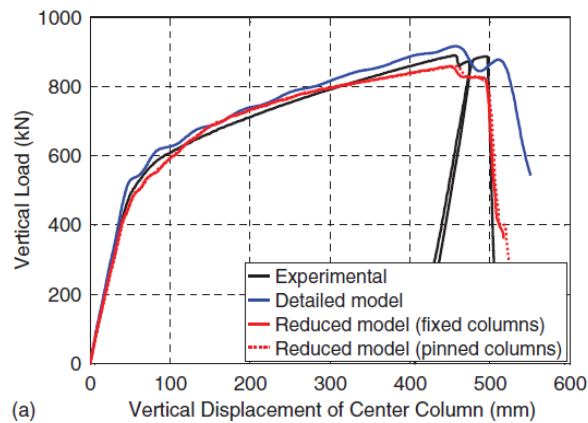


Figure 2.34. Vertical load vs. center column displacement (figure from Sadek et al. 2011)

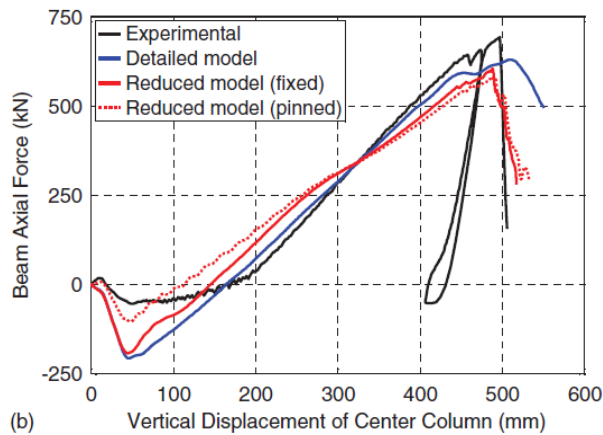


Figure 2.35. Beam axial force vs. center column displacement (figure from Sadek et al. 2011)

The results of the experimental and numerical data presented in this section all point to the same conclusion. The data reviewed in this section reveal two important pieces of information: steel beams have adequate ductility and strength to engage catenary behavior; and the axial tension forces and large rotations developed during catenary behavior require adequate connection performance. The following section will detail research into connection performance during progressive collapse events.

2.6 Connection Performance during Progressive Collapse Events

Prior to the 1994 Northridge earthquake, welded-flange-bolted-web (WUF-B) connections were predominantly used in seismic design of steel-framed structures (Roeder 2002). During the Northridge earthquake, many of these connections failed due to cracking that was initiated at the beam flange welds which propagated into the beam and column, resulting in considerable economic damage (Roeder 2002). These types of “pre-Northridge” connections failed due to their inability to accommodate large beam rotations during an extreme loading event. After these events, engineers began researching different connection types to better resist seismic loads. Both seismic and progressive collapse events induce larger-than-normal forces on a structure and require member ductility. Because of these similarities, research into connection performance in seismic events correlates well with progressive collapse events. Thus, several of the studies reviewed below involve cyclic loading of connections. While there may be differences in connection performance between this loading scenario and a missing column situation, these tests serve as an important basis for speculating on connection performance under a missing column scenario.

Much research has been conducted on the performance of both welded and bolted-type moment connections. The failure mechanisms and rotation capacity for

these types of connections vary. As was shown earlier in this chapter, large rotations are necessary in order to fully utilize catenary behavior in a steel beam. This section details the research into some of the moment-resisting connections that can be used in progressive collapse design. The scope is limited to moment-resisting connections because of their more-frequent use in progressive collapse designs as a result of their greater load-carrying capacity.

2.6.1 Research into Performance of Non-Proprietary Steel Connections

Roeder (2002) noted that welded flange-type connections tend to fail due to weld fracture at the beam flange-column interface, which can lead to column web crippling and unreliable inelastic deformation capacity. Bolted-flange-plate connections tend to yield due to tension in the gross area of the flange-plate with significant plastic rotation occurring due to bolt hole elongation. Thus, reviewing the performance of various bolted connections is of greatest interest to the present study.

The sudden removal of a column in a potential progressive collapse scenario results in rapid rates of loading to the members and connections in the vicinity of the removed or damaged column. Munoz-Garcia et al. (2005) analyzed several configurations of both flexible endplate and web cleat connections using the dynamic FE software, LS-DYNA. Figure 2.36 shows the parameters measured and the geometry of the different connection types.

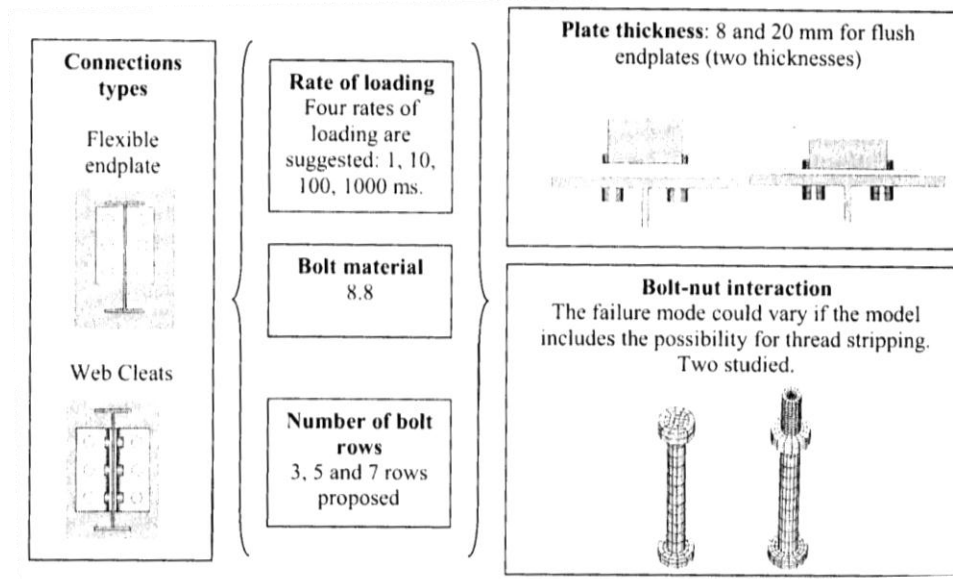


Figure 2.36. Connection geometry and measured parameters (figure from Munoz-Garcia et al. 2005)

An axial tensile force was applied to a steel beam stub which framed into a steel column connected by the specific connection type being analyzed. A monotonically increasing tensile load was applied over a specified time period: 1 millisecond (ms); 10 ms; 100 ms; and 1000 ms for each of the connection types. The endplate connections were shown to reach brittle failure by fracture of the net section at the bolts. The failure load decreased as the rate of loading increased (Munoz-Garcia et al. 2005). This is graphically shown in Figure 2.37, which details the results for a partial endplate connection with 7 rows of bolts in which the bolts were not subject to the effects of thread stripping. The size of this plate was not explicitly stated in the article. The results are compared with the statically applied load which causes failure of the connection.

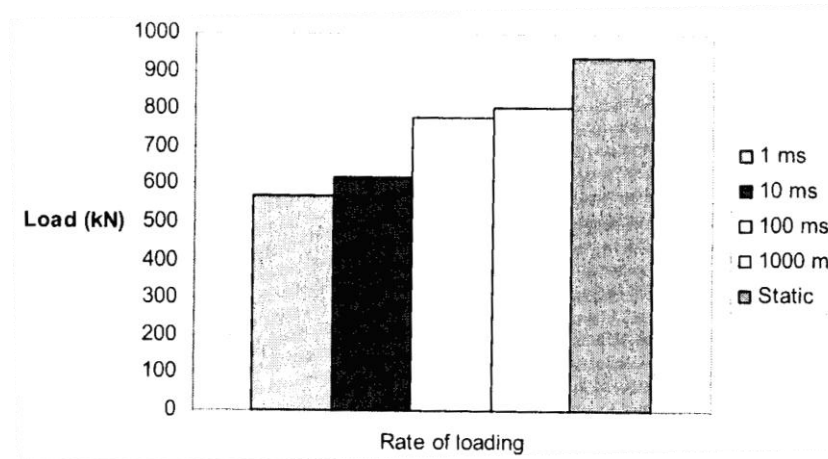


Figure 2.37. Rate of loading vs. strength (figure from Munoz-Garcia et al. 2005)

While the failure load for all dynamically loaded models is lower than the failure load from a static analysis, the results show that for lower rates of loading static connection strength can nearly be achieved. The response of the web cleat connections was found to have “higher deformation capabilities which increases the energy that can be absorbed” (Munoz-Garcia et al. 2005). These results show that for the high rate of loading expected in a column loss event, particular attention must be paid to connection detailing to achieve full strength. Specifically, Munoz-Garcia et al. (2005) noted that “greater attention has to be paid to the [heat-affected zone] in partial endplates, since the reduction in ductility present in this zone appears to be important”. These tests showed that for partial endplate connections, ultimate strength as a percentage of the static strength of the connection ranged from approximately 61.5% for a loading time of 1 ms to 87.9% for a loading time of 1000 ms.

Kim and Kim (2009) analyzed the behavior of three types of moment connections under a column removal scenario. The connections studied were: welded

cover plated flange (WCPF); welded reduced beam section (RBS); and welded unreinforced flange-welded web (WUF-W). The flanges of all three connection types were welded to the column. Two models, 3-story and 6-story, were analyzed with both having four bays. Each structure was designed for two seismic conditions, moderate and high, which led to different member sizes. The models were analyzed for a single removed column in the lowest story of the structure using the nonlinear analysis program code 'OpenSees' (Kim and Kim 2009). The column panel zones were modeled as rigid elements and the post-yield stiffness of the beams and columns was assumed to be 2% of the initial stiffness. The beams and columns were modeled using 'nonlinearBeamColumn' elements, which considered material plasticity and second-order effects (Kim and Kim 2009). "Limit state criteria for beam and column members and panel zone were not defined in the analysis" (Kim and Kim 2009).

The non-linear dynamic analyses were carried out by instantaneously removing a specific column from the model once it had reached static equilibrium (Kim and Kim 2009). Results of the analyses were compared to the specified loading condition as dictated by General Services Administration (GSA) publication, *Progressive Collapse Analysis and Design Guidelines* for nonlinear dynamic analysis (GSA 2003). This loading is: $DL+.25LL$. Figure 2.38 and Figure 2.39 summarize the results of the analyses for a 3-story structure in a moderate seismic region. All connection types allowed plastic hinges to develop in the beam and were therefore able to resist the plastic moment of the beam (Kim and Kim 2009). The graphs compare both vertical displacement at the location of the removed column as well as plastic hinge rotation versus elapsed time (Kim and Kim 2009). The results show that the RBS connection was able to undergo much larger vertical displacements (95 cm) as well as plastic

rotations (0.07 radians) than the other connections. Kim and Kim (2009) stated that, for these analyses, “In the RBS connections the plastic hinges generally formed at the reduced sections” indicating that these connections had sufficient capacity to resist the beam plastic moments. Both WUF-W and WCPF connections underwent vertical displacements of around 15 cm and plastic rotations of approximately 0.015 radians. However, these results do show that certain steel moment connections are able to sustain large vertical displacements as well as plastic rotations.

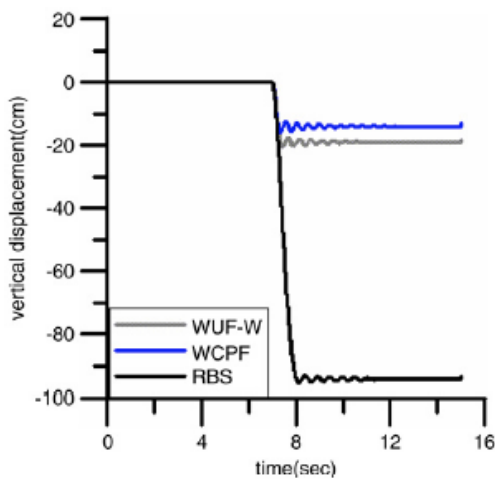


Figure 2.38. Vertical displacement vs. elapsed time for 3-story model in moderate seismic region (figure from Kim and Kim 2009)

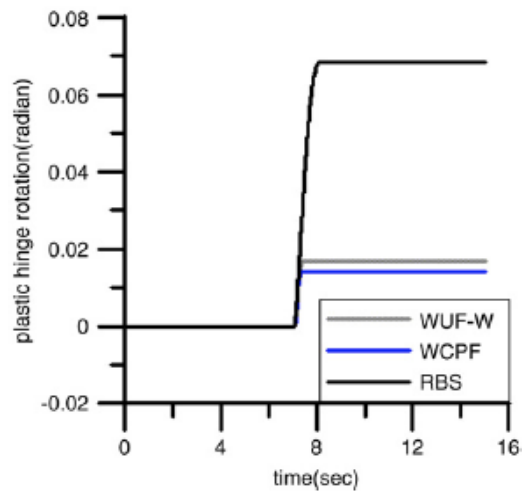


Figure 2.39. Plastic hinge rotation vs. elapsed time for 3-story model in moderate seismic region (figure from Kim and Kim 2009)

Popov and Tsai (1989) conducted several full-scale tests of connection rotation vs. load for various rolled steel shapes and moment connections. These tests compared bolted connections with welded connections. These tests were performed under cyclic loading, and Figure 2.40 details the results of these experiments.

Figure 2.40a represents a connection with both flanges and the web welded to the column. Figure 2.40b represents a reduced beam section connection with both flanges and the web welded to the column; a reduced beam connection works by reducing the width of the top and bottom flanges of the beam near the column that it is being connected. Figure 2.40c represents a fully bolted T-stub connection. The results show that the fully bolted T-stub connection achieves the greatest plastic rotation, 0.06 radians in this situation.

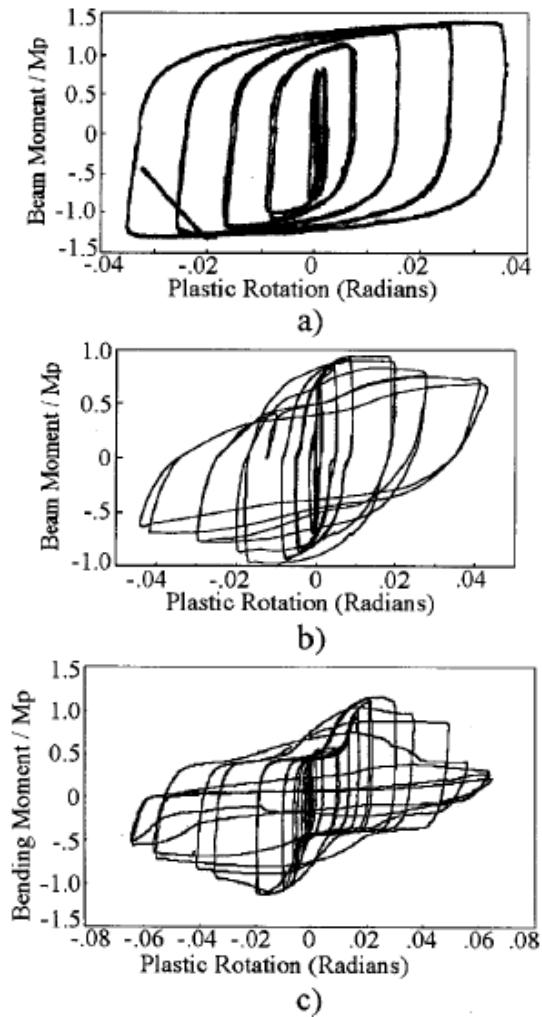


Figure 2.40. Beam rotation vs. cyclic loading for: (a) flanges and web welded to column; (b) RBS with both flanges and web welded to column; (c) bolted T-stub (figures from Popov and Tsai 1989)

Schneider and Teeraparbong (2002) conducted eight full scale experiments on bolted flange plate connections with varying geometries. The flanges of the steel beams were bolted to a cover plate which was then welded with a full-penetration weld to the column flange. The connections they investigated were designed to induce

either inelastic behavior in the flange plates or in the girder beyond the connection location. These modes of behavior are very ductile and therefore desirable when designing for events that require large amounts of energy dissipation. All connections were of similar geometry with varying girder and column sizes as well as number and size of bolts. Figure 2.41 shows the different connection types and their parameters in tabular form. Figure 2.42 graphically details the basic geometry for all connection types analyzed by Schneider and Teeraparb Wong.

The connection-beam-column configuration was tested using two 500 Newton (112 kip) hydraulic actuators that imposed predetermined cyclic deformations on the specimen. Figure 2.43 details the apparatus used to test the connection specimens.

| Specimen | Structural shapes | | Flange plate | | Comments |
|----------|-------------------|-------------------|--------------|---------------|--|
| | Girder | Column | Material | Bolts | |
| BFP 01 | <i>W</i> 24 × 68 | <i>W</i> 14 × 120 | A572 | Slip critical | Minimum strength design. Oversized bolt holes. |
| BFP 02 | <i>W</i> 24 × 68 | <i>W</i> 14 × 120 | A36 | Bearing | Minimum strength design. |
| BFP 03 | <i>W</i> 30 × 99 | <i>W</i> 14 × 211 | A36 | Bearing | Girder hinge. |
| BFP 04 | <i>W</i> 24 × 68 | <i>W</i> 14 × 120 | A36 | Bearing | Balanced failure mode. Extended flange plate to enhance ductility. |
| BFP 05 | <i>W</i> 30 × 99 | <i>W</i> 14 × 211 | A36 | Bearing | Similar to BFP 03. Oversized bolt holes in flange plate. 254 mm (1 in.) thick clamp plates. |
| BFP 06 | <i>W</i> 24 × 68 | <i>W</i> 14 × 145 | A36 | Bearing | Similar to BFP 04. Oversized holes in girder flange and flange plate. 254 mm (1 in.) thick clamp plates. |
| BFP 07 | <i>W</i> 24 × 68 | <i>W</i> 14 × 145 | A36 | Bearing | Similar to BFP 02. 15.9 mm (1/16 in.) ϕ bolt holes. |
| BFP 08 | <i>W</i> 24 × 68 | <i>W</i> 14 × 120 | A36 | Bearing | Reduced flange plate width. |

Figure 2.41. Parameters of test connections (adapted from Schneider and Teeraparb Wong 2002)

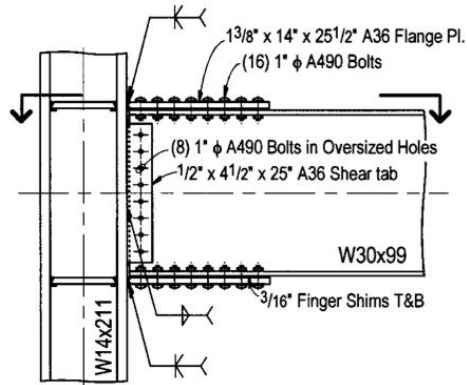


Figure 2.42. Example connection geometry (figure from Schneider and Teeraparbong 2002)

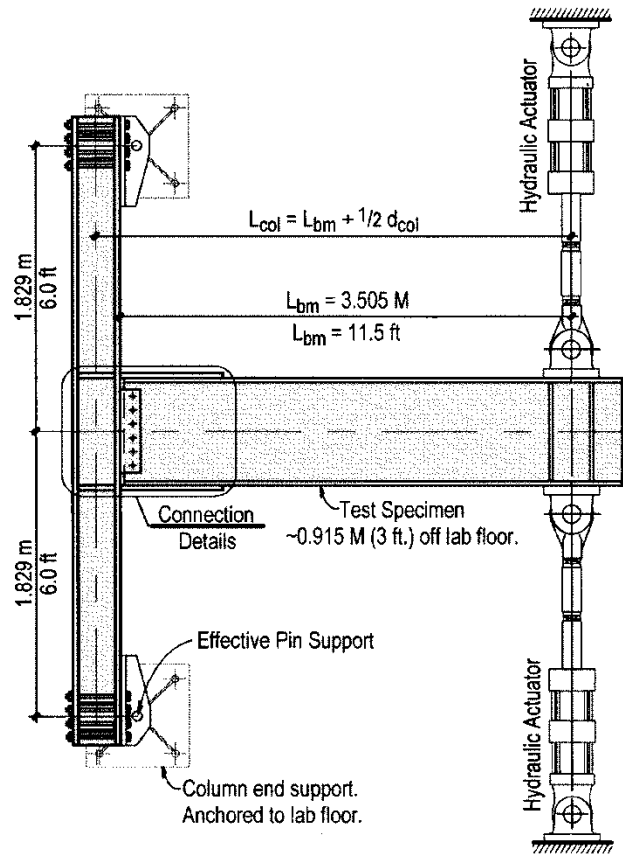


Figure 2.43. Testing apparatus (figure from Schneider and Teeraparbong 2002)

Figure 2.44 shows the normalized moment vs. plastic rotation plots for the tested connection geometries. The observed moment is normalized relative to the plastic moment capacity of the tested girder.

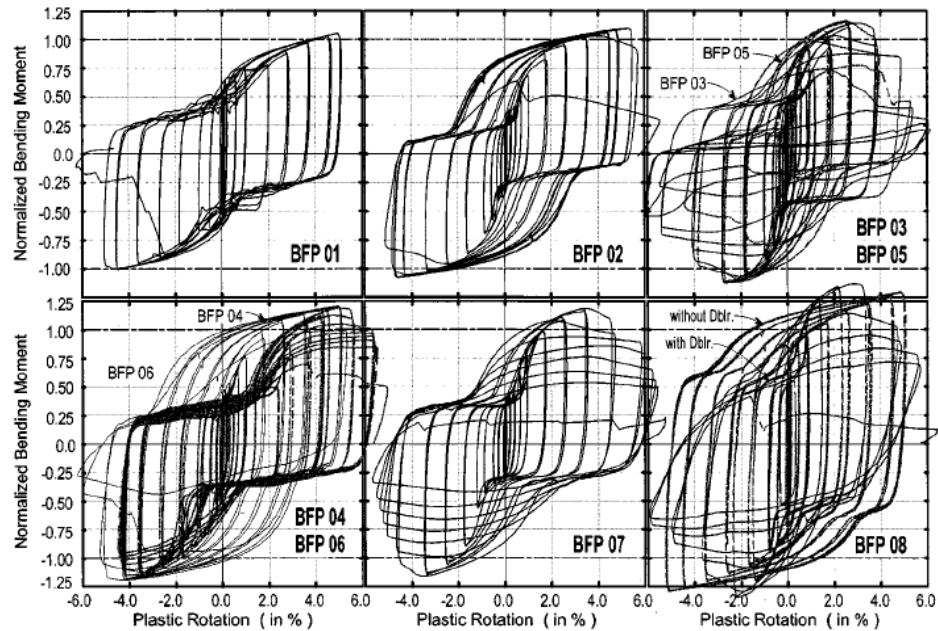


Figure 2.44. Moment vs. plastic rotation hysteretic graph (figures from Schneider and Teeraparbong 2002)

Schneider and Teeraparbong (2002) concluded these bolted flange plate type connections demonstrate large amounts of ductility, with all connection configurations reaching at least 0.035 radians of plastic rotation at high levels of moment. A maximum plastic rotation of 0.062 radians was observed for specimen BFP 06. The results of the experiment also showed that all specimens were able to resist moments equal to or greater than their calculated plastic moments. Bolt slip, flange plate

yielding, girder yielding, and panel zone yielding all contributed to the overall ductility of the system. This type of connection behavior is greatly preferred in design over the brittle failure modes displayed in welded beam flange-to-column flange connections. The experimental data collected by Schneider and Teeraparbong (2002) definitively concluded that bolted moment connections are able to develop the full plastic moment of a given beam along with accommodating large plastic rotations. They concluded that “girder hinging produced significant inelastic behavior for these connections” and “these full-scale tests demonstrated that BFP connections have significant ductility to sustain large inelastic deformation” (Schneider and Teeraparbong 2002). These characteristics are essential in initiating catenary action in frames.

Nader and Astaneh-Asl (1989) conducted shake-table tests on eight moment frames consisting of top and bottom angle connections and a double-angle shear connection. The experiments revealed that the connection was able to achieve total rotations between 0.005 radians and 0.04 radians. They concluded that the moment capacity of the connection was higher than expected and that “the catenary forces that were developed in the seated connections could double the expected plastic moment of such connections” (Nader and Astaneh-Asl 1989).

Bolted T-Stub connections are able to develop the full plastic capacity of a beam, which is necessary when designing for catenary behavior to mitigate progressive collapse (FEMA-355D 5-35). Figure 2.45 depicts the primary yield mechanisms in a bolted T-stub moment connection. When the yield mechanism of the connection is shear yielding of the bolts connecting the beam flange to the T-stub stem, bolted T-stub connections have very small inelastic rotations. However, when

the yield mechanism occurs due to flexural yielding of the T-stub flanges, inelastic rotation capacity greatly increases (FEMA-355D 5-35).

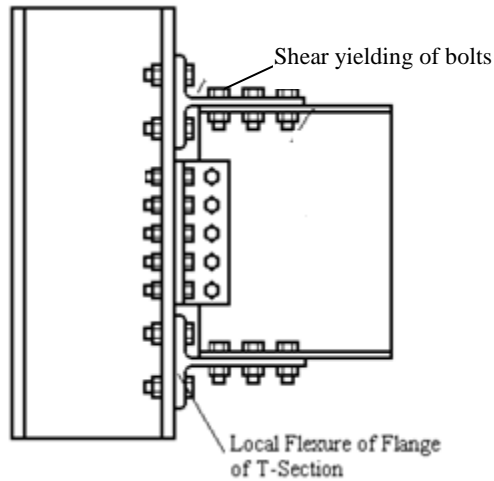


Figure 2.45. Primary yield mechanisms of bolted T-stub connection (adapted from FEMA 2000)

Leon et al. (1999) performed tests on twelve T-stub connections with varying details to analyze their behavior and failure modes. These tests showed that when the failure mode of the global system was located in the beam instead of the T-stub connection, plastic rotation was maximized. A maximum value of $\theta_p = 0.05$ radians was obtained from the twelve connection tests. It was also noted that larger beam depths led to greater plastic rotation capacity of the global system. The moment at failure was often observed to be higher than M_p , with a maximum ratio of moment at failure to M_p equal to 1.25 (Leon et al. 1999). Failure of the connection occurs when either the ultimate strength of one or more components is exceeded or fracture of an element occurs, resulting in loss of load-carrying capacity. Figure 2.46 depicts the

common failure modes associated with a bolted T-stub connection. Figure 2.47 illustrates a typical hysteretic curve for a full strength T-stub connection with a W24 beam.

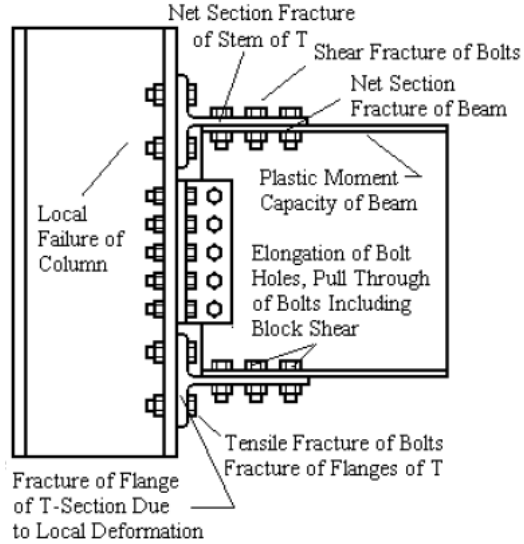


Figure 2.46. Common failure mechanisms of bolted T-stub connection (figure from FEMA 2000)

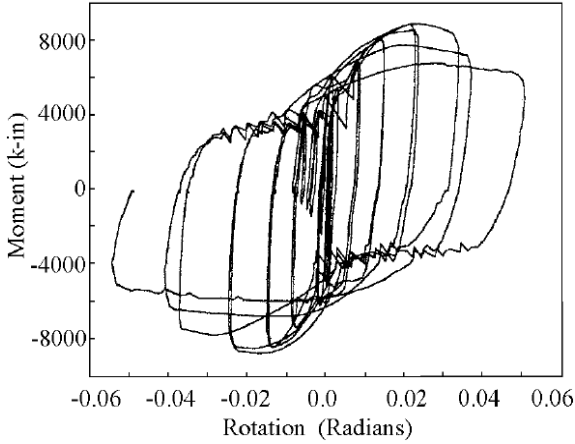


Figure 2.47. Typical moment-rotation curve for T-stub connection and W24 beam (figure from FEMA 2000)

Popov and Takhirov (2002) investigated “an alternative bolted connection having low installation cost and high reliability.” The reason for this was the failure of welded steel moment frame connections to achieve high ductility in seismic events. Popov and Takhirov (2002) explain how bolted connections, as opposed to field-welded connections, are less expensive and avoid brittle weld failures. They also described how the testing of full-size beam-to-column connections at Lehigh University showed that “bolted connections are capable of providing rigid moment connections with cyclic plastic rotational capabilities in excess of equivalent welded joints, but with the same rigidity as welded connections.”

Popov and Takhirov (2002) tested two separate connection geometries. The first, Specimen 1, is shown in Figure 2.48 and Specimen 2 is shown in Figure 2.49. All dimensions and geometry of the two connections were the same except for the stems of the T-stubs connected to the beam flanges. The T-stub used for Specimen 1 had a rectangular-shaped stem consistent with traditional T-stub connections. The T-stub used for Specimen 2 had a U-shaped stem which was shorter than the stem in Specimen 1. The T-stubs for both specimens were connected to the beam flanges by fillet welds and pre-tensioned bolts to “enforce the tee stem and the beam flange joint performance” (Popov and Takhirov 2002). For Specimen 1, four bolts were used for each beam flange; two bolts were used for each beam flange for Specimen 2.

The specimens were tested by using a hydraulic actuator to apply a cyclic load at the end of a cantilevered beam in incremental stages. Figure 2.50 shows the test setup utilized by Popov and Takhirov (2002).

The test results for both specimens showed very ductile behavior of the bolted T-stub connections. The maximum total rotation of both connections was

approximately 0.04 radians with plastic rotation of around 0.03 radians. Yielding of the T-stub flanges and bolts in the column was shown to greatly increase the rotation capacity of the connection.

Popov and Takhirov (2002), through experimental analysis, showed that these bolted T-stub connections also exhibit great ductility and rotation capacity while also developing the full moment capacity of the connected beam.

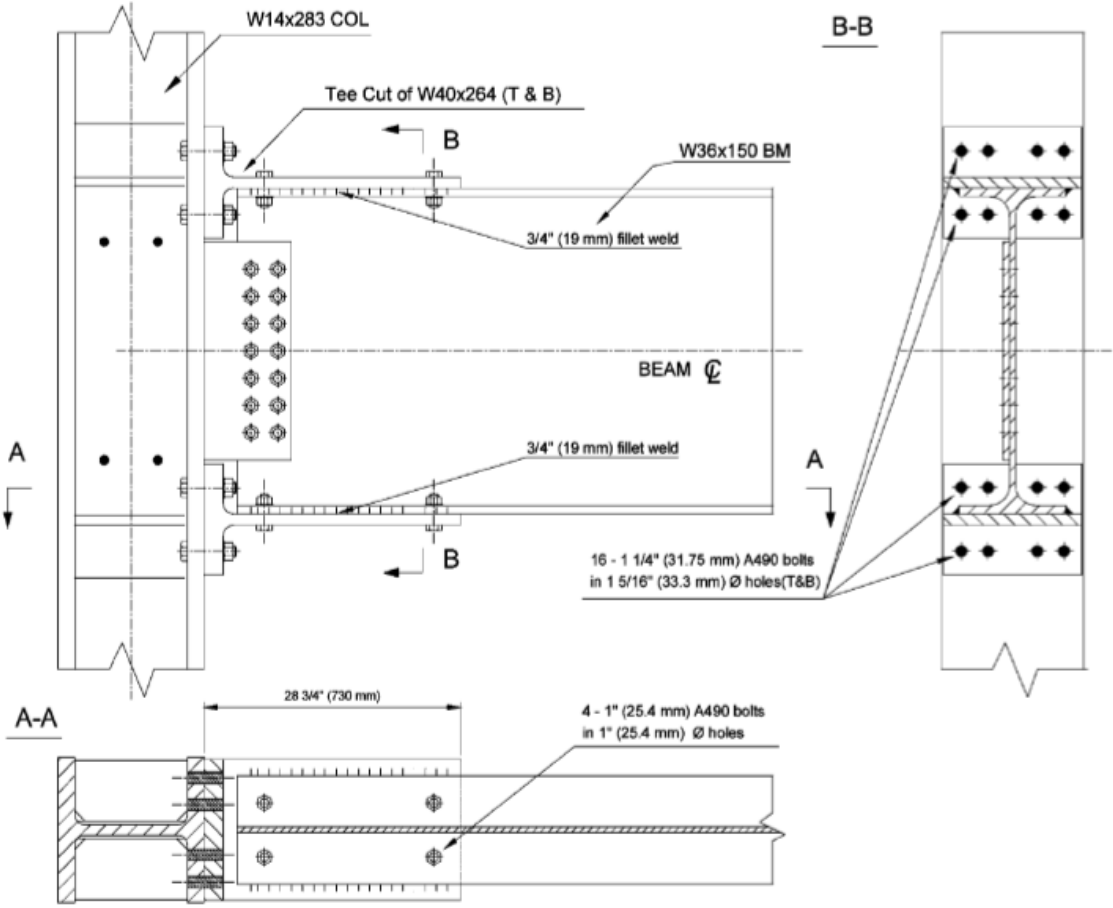


Figure 2.48. Specimen 1 (figure from Popov and Takhirov 2002)

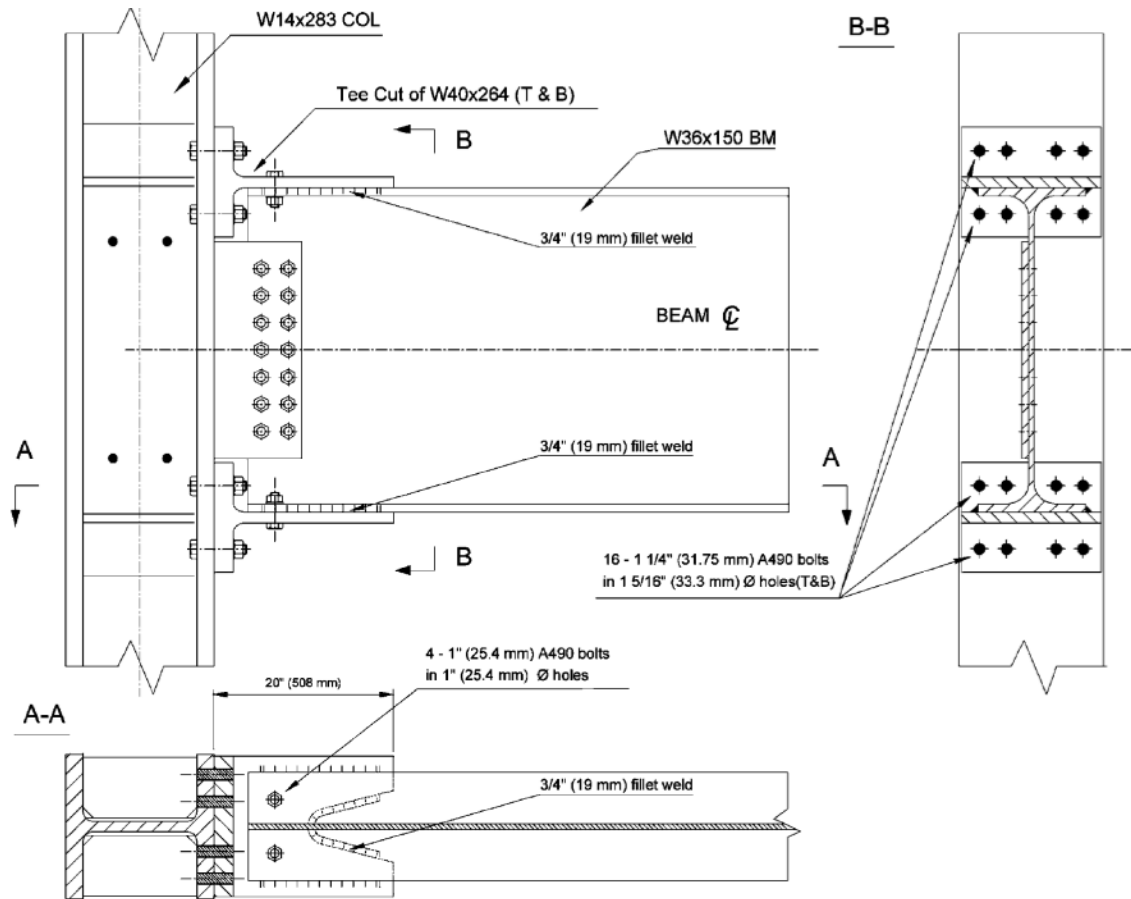


Figure 2.49. Specimen 2 (figure from Popov and Takhirov 2002)

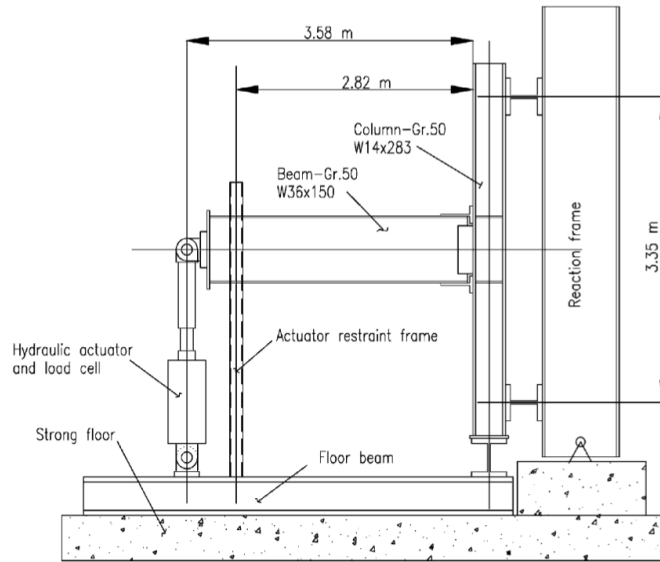


Figure 2.50. Experimental test setup (figure from Popov and Takhirov 2002)

Yang and Tan (2012) created FE models for “six types of conventional connections using ABAQUS finite element software”. The modeled connections represented a beam connection to a column which has been removed. Due to symmetry, only one quarter model was simulated and is shown in Figure 2.51 (Yang and Tan 2012). The column is represented by only one modeled flange. The steel beam was divided into two parts, with solid elements used at and near the connection and beam elements used for the rest of the length. The end of the beam, shown on the far right side in Figure 2.51, was supported by a pin. During the analysis, the column flange was pushed downwards using displacement control to simulate a removed column (Yang and Tan 2012).

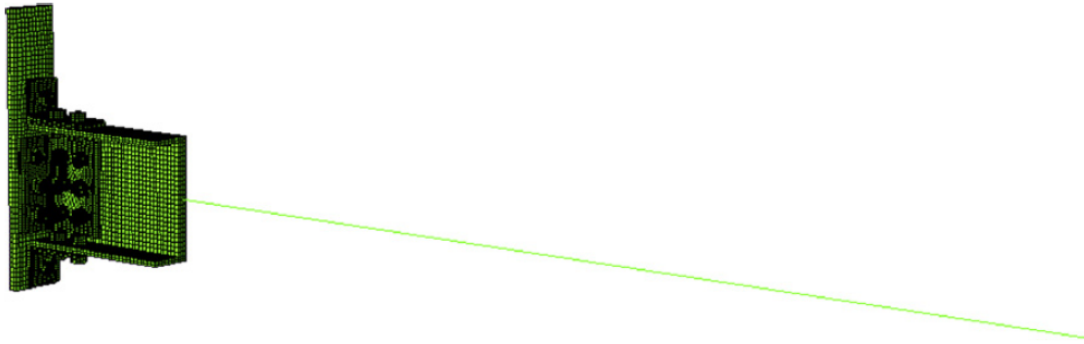


Figure 2.51. Finite element model (figure from Yang and Tan 2012)

Only the results for the connection designated as ‘flush end plate connection’ are detailed in this thesis. This is because the flush end plate connection is the only connection for which the rotation was graphically detailed. Figure 2.52 shows the deformed shape of the flush end plate connection. The modeled bolts in the FE analysis had their two ends connected with a “spring with limited stiffness to constrain free rigid body movement after bolts have fractured” (Yang and Tan 2012). This was done in order to prevent non-convergence of the model from occurring and resulted in the FE model agreeing well with the experimental data (Yang and Tan 2012).

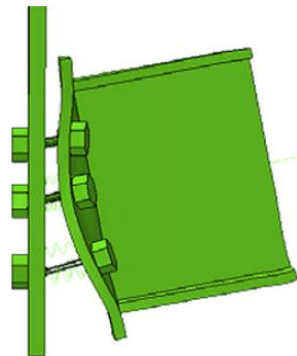


Figure 2.52. Flush end plate connection (figure from Yang and Tan 2012)

The FE analysis shows that the flush end plate connection is able to undergo very large total rotations, about 0.15 radians. It was also observed that, at total rotations greater than 0.05 radians, connection forces begin to be primarily axial and less from flexural action. This is due to the increase in catenary behavior at large rotations (Yang and Tan 2012). Figure 2.53 details the total connection reaction forces, which sums the connection forces from both flexural and catenary action, and those due to flexural action versus connection rotation. Yang and Tan (2012) noted that the allowable plastic rotation for a flush end plate connection in ASCE 41-06 is only 0.015 radians. Therefore, it can be seen that current design codes are likely overly conservative in approximating the maximum rotation of connections.

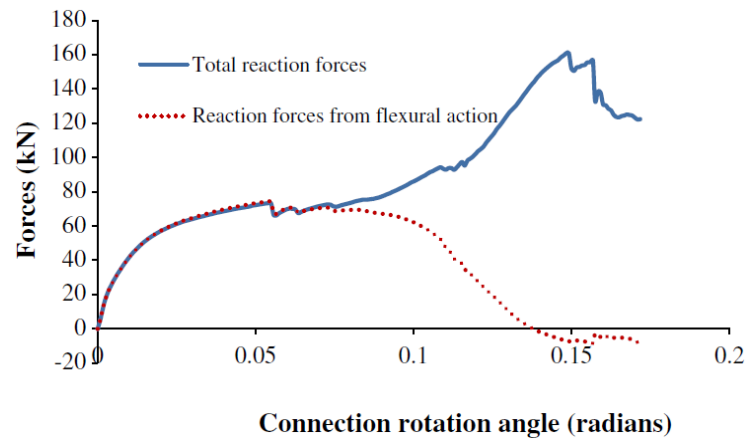


Figure 2.53. Total and flexural reaction forces vs. connection rotation (figure from Yang and Tan 2012)

Liu et al. (2005) investigated the effects of the stiffness of varying connections on the axial, or “tying”, forces developed in the connection during a column removal scenario. Using the non-linear FE computer program, LS-DYNA, they analyzed a 3-

story steel-framed structure designed per UK structural code (Liu et al. 2005). An exterior column was then removed and the structure was analyzed under the reduced loading permitted by UK structural code for damaged buildings. The beam size detailed in this summary is a UB457x152x67 beam section. The material strength is not explicitly stated in the article, but a typical UK value of 355 MPa (51.5 ksi) is assumed. Figure 2.54 shows that rigid and semi-rigid connections develop substantially lower tying forces than pinned and semi-pinned connections. “This is because as the joint stiffness increases the resistance mechanism of the damaged building changes from one solely reliant on catenary action to one that resists loads by a combination of tying forces and Vierendeel action, so the tying force in the remaining structure is reduced as the bending moment plays an increasingly influential role” (Liu et al. 2005).

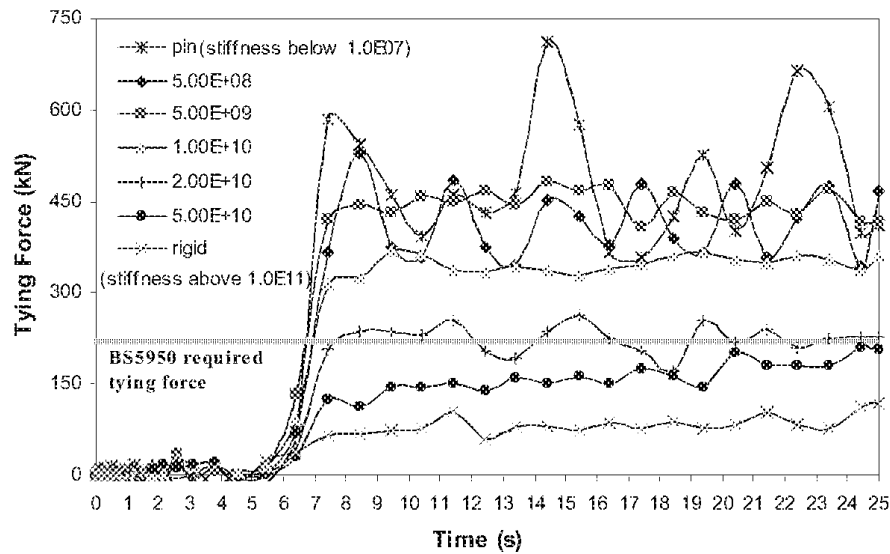


Figure 2.54. Tying force vs. connection stiffness (figure from Liu et al. 2005)

Tying forces range from approximately 80 kN to 720 kN (18 kips to 162 kips) based on connection stiffness. The tying force of 720 kN (162 kips) is more than three times greater than the required tying force of 222 kN (50 kips) per UK code BS6399 (Liu et al. 2005). These values correspond to a 2.6% to 23.8% range of tying force as a percentage of axial yield force (682 kips). Therefore, it is shown that for a steel-framed structure, rigid connections are ideal for minimizing connection forces during a column removal event. Regardless, connections must be designed for the large axial forces induced during a progressive collapse event.

Karns et al. (2009) summarized the results of full-scale and FE tests into the behavior of several types of steel beam-to-column connection types. The connections ranged from fully-restrained (FR) moment connections to semi-rigid and pinned connections. Two of the connections, welded beam flange to column flange (WUF-B) and SidePlate™, were subjected to both a full-scale blast event as well as an FE analysis under a column removal scenario. Other connection types tested were bolted double split tee, reduced beam flange section (RBS), bolted double angle, and bolted single shear tab (Karns et al. 2009). All tests utilized W18x35 steel beams with a yield stress of 50 ksi. The maximum axial tensile capacity of this section is 2291 kN (515 kips).

For all scenarios, a monotonic vertical load was applied at the location of a “missing” column after a blast event. The results of the testing that both FR and semi-rigid moment connections are capable of undergoing large rotations at the location of the “missing” column while developing large moments and axial forces. Pinned connections were also shown to have some ability to carry the loads from a “missing” column event. Most FR and semi-rigid connections, not including SidePlate, were

able to undergo rotations of at least 0.08 radians prior to loss of capacity, as well as develop upwards of 289 kN (65 kips) of axial tensile force. This correlates to 12.6% of the maximum tensile axial force of the beam. Figure 2.55 and Figure 2.56 detail the results of the experiments by Karns et al. (2009).

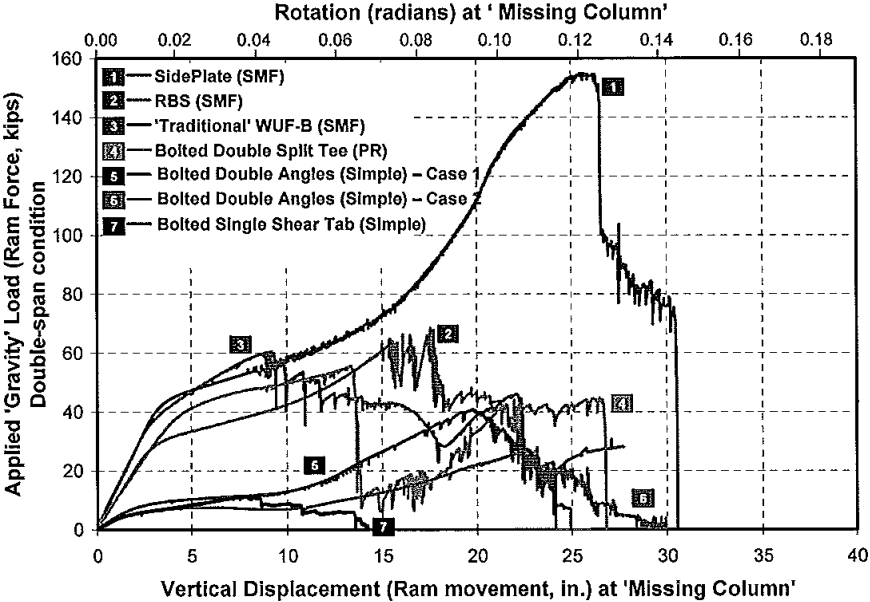


Figure 2.55. Vertical displacement and rotation at “missing” column vs. applied load (figure from Karns et al. 2009)

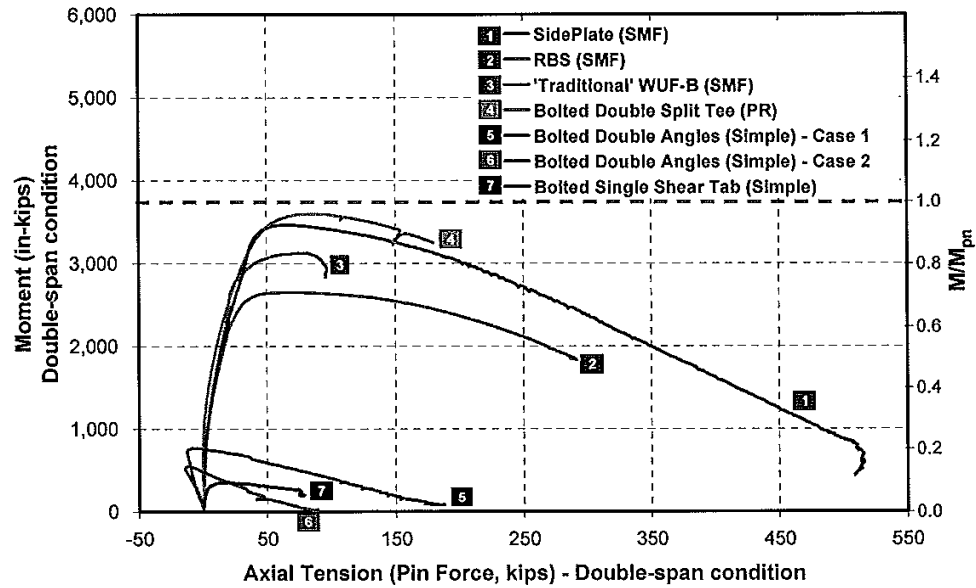


Figure 2.56. Axial tension vs. moment (figure from Karns et al. 2009)

Pirmoz (2009) conducted nonlinear finite element modeling, using the program ANSYS, of bolted angle connections to determine their rotation and performance under a column removal scenario. The analysis revealed maximum total connection rotations of approximately 0.03 radians for W8x21 and between 0.05 and 0.06 radians for W14x38 beams (Pirmoz 2009). In addition, equations were developed to calculate the rotation at a specific moment for bolted angle connections. These equations were developed by curve-fitting to the analytical data of the finite element models and observed that “it has a relatively good accuracy for specimens in the range of studied connection” (Pirmoz 2009).

Xu and Ellingwood (2011) used finite element modeling to analyze the behavior of a welded flange-bolted web (WFBW) connection. The push-down models analyzed also took into account fracture of the connection. Their results revealed that

a WFBW connection can achieve a total rotation of approximately 0.042 radians prior to fracture of the flanges (Xu and Ellingwood 2011).

The data presented in this section showed that a variety of steel connection are capable of undergoing the large rotations associated with initiating catenary behavior of beams and detailed in Section 2.5 of this thesis. Under experimental and numerical cyclic loading tests, several connections were shown to have total rotation capacities as high as 0.062 radians. These rotation capacities coupled with the data presented in Section 2.5 of this thesis indicate that it is possible for a beam-connection system to undergo the plastic rotations required to initiate, but not fully develop, catenary behavior. However, FE model analyses of beams under monotonic loading, such as presented by Yang and Tan (2011), show that some connections may have the ability to undergo rotations of about 0.15 radians.

2.6.2 SidePlate™ Connection

One of the most pressing issues concerning progressive collapse design is the beam-column-beam continuity at the location of a missing column. In order for two previously independent beams to act as one continuous span, the connection at the missing column location must be adequate enough to resist the large moment and tensile forces developed. One such solution to the continuity problem is the use of the SidePlate™ moment connection system, developed in response to the failure of pre-Northridge earthquake connections.

Figure 2.57 details a typical SidePlate™ connection configuration. In this configuration, the beam itself is not directly attached to the column, but is rather terminated at a small distance away from the column face. Horizontal and vertical steel plates are welded to both the beam and the column to transfer the internal forces.

Steel plates may also be utilized to connect the outer edge of the beam flanges to the beam on the opposite side of the column to ensure force distribution and continuity in the case of a missing column. However, SidePlate™ is a proprietary connection and requires large amounts of welding as well as non-traditional beam and column geometries to allow for proper alignment of the steel plates.

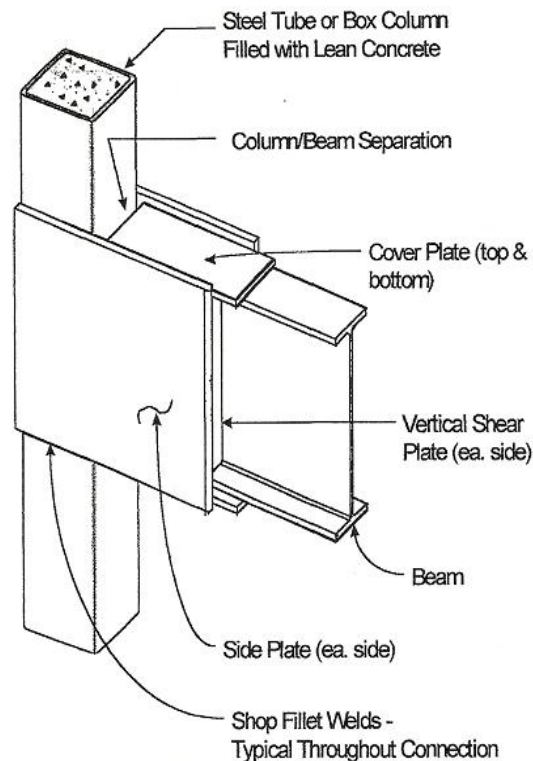


Figure 2.57. Typical SidePlate™ Moment Connection Configuration (figure from SidePlate™ 2012)

2.7 Summary

Current codes, such as UFC and GSA, outline several methods for design to mitigate progressive collapse. In the Alternate Path Method, elements must be

designed to bridge over a damaged column in order to arrest the collapse of a portion or all of the structure. The members must be designed according to current codes such as AISC and ACI. Using these codes, beams are designed for a nominal flexural capacity, at which point the beam is assumed to have no more load-carrying capacity.

However, research has shown the ability of steel beams to utilize a phenomenon known as catenary action to greatly increase its load-carrying capacity past its flexural capacity. Catenary behavior occurs after a sufficient number of plastic hinges develop. Research summarized in Section 2.5 of this thesis indicates that steel beams have adequate ductility to develop large catenary forces after their flexural capacity has been reached. In order to utilize catenary behavior, connections must also be designed to resist the large flexural and axial forces generated during catenary action.

Substantial amounts of research and experimental data have shown that several types of steel connections are able to withstand large rotations. Section 2.5 of this thesis details the results of several experimental and numerical data on several types of connections. The results show that many conventional connections, if detailed correctly, are able to undergo the necessary rotations and resist some level of catenary forces developed in the beams. The research summarized in the tables below indicates that steel connections and beams have the ability to undergo rotations of 0.067 radians prior to failure (Hoffman and Fahnestock 2011), ignoring the results of Kim and Kim (2008) where connection failure was excluded. For these levels of rotation, it is possible to achieve at least 40% of the beam yield strength in axial tension (Khandelwal and El-Tawil 2007). This substantial increase in load-carrying capacity above the flexural capacity of a steel beam is the basis for considering catenary action

as an effective means of mitigating failure of steel-framed structures under extreme loads.

Table 2.1, Table 2.2 and Table 2.3 below summarize the results of the data reviewed in this chapter. Table 2.1 details the required rotation necessary for a specific percentage of catenary action to be achieved. Table 2.2 and Table 2.3 detail the available rotation of certain connections. Rotation values are specified as either total rotation, which is the sum of elastic and plastic rotation, or plastic rotation, depending on the metric used by the original author.

Table 2.1. Summary of data of required rotation for catenary action

| Study | Rotation | Corresponding Axial Load | Type of Connection | Analysis Method | Residual Stresses / Geometric Imperfections | Significant Assumptions & Results |
|--------------------------------|---|-------------------------------------|--|------------------------|--|---|
| Karns et al. (2009) | 0.08 radians | 12.6% axial yield | Detailed modeling of various connection types | LS-DYNA | None | Terminated at connection /beam fracture Total Rotation |
| Khandelwal and El-Tawil (2007) | 0.08 for RBS 0.06 for non-RBS | 42% axial yield 43% axial yield | Modeled shear tab and merged beam flange nodes to column flange nodes 40% section reduction for RBS | MPP-DYNA | None | Terminated at local beam buckling Plastic Rotation |
| Kim and An (2008) | 0.075 radians 0.25 radians | 25% axial yield 100% axial yield | Merged beam flange nodes to column flange nodes | OpenSees | None | No connection failure No specific termination criteria Total Rotation |
| Lee et al. (2008) | 0.06 to 0.10 radians 0.11 to 0.172 radians | 50% axial yield 100% axial yield | Merged beam flange nodes to column flange nodes | ABAQUS | None | No connection failure No specific termination criteria Varying L/D ratios Total Rotation |
| Sadek et al. (2011) | 0.082 radians | 14 % axial yield | Modeled welded beam flange to column and bolted shear tab to beam web | LS-DYNA | None | Terminated at connection /beam fracture Total Rotation |

Table 2.2. Summary of FEA data of available rotation for different connections

| Study | Rotation | Type of Connection | # of Specimens | Analysis Method | Loading Scenario | Significant Assumptions & Results |
|-------------------------------|---------------------------------|---|-----------------------|------------------------|-------------------------|---|
| Hoffman and Fahnestock (2011) | Range of 0.013 to 0.067 radians | Generic moment connection in framed structure | 12 | ABAQUS Dynamic | Push-down | Total Rotation |
| Kim and Kim (2008) | 0.07 radians | RBS | 1 | OpenSees | Push-down | No connection failure |
| | 0.015 radians | WUF-W and WCPF | 2 | | | Plastic Rotation |
| Pirmoz (2009) | radians | Bolted angle with W8x21 beam | 10 | ANSYS | Push-down | Fracture of bolts and steel not considered |
| | Range of 0.05 to 0.06 radians | Bolted angle with W14x38 | 7 | | | Total Rotation |
| Yang and Tan (2011) | 0.15 radians | Bolted flush end plate | 1 | ABAQUS | Push-down | connection force was axial after 0.05 radians |
| Xu and Ellingwood (2011) | 0.042 radians | WFBW | 1 | FE Model | Push-down | Total Rotation |

Table 2.3. Summary of experimental data of available rotation for different connections

| Study | Rotation | Type of Connection | # of Specimens | Analysis Method | Loading Scenario | Significant Assumptions & Results |
|-------------------------------------|---|--------------------------------------|----------------|-----------------|------------------|-----------------------------------|
| Leon et al. (1999) | Range of 0.015 to 0.05 radians | Bolted T-stub | 10 | Experimental | Cyclic load | Plastic Rotation |
| Nader and Astaneh-Asl (1989) | Range of 0.005 to 0.04 radians | Top & bottom angles | 8 | Experimental | Cyclic load | Total Rotation |
| Popov and Tsai (1989) | 0.035 radians 0.04 radians 0.06 radians | WUF-W Welded RBS Bolted T-stub | 1 1 1 | Experimental | Cyclic load | Plastic Rotation |
| Popov and Takhirov (2002) | 0.04 radians both tests | Bolted T-stub | 2 | Experimental | Cyclic load | Total Rotation |
| Schneider and Teeraparb Wong (2002) | Range of 0.035 to 0.062 radians | Bolted flange plate | 8 | Experimental | Cyclic load | Plastic Rotation |

As presented in Table 2.1, Table 2.2 and Table 2.3, there is a significant amount of data quantifying the maximum total and plastic rotations for a variety of steel connection types. These data were used to determine a prescribed failure rotation for which the models analyzed in Chapter 4 of this thesis were assumed to fail. This value was taken to be a total rotation of 0.05 radians, measured at a location two feet from the girder support. The previous research detailed in this thesis clearly shows that a total rotation value, elastic rotation plus plastic rotation, of 0.05 radians is an acceptable and legitimate limiting value. Total rotation, instead of plastic rotation, was used as the limiting parameter in the analyzed models for two reasons: First, the majority of the research presented in this chapter measured total rotations instead of plastic rotations; Secondly, since total rotations include both elastic and plastic rotations, using total rotations is slightly more conservative than using plastic rotations. For comparison, the elastic rotation of the fixed support girders that will be analyzed in Chapter 4 is 0.0035 radians. Thus, the allowable plastic rotation is effectively 0.0465 radians.

The research presented in following chapters of this thesis aim to quantify the forces and rotations that must be resisted in both the steel beams and connections in order to efficiently utilize catenary behavior.

Chapter 3

METHODOLOGY

This chapter presents the methodologies related to this research. This includes the methodologies used in selected past FEA-based research related to connection forces and rotations in structural steel components undergoing catenary action. The methodology utilized for the present thesis is also detailed in this chapter. This methodology is the basis for the results presented in Chapter 4.

Because the present research is carried out on compact beams, this geometric definition is first reviewed in Section 3.1. Section 3.2 provides an overview of selected past FEA-based research which relates to catenary action in steel beams and the behavior of steel connections under large loads. The physical configuration represented and analysis assumptions used in this prior work is included in Section 3.2.

Section 3.3 details the design process that was used to select the member sizes that were utilized in the parametric studies presented in this thesis. The AISC design equations used and design assumptions made will be presented in this section. Section 3.4 details the FE methods used in the research presented in this thesis. The assumptions and modeling techniques used are overviewed, including: geometric imperfections; the residual stress patterns; support conditions analyzed; lateral bracing modeling techniques; material properties of the modeled components; and the loading methods utilized. Section 3.5 outlines the methods and techniques used to evaluate the data from the FEA analysis, including: selection of cross-sections of beam geometry

for stress analysis; beam rotation calculations; and the process for obtaining connection force data. Section 3.6 presents a method for validating the modeling assumptions and techniques used in this thesis. Lastly, Section 3.7 will summarize the chapter.

3.1 Geometric Properties of Steel Components

There are several important geometric properties which are important in quantifying the load-carrying of steel beams defined in the AISC 13th Edition Steel Design Manual (2005). These include web slenderness and flange slenderness as well as lateral bracing distance. AISC provides formulae for these properties which influence load-carrying capacity. The flange slenderness ratio for flexure in singly-symmetric rolled shapes is defined by the following equation,

$$\lambda_f = \frac{b_f}{2t_f} \quad (\text{Equation 3.1})$$

while the web slenderness ratio for flexure in rolled shapes is defined by,

$$\lambda_w = \frac{h}{t_w} \quad (\text{Equation 3.2})$$

In order for steel beams to be able to achieve their full plastic moment capacity, the flanges and web slenderness ratios must satisfy compactness limitations along with bracing distance limitations. For flanges, the slenderness ratio must satisfy the following equation to be considered compact,

$$\lambda_f \leq \lambda_p = 0.38\sqrt{E/F_y}. \quad (\text{Equation 3.3})$$

In order for webs to be compact, their slenderness ratios must satisfy the following equation,

$$\lambda_w \leq \lambda_p = 3.76\sqrt{E/F_y}. \quad (\text{Equation 3.4})$$

However, AISC 13th Edition Steel Manual (2005) provides more stringent compactness ratios for seismic design. These more closely represent building response during progressive collapse events in that the member and connection demands are high during a seismic event, similar to those in a progressive collapse scenario. For seismic design, the flange slenderness ratio must satisfy the following equation to be considered compact,

$$\lambda_f \leq \lambda_{p,s} = 52/\sqrt{F_y} . \quad (\text{Equation 3.5})$$

The web slenderness ratio must satisfy the following equation in order to be considered compact for seismic design,

$$\lambda_w \leq \lambda_{p,s} = 520/\sqrt{F_y} . \quad (\text{Equation 3.6})$$

Both of these compact slenderness ratios for seismic design assume a Young's Modulus value, E, of 29,000 ksi.

Lateral-torsional buckling is a failure mode which can occur when the compression flange of a steel beam is not sufficiently braced. AISC code details limiting braced lengths for varying beam geometries in order to determine moment capacity. For doubly-symmetric members the maximum unbraced length, L_b , to allow the plastic moment to be reached is given by the following equation,

$$L_b \leq L_p = 1.76r_y \sqrt{E/F_y} . \quad (\text{Equation 3.7})$$

The AISC Steel Manual provides tables, an excerpt of which is shown in Table 3.1, which provide values of L_p for most W-Shape steel sections.

The compactness and bracing criteria presented in this section must be met by flexural members so that their plastic moments can be reached. It is only after a sufficient number of hinges form that catenary action can be achieved. Hinges form when the flexural capacity of a member is reached at a certain section. If the member

is not sized and detailed appropriately, per compactness and lateral bracing criteria, the load which causes hinges to form will be less than the plastic moment of the section. Thus, because the full flexural resistance of the member will be utilized by designing the member to reach M_p as described in Section 3.3, the load at which catenary action will begin is relatively high for the given member.

Table 3.1. AISC Z_x table with limiting braced lengths (table from AISC 2005)

| Shape | | Z_x in. ³ | M_{px}/Ω_b | | M_{rx}/Ω_b | | BF | | L_p ft | L_r ft | I_x in. ⁴ | V_{nx}/Ω_v | |
|----------------------|--|---------------------------|-------------------|--------|-------------------|--------|------|------|-------------|-------------|---------------------------|-------------------|------|
| | | | kip-ft | kip-ft | kip-ft | kip-ft | kips | kips | | | | kips | kips |
| | | | ASD | LRFD | ASD | LRFD | ASD | LRFD | | | | ASD | LRFD |
| W36×800 ^h | | 3650 | 9110 | 13700 | 5310 | 7980 | 47.5 | 71.4 | 14.9 | 94.8 | 64700 | 2030 | 3040 |
| W36×652 ^h | | 2910 | 7260 | 10900 | 4300 | 6460 | 46.8 | 70.4 | 14.5 | 77.8 | 50600 | 1620 | 2430 |
| W40×593 ^h | | 2760 | 6890 | 10400 | 4090 | 6140 | 55.5 | 83.5 | 13.4 | 63.8 | 50400 | 1540 | 2310 |
| W36×529 ^h | | 2330 | 5810 | 8740 | 3480 | 5220 | 46.5 | 70.0 | 14.1 | 64.4 | 39600 | 1280 | 1920 |
| W40×503 ^h | | 2310 | 5760 | 8660 | 3460 | 5200 | 54.7 | 82.2 | 13.1 | 55.3 | 41600 | 1290 | 1940 |
| W36×487 ^h | | 2130 | 5310 | 7990 | 3200 | 4800 | 46.1 | 69.3 | 14.0 | 60.0 | 36000 | 1180 | 1770 |
| W40×431 ^h | | 1960 | 4890 | 7350 | 2950 | 4440 | 53.6 | 80.6 | 12.9 | 49.0 | 34800 | 1110 | 1660 |
| W36×441 ^h | | 1910 | 4770 | 7160 | 2880 | 4330 | 45.2 | 68.0 | 13.8 | 55.5 | 32100 | 1060 | 1590 |
| W27×539 ^h | | 1890 | 4720 | 7090 | 2740 | 4120 | 26.1 | 39.2 | 12.9 | 88.6 | 25600 | 1280 | 1920 |

3.2 Methods of Analysis in Previous Related FEA Research

Experimental tests are a time consuming and expensive manner with which to conduct research. In recent years, finite element analysis (FEA) computer programs have become a powerful tool to research structural behavior. Programs such as ABAQUS and LS-DYNA are useful in reaching a better understanding of structural

behavior. This section details how researchers have utilized FEA programs as a tool to compliment and sometimes verify experimental data relating to connection and beam behavior under extreme loads. The focus of this section is on a single study since the same software utilized in this thesis was used in the study. Also, the study presented focused on bolted moment connections which were also utilized in this thesis.

Takhirov and Popov (2002) utilized the finite element program, ABAQUS, to perform a cyclic load test on bolted steel beam-to-column connections. Takhirov and Popov created several models to analyze bolted T-Stub moment connections. The T-Stubs were fillet welded to the beam flanges and then connected by pre-tensioned high-strength 1¼" diameter bolts to the beam flanges as well. The beam web was connected to a shear tab plate with 1" diameter bolts and the shear tab plate was directly welded to the column flange. The T-stub connection flanges were connected to the column flange with 1¼" diameter bolts. Another connection model used a welded cover plate connection being welded to both the column flange and beam flanges. These models used shell elements and were tested to study the behavior of the overall connection performance. In another test, solid elements were used to model a single T-stub and study its behavior under direct tensile load.

The column-connection-beam system was modeled using two-dimensional reduced-integration shell elements, ABAQUS designation S4R, located at the center plane of the corresponding shell. A Cartesian coordinate system was used during the analysis and is shown in Figure 3.1, which details the orientation of the system.

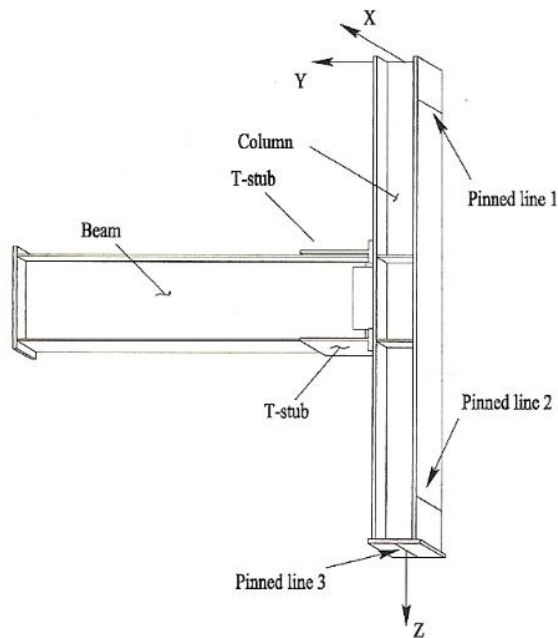


Figure 3.1. Coordinate system, boundary conditions, and mesh of shell analysis (figure from Tahkirov and Popov 2002)

Continuity plates were modeled with shell elements as well and were located at the corresponding elevations of the beam flanges. Continuity plates are plates which are welded to the column at the elevation of the beam flanges. They are used to increase the strength of the column due to the high shear force in the column at the connection and to provide a continuous line of force from the flanges of one beam to the next. Two doubler plates were also modeled on both sides of the column web and were located between the continuity plates to increase the web thickness in the column panel zone. The T-stub connection was modeled with shell elements with the stem and flange attaching to the beam and column, respectively. The high-strength bolts used to connect the T-stub to the column and beam flanges were modeled as spring elements with bilinear stiffness corresponding to the stiffness of the actual bolts while

welds were modeled by merging the nodes of the connecting elements. The node located at the center of the bolt was restrained to have the same displacement for both the bolt and the connecting element in any direction. The shear tab was indirectly modeled by directly connecting the beam web to the column flange by merging the coincident nodes. Figure 3.2 which shows the finite element mesh of the shell elements used to model the structural components.

An eigenvalue analysis was performed on the shell model to impose initial imperfections into the members during the load cycle. The first phase of the analysis applied a total load of 30 kips at the tip of the beam to induce a bending moment in the beam and at the connection. Using the modified Riks method, the second phase utilized a load-displacement analysis which was performed on the model with the displacement being applied to and controlled by the nodes at the tip of the beam (same location as for first phase), with a target ultimate displacement of 6 inches. Figure 3.2 shows the final deformed shape of the global shell model analysis.

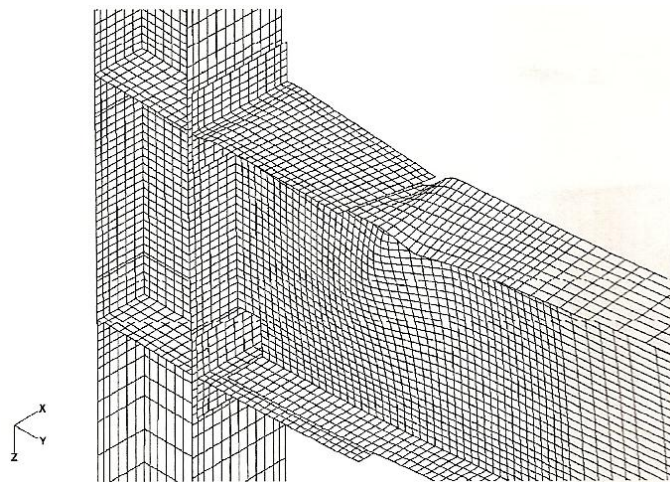


Figure 3.2. Deformed shape of global shell analysis model (figure from Takhirov and Popov 2002)

In a separate local analysis, solid elements were utilized in the analysis of the T-stub connection. Utilizing symmetry, a quarter model of the T-stub connection was used in the analysis, which is shown in Figure 3.3 along with the finite element mesh using solid elements for the bolts, washer, and the T-stub. However, the T-stub is not expected to be perfectly symmetric about the y-axis as the bolts would likely have different forces with varying x-position. A tension test in the local Z-direction was used to analyze the behavior of the T-stub flange utilizing displacement control with a maximum end displacement of 0.3 in. The target value of T-stub flange displacement of 0.3 inches corresponds to a relative beam rotation of 0.008 radians. This value was obtained by measuring the gap between the T-stub flange and the column face, which was modeled as a rigid surface using ABAQUS with the same mesh pattern as the T-stub flange. Results from the analysis showed that the bolts underwent plastic deformation under both tensile and flexural forces.

The high-strength bolts used in the solid element analysis were modeled using two cylinders with different diameters. The diameters of the heads of the bolts were equal to the average diameter of the actual hexagonal bolt head. The shank diameter of the bolts was 1-1/4 inch. Figure 3.4 shows the final deformed shapes of the T-stub solid elements analyses for both the connection and the bolts. The zones in the Figure refer to locations of active yielding in the model.

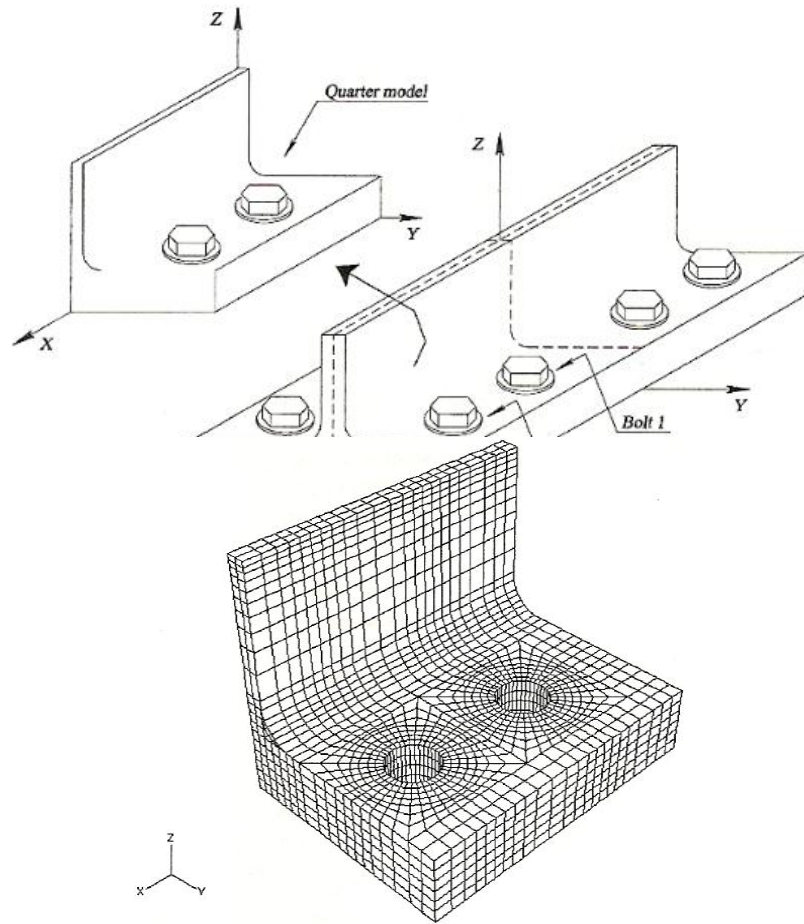


Figure 3.3. Quarter model and mesh of solid T-stub connection analysis (figure from Takhirov and Popov 2002)

The results from the tests performed by Takhirov and Popov (2002) show that bolted T-stub moment connections are able to undergo plastic deformations which are necessary for catenary action to occur in beams. These results, in conjunction with other previous research, were used to define the prescribed total failure rotation of 0.05 radians utilized in this thesis. However, the models analyzed in this thesis used

simplified connections consisting only of restrained nodes instead of the detailed connections used in Takhirov and Popov (2002). While the models analyzed in this thesis were more simplified than detailed in Takhirov and Popov (2002), the prescribed failure rotation of 0.05 radians indirectly accounts for a variety of failure modes for various ductile fully-restrained moment connections.

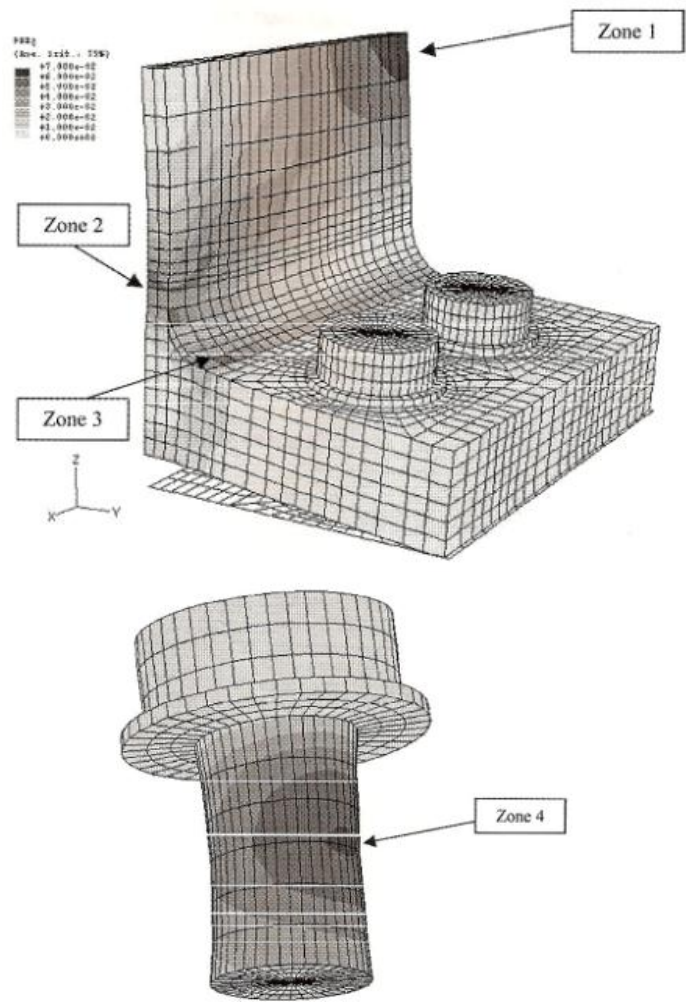


Figure 3.4. Deformed shapes of T-stub connection and bolts for solid element analysis (figure from Takhirov and Popov 2002)

3.3 Methodology of Design of Girder and Beams

The first step in conducting the modeling presented in this thesis was to design a steel framing plan typical of mid-rise building construction. The resulting member sizes were modeled to determine their response under an idealized missing column scenario. The framing plan is designed to current code requirements. A plan view of a 2-bay by 2-bay 10-story steel-framed building, shown in Figure 3.5, was used for the structural member design. This design is applicable to a building with any number of bays and/or stories, as long as the bay dimensions are the same. This layout was chosen as representative of a typical structure.

The plan dimensions of the building were assumed to be 56 feet long by 80 feet wide. Typical load values found in building construction were utilized, with a dead load, D , of 45 pounds per square foot and a live load, L , of 100 pounds per square foot being applied. The dead load corresponds to a four inch concrete slab on metal decking. The dead load corresponds to a four inch thick lightweight concrete slab on steel decking. The live load is a typical value for office buildings with file rooms obtained from ASCE 7 (2005). The following AISC LRFD load combination equation was used to obtain the design load:

$$Load_{Design} = 1.2 * D + 1.6 * L. \quad \text{(Equation 3.8)}$$

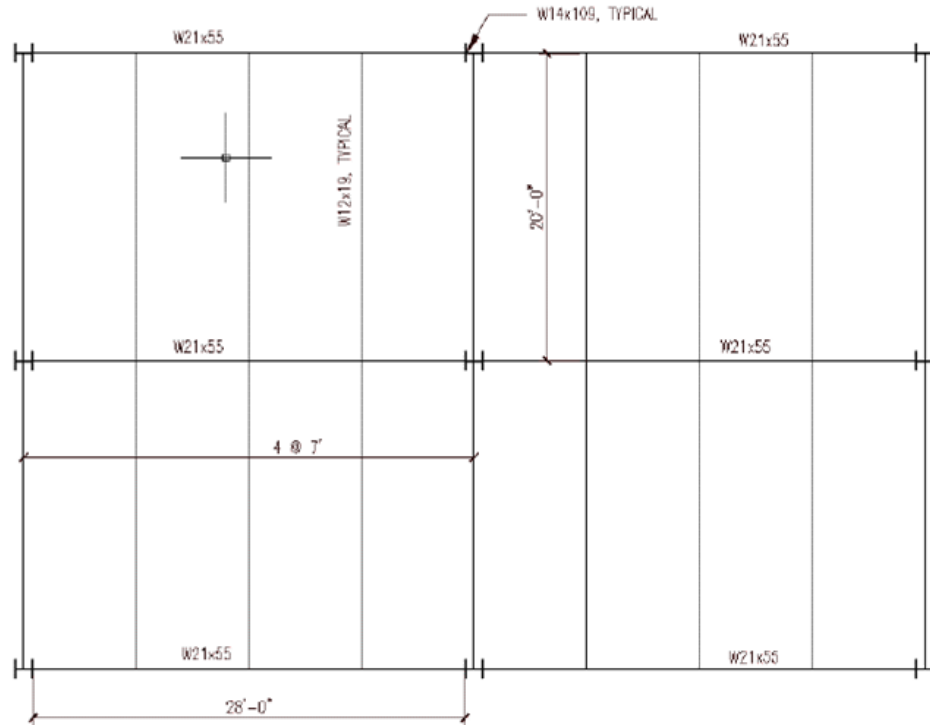


Figure 3.5. Framing plan for member design

The girder and beams were assumed to be continually braced along their compression flanges from the concrete slab. The steel was assumed to be Grade 50, with a Young's Modulus value, E , of 29,000 ksi. The design moment for the beams, $M_{u,beams}$, was calculated to be 76.3 ft-kips. The design moment for the girder assuming fixed supports, $M_{u,girder}$, was calculated to be 427.7 ft-kips. In this thesis, models were created for both fixed support and shear support girders. Therefore, the design of the girders previously described would lead to an under-designed girder with shear supports. However, using the same girder dimensions for models with both types of support conditions is necessary to be able to make direct comparisons of the results. Table 3-2 of the AISC LRFD Steel Design Manual was used to appropriately size the

girder and beams for the steel-framed building. This table gives values for nominal plastic moment capacity of various structural members. A W12x19 section, nominal plastic moment capacity of 92.6 ft-kips, was selected for the beams and a W21x55 section with a yield stress of 55 ksi, nominal plastic moment capacity of 566.5 ft-kips, was selected for the girder. The lateral bracing length of 7 feet, which is assumed to be provided by the beams, is sufficient to allow the W21x55 girder to fully develop its plastic moment capacity. The beams are assumed to be continuously braced.

3.4 Finite Element Analysis

The finite element analysis (FEA) method is an extremely powerful tool for analyzing behavior in structural members. FEA can be utilized to analyze structural problems with varying boundary conditions, loading conditions, as well as variations in the cross-section and material properties of a given element or system of elements.

FEA discretizes the desired domain into a finite number of nodes and elements. The primary dependent variables are approximated at the location of the nodal points (Kaliakin 2001). The domain is “subdivided into a finite number of non-overlapping subdomains or elements” which are connected together at the location of the nodes on their respective boundaries (Kaliakin 2001). The interpolation functions used in FEA are integrated in order to obtain a result over each discrete element, and are used in determining stresses and displacements over elements. Typically, polynomial equations are used as the interpolation functions “since they are easy to manipulate mathematically” (Kaliakin 2001). However, trigonometric functions and functions formed by adding a Fourier series to a polynomial have also been successfully utilized (Kaliakin 2001).

3.4.1 FEA Programs Utilized

For analyses presented in this thesis, the model geometry was first created in AutoCAD2004. The geometries were then loaded into a commercially-available finite element pre- and post-processor that is compatible with ABAQUS. The pre-processing program was utilized to create the mesh for the model geometries and also apply support conditions and loading conditions. ABAQUS (version 6.11-1) was utilized as a finite element solver and post-processing unit for analyses in this study. Non-linear material input was manually input in the ABAQUS input files.

3.4.2 Assumptions and Modeling Techniques

A W21x55 girder, the basis for which was presented in Section 3.3, was used for all analyzed models presented in this thesis. A yield stress of 55 ksi was used to represent Grade 50 steel with a 10% over-strength factor (as recommended by DoD 2010 and GSA 2003). Two 28-foot spans of the W21x55 were modeled as a single span with the assumption of an immaculately removed mid-span column, which assumes no damage to the beam-column connections or to the beams themselves. This assumption is consistent with the modeling techniques presented in both the GSA (2003) and DoD (2010) progressive collapse design criteria.

In order to more accurately represent a typical rolled W-shape, geometric imperfections were imposed on the models. In this manner, more realistic results could be obtained from the FEA models. The magnitude and orientation of the geometric imperfections used in this study were taken from the tolerances presented in Table 1-22 of the AISC 13th Edition Steel Construction Manual (2005). The three geometric imperfections modeled in this thesis were: flange out-of-squareness or flange tilt; sweep of the compression flange; and web out-of-plane bowing. The

maximum allowable imperfection magnitudes were used in this study to provide a conservative result, and are quantified below, where T and T' are defined in Figure 3.6:

$$\text{Flanges Out-of-Square: } T + T' = \frac{5}{16} \text{ "}$$

$$\text{Sweep: } \frac{1}{8} \text{ "} \times \left(\frac{\text{Length}(ft)}{10} \right) = 0.35 \text{ "}$$

$$\text{Web Out-of-Flatness: } \frac{3}{16} \text{ "}$$

The values for sweep and web-out-of-flatness from AISC (2005) are directly applied to the model. The flange-out-of-squareness is only applied to the top flange due to limitations of the imperfection program described below. The magnitude of the flange-out-of-squareness tolerance is assumed to be equally distributed between the two flanges, so that T' and T are equal to 5/32". Furthermore, it is assumed that the flange tilt is equal on either side of the web so that the applied imperfection, using the program described below, is 5/64".

Figure 3.7 graphically represents the definitions of sweep for W-shapes and in this work this sweep is applied solely to the compression flange in order to maximize the distortion of the cross-section and because this is more relevant to the buckling which these imperfections exacerbate. A value of 28 feet, the span of a single W21x55 member, was used for the length in the sweep equation.

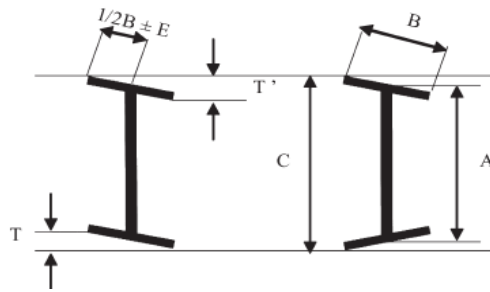


Figure 3.6. Flange out-of-squareness (figure from AISC)

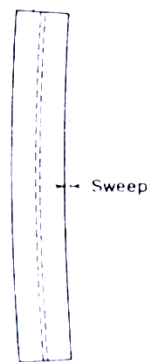


Figure 3.7. Sweep for W-shapes (figure from AISC)

In order to apply the necessary imperfections to the model geometries, the program Imperfection.FOR was utilized. This program was developed by Yang, et al (2005) to apply geometric imperfections in an FEA modeled steel beam. The program requires an input file containing geometric data from the models and the magnitude of the desired imperfections. The first line of input includes dimensions of the member and number of nodes in the model. The second and third lines of input are the distances between bracing and stiffeners of the member, which dictate the lengths of the sinusoidal wave that describes the variation in magnitude along the length of the girder. For models in this thesis, these distances were assumed to equal the initial

span of the girders prior to removal of the mid-span column, which is taken as 28 feet, given the relatively robust nature of rolled sections (in comparison to the shorter lengths used for plate girders in the prior work of Barth et al 2005). Line 4 of Figure 3.8 corresponds to the magnitude of sweep; Line 5 corresponds to the magnitude of web out-of-flatness; and Line 6 corresponds to the magnitude of flange out-of-squareness or flange tilting. The imperfection text file input used in this study is shown in Figure 3.8.

```
24913, 4.11, 0, -.0000000000000391, 20.278, 8.22, 8.22, 2, 2, 0
336, 336
336, 336
0.35, 0.35,
0.1875, 0.1875
0.078125, 0.078125
```

Figure 3.8. Text file input for Imperfection.FOR

A residual stress pattern was also utilized for the analyzed models to most accurately represent true behavior of the beam. Previous research of steel beam behavior under extreme loads leading to catenary action did not quantify or detail the effects of residual stresses. A linear residual stress pattern for rolled steel wide flange shapes developed by Galambos and Ketter (1959) was used for the models in this thesis. This residual stress pattern was used due to the credibility of Galambos in the field of structural steel behavior as well as for its ease in applying to the finite element analysis (FEA) models. Figure 3.9 graphically shows the assumed residual stress pattern and associated equations as developed by Galambos and Ketter (1959).

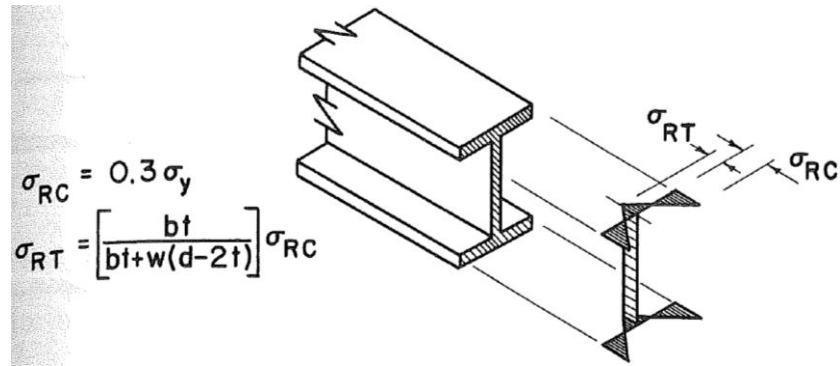


Figure 3.9. Residual stress pattern (figure from Galambos and Ketter 1959)

The yield stress, σ_y , is equal to 55 ksi for the models analyzed in this thesis. Therefore, the residual stress value, σ_{rc} which is the compressive stress at the tips of the top and bottom flange, was calculated to equal 16.5 ksi. Similarly the residual stress value, σ_{rc} which is the tensile stress along the entire web depth, was calculated to equal 6.2 ksi. Since the flange cross-section of the girders modeled consisted of eight shell elements across the length, the linear residual stress pattern was discretized using the average residual stress expected over the width of the element and is graphically presented Figure 3.10. The residual stress values were input into the ABAQUS input file using the command *INITIAL CONDITIONS. Initial stress values were assigned to elements based on their location in the web or flange of the member. The interested reader may wish to refer to Szalai and Papp (2005), who document the accuracy of this simple residual stress profile in comparison to more complicated and modern suggestions.

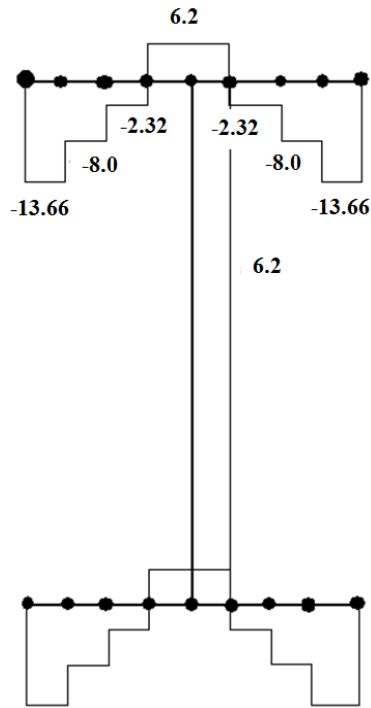


Figure 3.10. Discretized residual stress pattern

In typical building construction, beams and girders are connected to one another and adjacent columns using either bolts or in-field welds. These connections are either called shear connections or moment connections. Both of these types of connections, shear and moment, were modeled and analyzed in this. The rationale for using these two support conditions was to quantify the effects of two extremes of support conditions on the flexural and catenary behavior of the steel girder during an extreme loading event. However, as will be explained below, the shear connections modeled represent more of a practical extreme versus a theoretical extreme of a true pin support. The results for the varying support conditions were also used to quantify differences in connection forces.

Both types of connections were modeled utilizing nodal restraints at the girder ends to model the desired support type. The applicable translational and rotational degrees of freedom were restrained for the specific connection type being modeled. Each degree of freedom had a number associated with it. Values between 1 and 3 represent restrained translation and values 4 through 6 represent restrained rotation about the three axes. Therefore, for the fixed or moment connection, each node at the girder ends was fully restrained in all six degrees of freedom. In this manner, the model represented a girder with a fully-rigid moment connection.

The shear connection was modeled by restraining specific nodes along the web at the ends of the girder where bolts are typically placed in common construction practice. The vertical centerline of the bolt line was located at the end of the girder. A total of eight nodes were restrained in a vertical line at each end of the girder. The nodes were spaced at approximately 2 inches vertically from each other to represent a 2 inch spacing of the bolt centerlines centered vertically on the girder. The nodes were only restrained in each of the three translation degrees of freedom and no rotation was restrained. A total of eight nodes at each girder end were restrained in this manner. The restrained nodes were located approximately two inches from the ends of the girder and were vertically spaced at approximately two inches as well. In this manner, the model represented a bolted shear connection which is widely used in construction. Although the use of several bolts inline vertically will cause some level of flexural resistance at the connection, results presented in Chapter 4 show that flexural stiffness is less compared to a fully-rigid moment connection.

Lateral bracing was modeled to allow the girder to achieve its plastic moment capacity through flexural response. Lateral bracing for the girder was

assumed at the locations of the framed-in beams. This bracing was modeled using beam elements corresponding to the properties of a W12x19 member (selected on the basis of the discussion in Section 3.3) at the locations of the framed-in beams along the web of the girder. The beams were connected to the middle of the girder web by merging the two coincident nodes together. The beam supports were fully restrained in all degrees of freedom, except for vertical translation. This allowed for the entire applied vertical load to be directly resisted by the girder. ABAQUS's 'beam general section' element type was utilized to model the lateral bracing for the analyses that modeled lateral bracing as beams. Using the 'beam general section' command line, the applicable section properties of the W12x19 beam were accurately modeled. The input for the command was the cross-sectional area of the W12x19 member as well as the moments of inertia about the principal axes.

Bearing stiffeners were utilized in the models to provide bearing strength at the location of the supports and one pair of double sided transverse web stiffeners were used at mid-span of the girder for the applied concentrated load. These stiffeners were located on both sides of the web. They were attached to the girder flanges and web in to represent a welded connection. The stiffeners were designed in accordance with AISC 13th Edition Steel Construction Manual using LRFD. The mid-span transverse stiffener was designed for a factored load of 900 kips, equal to a concentrated load equal to the column force assuming 9 stories above the removed member. Each bearing stiffener at the ends of the girder were designed for half of the total possible applied vertical load including the beam load and self-weight, equal to 515 kips.

The material properties of the beams and girder were assumed to be those of typical structural steel. Steel behaves in an elastic-plastic manner and was modeled as

such. The Young's modulus, E , of the steel was taken to be 29,000 ksi and the steel was assumed to have a yield stress of 55 ksi (based on assuming Grade 50 steel with a 10% over-strength factor). Stress versus strain data was gathered from steel coupon tension tests performed by Righman (2005). Specifically, the data set labeled '0.3125" AUG 50 ksi' was used for the models in this thesis. This experimental data was utilized to obtain a realistic non-linear stress-strain behavior of the steel used as the basis for the material behavior and plastic properties of the girders analyzed in this thesis. The tension test results from Righman (2005) were used for several reasons: First, the steel plate used in the test was Grade 50, the same as the material of the steel used in this thesis; Second, the actual yield stress of the plate was equal to 55 ksi which is the yield stress value used in the models presented in this thesis; Third, the thickness of the plate tested was 0.3125 inches which is very similar to the modeled web thickness of 0.375 inches used in this thesis.

The ABAQUS command, *PLASTIC, was used to model the plastic behavior of the steel in the analyses. Figure 3.11 shows the command line used in the input files for the models presented in this thesis. Each input line requires a value for true stress on the left and the corresponding value of true plastic strain on the right. The first line of input is the stress at which the material first yields. For the models in this thesis, four lines of data for nonlinear modeling were used. Figure 3.12 plots the data displayed in Figure 3.11 with the material input obtained using methods validated in Barth et al. (2005).

| *PLASTIC | |
|----------|--------|
| 55.104 | 0.0000 |
| 55.606 | 0.0090 |
| 72.228 | 0.0288 |
| 105.102 | 0.4018 |

Figure 3.11. Plastic command line used in analyses

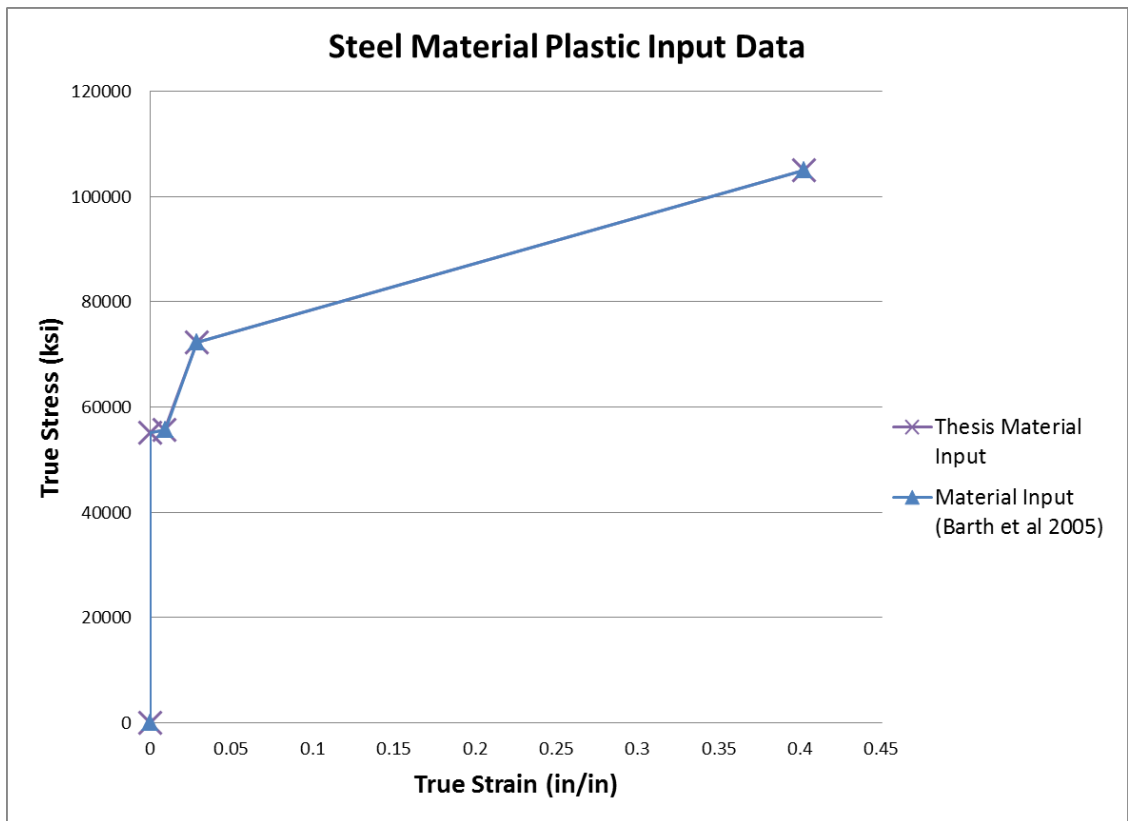


Figure 3.12. Steel material plastic input data

Several loads were used in the models analyzed in this study. The dead load of the steel girder, loads from the tributary areas of the framed-in beams, and the load from the missing column were applied to the girder. The load from the “missing” column was assumed to be the load of the column supporting the nine stories above it. This load was input in the *CLOAD command of ABAQUS as the reference load for the Riks analysis. A live load of 100 psf and a dead load of 45 psf was applied to the floor supported by the beams. Each beam’s total length was 20 feet and the beams were spaced 7 feet apart. Half of the total load on each beam was assumed to distribute to its support and the other half was applied to the girder, resulting in a total tributary area of 140 square feet ($7' * 10' * 2$ beams framing into each girder cross-section) for each concentrated beam load on the girder. These loads, with a dead load factor of 1.2 and reduced live load factor of 1.0 represent the dead load factor used in traditional design and a reduced live load factor based on GSA (2003) rationale of using a reduced live load factor during extreme events. Although the live load factor used here is more conservative than GSA (2003), two times the effective load factor for a static analysis, which would be 0.5 per GSA (2003). The dead load factor is typical for LRFD design and the reduced live load factor was used to account for the likelihood that the full design live load would not be present during an extreme loading event.

This resulted in a concentrated load of 21.6 kips applied at the location of the connection with the framed-in beams, which occurs at the center of the girder web at 7 foot intervals along the girder length, consistent with the framing plan shown in Figure 3.5. The mid-span load applied to the girder at the location of the missing column was increased incrementally using the Riks method in ABAQUS. The unit weight of steel

was taken to be 490 pounds per cubic foot. The steel unit weight was converted to mass and used as an input in the ABAQUS file to calculate the girder and beam self-weight.

The various loads were applied to the girder in steps using the *STEP command in ABAQUS. The first load step applied the self-weight of the girder using the *DLOAD command in ABAQUS. The concentrated loads from the framed-in beams were applied in three load step increments of 5.5 kips and one increment of 5.1 kips until the full magnitude was reached. This was performed to monitor and analyze the model behavior in incremental steps as opposed to one large load step and also to more accurately model and obtain data for the elastic behavior of the girder prior to yielding. Lastly, the mid-span concentrated load from the missing column was applied to the girder using the modified Riks method (Dassault Systemes 2011). The modified Riks method is generally used to predict unstable, geometrically nonlinear collapse of a structure, which is useful in analyzing catenary behavior, a primary interest in this work.

3.5 Quantification of Data to be Acquired from FEA Analysis

In order to best understand the catenary behavior of the girder analyzed in this study as well as the forces generated in the connections, appropriate methods of data analysis were developed. First, several cross-sections of the girder were selected for evaluation. At these cross-sections, the percentage of the web depth in tension was calculated in order to analyze the manner in which the girder carried increasing load. This data was evaluated relative to beam rotations to determine the extent to which catenary behavior is developed at feasible levels of rotation in steel beams subjected to abnormally large loads. Beam rotations were also measured to evaluate the

relationship between applied load and connection forces versus rotation to determine magnitudes of connection force that should be considered in such design scenarios. Calculation of beam rotations is discussed in more detail in Section 3.5.3.

3.5.1 Selection of Cross-section Cuts

Utilizing the geometric and loading symmetry of the girder, cross-section cuts were determined for half the length of the girder. A total of 3 cross-sections were selected for analysis. Since the behavior of the girder was assumed to be identical on both sides of mid-span, i.e. symmetric behavior, the cross-sections were all located on one half of the girder. These cross-sections were located at the following distances measured from the mid-span of the girder: Cross-section at 28 inches because this value is near the girder mid-span; Cross-section at 224 inches because this was located near the assumed girder inflection point; and cross-section at 324 inches because this was located near the girder connection. Charts detailing the exact location of the cross-section cuts are presented in Section 4.2.

3.5.2 Tension Depth Analysis

Typical flexural response of symmetric I-shaped beams requires that half of the cross-section be subjected to tensile stress while the other half is subjected to compressive stress. However, catenary action necessitates that the majority of the cross-section be subjected to tensile stress to carry load beyond the flexural capacity of a section. A parameter, the tensile depth ratio (TDR), was developed to quantify the fraction of the web subjected to tension. This ratio is given by:

$$TDR = D_{Tension} / D_{Total} \cdot \quad (\text{Equation 3.9})$$

This ratio was plotted versus applied load to the girder for the various cross-section cuts, the charts of which are presented in Section 4.3. Comparisons of these charts were analyzed for different conditions: presence or absence of residual stresses; presence or absence of geometric imperfections; and differing types of support conditions.

3.5.3 Beam Rotation Calculations

Rotation capacity and ductility of a steel girder is another important factor in the analysis of catenary behavior and connection forces. Beams and their connections must be ductile enough to allow for large beam deflections in order catenary action to be initiated and prior studies suggest that rotation capacity is a limiting factor in the amount of catenary action that can be realistically developed (e.g., Khandelwal and El-Tawil 2007). Therefore, charts were constructed for the various models plotting rotation versus applied load and are presented in Section 4.2. The rotation was calculated with respect to a point located at a distance of two feet from the end of the girder. The rotation at a location two feet from the end of the girder was calculated to represent the total connection rotation, similar to the values presented in Chapter 2. The rotation of the girder in units of radians, θ , was calculated using the following formula:

$$\theta = \text{Tan}^{-1}(\Delta/L). \quad (\text{Equation 3.10})$$

The value Δ represents the vertical deflection of the girder at the point where the rotation is calculated (i.e., 2 feet from girder end or mid-span) while the value L represents the length from the support to the point where the rotation was calculated. As discussed in Section 2.7, the total rotation (elastic plus plastic rotation) is used for analysis in this thesis.

3.5.4 Axial Girder Connection Forces

In structural design, beam-to-column connections in gravity load systems are not designed to resist axial force. Any axial forces which develop in the structural members of a gravity system are assumed to be negligible and are thus ignored. However, catenary action of a steel beam under extreme load causes large axial forces in order to achieve static equilibrium. Therefore, quantification of axial connection forces is of great importance if a structure is to be designed to resist progressive collapse through means of beam catenary action. It is possible that these forces would cause connections that are detailed through traditional means to fail at relatively low loads compared to the beam capacity.

The axial connection forces calculated in the analytical models presented in this thesis were plotted versus the connection rotation to determine their magnitude in Section 4.4. In order to achieve this, the axial force component of each nodal restraint at the end of the girder was summed for each load step to obtain the total axial connection force at the girder ends.

3.6 Verification of Results

In order to verify the accuracy of the analysis and results of the models presented in this thesis, a verification model was constructed and compared with the results of an FEA model of the same girder conducted by Righman (2005). A steel plate girder experimentally tested by Righman (2005) and modeled using the FEA program, ABAQUS, was used for the verification process. The girder (Righman's Girder 6MG) was modeled and the results were compared with the data obtained by Righman. Figure 3.13 details the geometry of the experimentally tested girder and the

constructed finite element model. Similar to the previous models detailed in this thesis, ABAQUS was utilized to analyze the model.

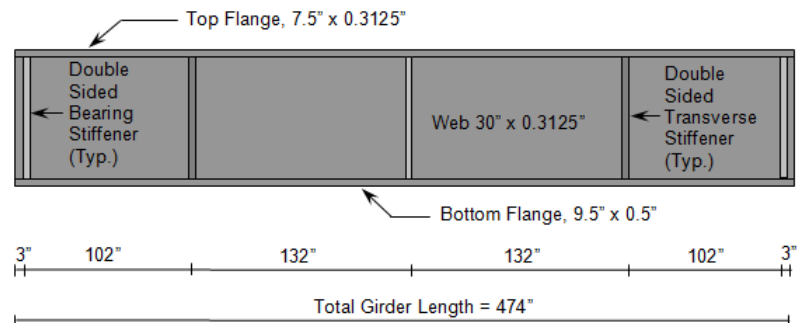


Figure 3.13. Geometry of experimentally tested steel plate girder

A residual stress pattern, applied in the same manner described in Section 3.4.2 but using values obtained from Righman (2005), was used in the input file for modeling the girder. Imperfections measured at the time of the experimental test were also input into the input file in order to accurately capture the plate girder geometry. The material property input is the actual non-linear measured properties of the experimental girder through curve fitting stress-strain data obtained from standard tension coupons. The top, compression, flange was modeled with a yield stress of 62.6 ksi; the bottom, tension, flange was measured with a yield stress of 64.6 ksi; and the web was modeled with a yield stress of 58.5 ksi. Lateral bracing was modeled at both of the transverse stiffeners as well as the mid-span stiffener by restraining out-of-plane translation of the web nodes at these locations. The modified Riks method presented earlier in this chapter was used to incrementally increase a concentrated load at mid-span of the girder.

A load vs. displacement curve was constructed from the FE data of the validation model and is shown in Figure 3.14. The data line labeled ‘Cotter’ represents the data from the verification girder FE model. The other data lines represent various models run by Righman to predict the experimental behavior of the girder.

The verification girder FE model and the Righman models correspond well. The initial stiffness of the verification girder model follows closely with the Righman models, as does the peak concentrated load and displacement. The post-yield behavior also approximately parallels with the Righman FE data. These data analyses confirm that the method used in thesis to analyze structural behavior is accurate and can be verified against previous data.

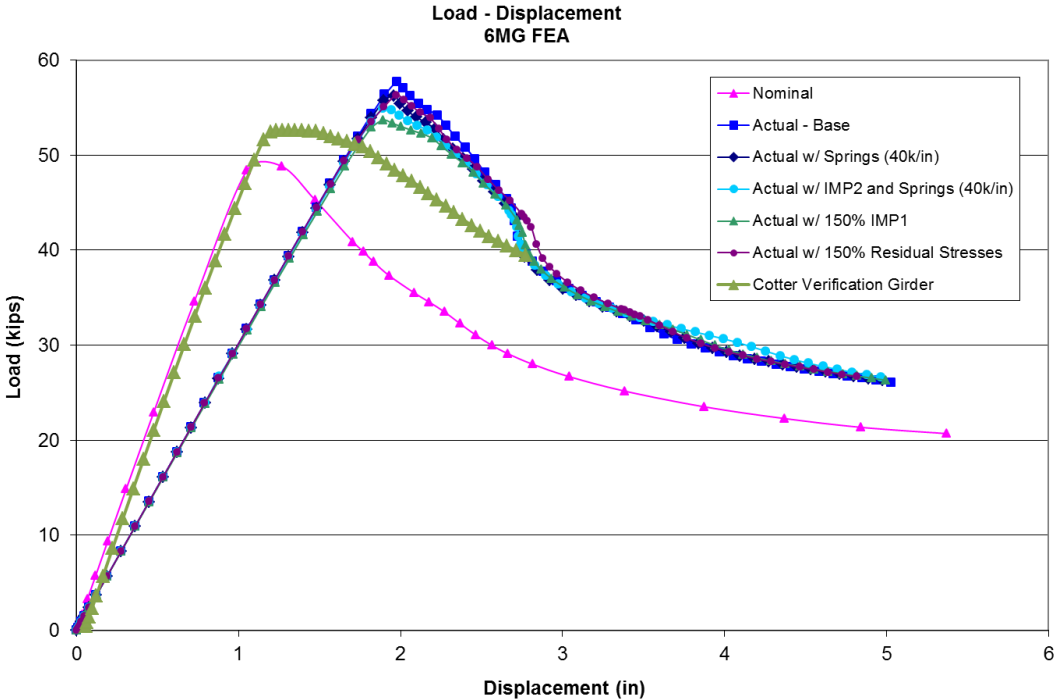


Figure 3.14. Comparison of verification girder FE with Righman data

3.7 Summary

This chapter has presented the methods of analysis used in past and the present research. An overview of the finite element method of analysis was also given in this chapter. The structural design of the girder and beam sizing, complying with AISC 13th Edition (2005), was presented along with several methods of quantification used to predict the catenary behavior of the models analyzed along with rotations of the girder and the connections.

A previously modeled steel plate girder, by Righman (2005), was used to compare the accuracy of the methodologies and assumptions used in this thesis. An FE model was analyzed, using ABAQUS, and was determined to accurately predict the same behavior shown in the Righman (2005) models. The results confirm that the methodologies used in this thesis reliably account for the effects of geometric imperfections and residual stresses, two primary variables investigated in this research.

Chapter 4

PARAMETRIC STUDY

This chapter is organized into five main sections: parametric values; connection rotation results; web depth percentage in tension results; connection force results; and a summary of the chapter. The first section, parametric values, details the variables which were used in the analyzed models found in this chapter. The connection rotation results present and quantify the rotation behavior of the models because it was determined that connection rotation was the limiting factor governing the load-carrying capacity of the members considered. The percentage of web depth in tension results section quantifies and details the model results in order to determine the extent to which catenary action develops in practical steel beams. The connection force results quantify the forces at the girder connection that are required to be resisted during a ‘missing’ column event. Lastly, the summary section presents the overall conclusions of the chapter.

Several graphs, which are presented in the following sections, were created to detail the results of the analyzed models. The graphs compared the connection rotation results, percentage web depth in tension results, and the axial connection force results for four different models that were analyzed in this work. The connection rotation data and percentage of web depth in tension graphs express the data relative to the total applied vertical load in the analyzed model. The total applied vertical load, including the beam self-weight, applied beam loads, and applied column load, was used in all graphs. The applied beam loads correspond to typical infill beam loads in

an office building or similar structure. The applied column load corresponds to the large concentrated load which would be applied to the mid-span of the girder in the event of a ‘missing’ column scenario and is increased as an independent variable throughout the analyses via a Riks analysis algorithm. The axial connection force graphs were plotted versus the connection rotation for each analyzed model.

As reference points, each graph shows the un-factored flexural capacity of the girder, assuming yield stress of 55 ksi, as well as the applied load which causes a beam rotation of 0.05 radians at a location two feet from the support. This rotation represents the connection rotation of the model because, as discussed in Chapter 2, previous literature has shown that a rotation of 0.05 radians for steel beams is the approximate maximum rotation which can be achieved for practical end connections. The flexural capacity of the girder was calculated to be the full plastic moment, M_p , of the member. The method of calculating the beam rotation is detailed in Section 3.5.4. The data points on all of the graphs presented in this chapter represent each discrete load step and the corresponding results associated with it.

4.1 Parametric Values

The goal of the research presented in this thesis is to quantify the catenary action and connection forces of a steel girder under an extreme loading scenario in which a mid-span support column is suddenly removed. The girder is assumed to be braced by steel beams at discrete locations along its length. Several variables were studied to identify their influence on the behavior of the beam under such a loading scenario. These variables are: type of end supports, presence of residual stresses and presence of geometric imperfections.

Residual stresses and geometric imperfections were selected as variables because it is a more realistic method of modeling actual beams that has not been previously researched to the best of the author's knowledge. Furthermore, the presence of tensile residual stresses may decrease the ultimate force which causes tensile failure of the girder. Additionally, it was desirable to investigate whether the influence of geometric imperfections on the compression region of the beam would cause different stress distributions to occur as the girder transitioned from a flexural to catenary response (compared to girders lacking geometric imperfections).

The majority of past experimental and finite element analyses presented in Chapter 2 of this thesis concerned members with fixed end supports and moment connections would most likely be used if a structure was designed to resist progressive collapse. Therefore, most of the models analyzed in this chapter similarly had idealized fixed end supports in order to replicate the behavior of a typical moment connection. Three models with fixed end supports were analyzed, each with the same type and location of lateral bracing supports. One model with fixity similar to that of a typical shear tab connection was also analyzed in order to quantify the difference due to varying support types.

Table 4.1 details the various parameters of each of the analyzed models. The first number of a specific model refers to the support condition of the model; i.e. "1" corresponds to fixed supports and "2" corresponds to shear connection supports. The second number refers to the combination of residual stresses and geometric imperfections used in the model. Specifically, "1" in the second digit of the analysis label corresponds to model including both residual stresses and geometric imperfections while a "3" in this location signifies that neither residual stresses nor

geometric imperfections are implemented. Thus, Model 1-3 was analyzed with fixed supports and neither geometric imperfection nor a residual stress pattern in order to establish a baseline for comparison to other models in this work and serves as a comparison to previous similar work (e.g., Khandelwal and El Tawil 2007). A “2” as the second digit of the model’s label indicates that only residual stresses but not geometric imperfections were considered.

Table 4.1. Parametric combinations used for analyzed models

| MODELS ANALYZED | | | | |
|--------------------------------------|------------------|------------------|------------------|------------------|
| | Model 1-1 | Model 1-2 | Model 1-3 | Model 2-3 |
| Girder Size | W21x55 | W21x55 | W21x55 | W21x55 |
| Support Condition | Fixed | Fixed | Fixed | Shear |
| Residual Stresses Used? | Yes | Yes | No | No |
| Geometric Imperfections Used? | Yes | No | No | No |

The specific residual stress pattern and geometric imperfection input was previously outlined in Section 3.4.2 of this thesis. The results of these models are located in Sections 4.2 and 4.3 of this chapter. The models were analyzed using the finite element analysis (FEA) program, ABAQUS version 6.11. The subsections below detail the other relevant details of the models.

4.1.1 Beam Dimensions

The steel girder used in all analyzed models presented in this chapter was a Grade 50 W21x55 AISC steel rolled section with an assumed 10% over-strength factor (as recommended by DoD 2010, and GSA 2003). This section was designed based on a representative office building-type structure. Design of the fixed support steel girder used for analysis in this thesis is presented in Section 3.3 of this thesis. The same girder size is used for analysis the shear connection model for consistency. A standard bay size of 28 feet by 20 feet was used, with the girders spanning 28 feet and the infill beams spanning 20 feet. A plan view of the typical bay spacing is shown in Section 3.3 of this thesis. The nominal moment capacity of the W21x55 girder, with a yield stress of 55 ksi, was calculated to equal 566.5 ft-kips.

A supporting column was assumed to be immaculately removed from the structure, with no damage to surrounding components, and the two girders were assumed to act continuously with a new unsupported span of 56 feet (i.e., the connection between the two girders is assumed to be uncompromised during column removal, consistent with current progressive collapse guidelines (DoD 2010 and GSA 2003). Additionally, the models were analyzed with bearing stiffeners on both sides of the web at mid-span and also at a distance of six inches from the ends of the beam, i.e., 6 inches from where the supports are applied. As detailed in Section 3.3, the stiffeners were designed according to the AISC Steel Construction Manual 13th Edition (2005) for the large concentrated loads at the mid-span and supports of the W21x55 girder.

4.1.2 Lateral Bracing

The vast majority of steel girders in typical building construction are assumed to be braced by infill beams and/or composite concrete slabs to resist the effects lateral-torsional buckling. The potential influence of slabs is neglected herein; however, the girder models presented in this chapter were analyzed with infill beams serving as lateral bracing. Specifically, a total of seven infill steel beams were assumed to provide lateral bracing for the girder at increments of seven feet. The infill beams were located at increments of seven feet along the 56 ft. span length of the girder for a total of seven intermediate locations. Lateral movement at the supports is restrained by the boundary conditions of the model, which are detailed below in Section 4.1.4. As described in Section 3.4.2, the infill beams were modeled to each have a length of 20 feet. The beams were modeled using the ‘beam general section’ element type in ABAQUS. This command allows the user to define the geometric properties of the beam as well as the axial stiffness. Therefore, the axial stiffness of the lateral support provided by the infill beams to the girder can be accurately predicted.

The beam and girder were connected by merging the coincident nodes in order to form a rigid connection. The beam end nodes were restrained in all degrees of freedom except for vertical translation so as not to restrain the deflection along the length of the girder. The intersection of the infill beams and the girder was modeled to occur at mid-height of the girder, which from the visual output from the model shown in Figure 4.1 was demonstrated as appropriately restraining lateral-torsional buckling (LTB) behavior due to the above-described constraints and stiffness properties applied to the beam elements.

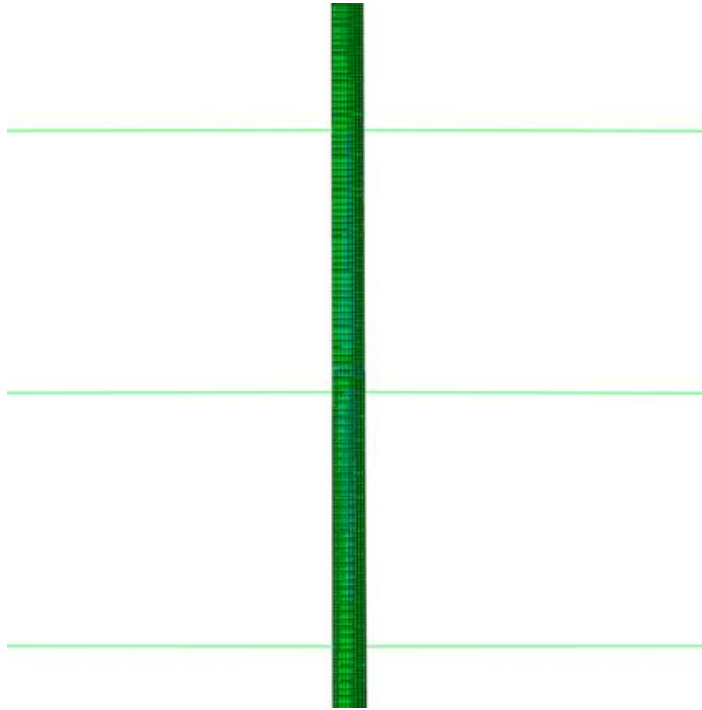


Figure 4.1. Lateral bracing preventing LTB at flexural capacity

4.1.3 Loads

Three primary types of load were applied to the member in discrete load steps: model self-weight; loads transferred from beams; and the ‘missing’ column load. First, the self-weight of the beams and girder was applied using the density of the members and the *DLOAD command in ABAQUS. Next, the concentrated load from each of the infill beams was applied in four equal increments so the behavior of the girder could be analyzed at discrete intervals. The total applied concentrated load from each of the infill beams was 21.6 kips, as calculated from applied dead and live loads in Section 3.4.2. Thus, each of the four increments of this loading applied a load of 5.4 kips at the location of the in-fill beams which was located in the middle of the girder web. Lastly, using the modified Riks method in ABAQUS (described in

Section 3.4.2 of this thesis), the ‘missing’ column load was applied at mid-span of the girder. This mid-span concentrated load was incrementally increased based on the calculations of the modified Riks algorithm. The mid-span load was continuously increased until the analysis reached a total of 100 load steps. At this analysis termination point, the girder rotation was well beyond the prescribed failure rotation of 0.05 radians and was thus neglected. Sections 4.2 and 4.3 detail the effects of this loading on the girder’s structural behavior.

4.1.4 Support Conditions

As described in the beginning of Section 4.1, two support conditions were analyzed to study their effects on the girder behavior. Both moment connections and shear connections were modeled since they constitute the overwhelming majority of steel connections in typical building construction. As detailed earlier, three of the four models analyzed in this chapter were modeled with fixed support conditions. Most of the models analyzed in this chapter are moment connections since they provide more redundancy and strength than shear connections, and are thus more likely to be used in progressive collapse design scenarios. This also allows for more direct comparisons with the results in the existing literature.

The fixed end supports were modeled by restraining translation in all directions of the girder end nodes along both the web and the flanges. Moment is also resisted in all directions as a result since, for example, both the top and bottom flanges are restrained and thus create a resisting force couple resisting flexure about the longitudinal plane of the girder. The shear connection supports were modeled by restraining translation of the web nodes in all three global axes at the end of the girder, where bolts would likely be located for a typical shear connection. Eight nodes,

corresponding to eight bolts, were restrained at each end of the girder and spaced at approximately two inches apart in the vertical direction. There were a total of 21 nodes in the depth of the girder web, but only those locations which corresponded to likely bolt locations were restrained. These support conditions are detailed in Section 3.4.2 of this thesis.

4.1.5 Residual Stresses

Residual stresses occur in rolled steel shapes due to different rates of cooling over the cross-section of a given member. This results in initial compressive and tensile stresses imposed on the steel member prior to loads being applied. During the literature review for this thesis, no investigation into the effects of residual stresses on catenary action of steel beams in progressive collapse scenarios was found. Therefore, the models in this thesis are analyzed with and without a residual stress pattern to determine the effects, if any, on the resulting behavior of a steel girder in the scenario considered herein.

The residual stress pattern used in this thesis is based on the proposed pattern developed by Galambos and Ketter (1959). This pattern was selected due to the wide credibility of the authors and due to its simplicity in application. The details of the residual stress pattern used in the models presented in this chapter are found in Section 3.4.2 of this thesis. This pattern was applied to the cross-section of the model by using the command line “*Initial Conditions” in the ABAQUS input file. The residual stress pattern was discretized in order to be able to apply it to the shell elements of the model as detailed in Section 3.4.2.

4.1.6 Geometric Imperfections

Rolling a steel member with no geometric distortions of the flanges and webs is nearly impossible. Therefore, the American Institute of Steel Construction (AISC) provides limitations for the amount of distortions allowed in a rolled steel section. There are three types of geometric imperfections included in the models: web out-of-flatness, which is distortion of the web perpendicular to its face; sweep, which is lack of alignment in the vertical plane of the longitudinal centroids of the top and bottom flanges; and flange tilt, which is the amount the flange is rotated from an angle of 90 degrees with the web. A more detailed discussion of the geometric imperfections used in this thesis is presented in Section 3.4.2.

Similar to what was found regarding residual stresses, a literature review of previous data indicated that no study was performed on the effects of geometric imperfections on catenary action in steel beams in progressive collapse scenarios. Therefore, models were analyzed with and without geometric imperfections to obtain a better understanding of their effect, if any, on the behavior of a steel girder in this situation. As described in Section 3.4.2, geometric imperfections were applied to the models by using a program created by Yang et al (2005) to apply nodal displacements corresponding to geometric imperfection input. This allowed the user to control the amount of web-out-flatness, sweep, and flange tilt in the model. A more detailed discussion of the geometric imperfections input and application is presented in Section 3.4.2.

4.2 Connection Rotation Results

In this section, the applied load versus beam rotation at the connections will be presented for the four analyzed models. The connection rotation was taken as the

rotation of the analyzed girder at a location two feet from the support, as described in Section 3.5.3. Two graphs were created to compare the rotation results of the fixed support models as well as compare the results of Model 1-3 and Model 2-3, which shows the effects of differing support conditions. While connection rotation is used throughout this chapter to analyze the results of the models, rotation at mid-span was also calculated using the method described in Section 3.5.3. Figure 4.2 shows the comparison between the two rotations for Model 1-1. The behavior for the other three models analyzed in this chapter is similar to that of Model 1-1.

One preliminary observation that is shown in Figure 4.2 and similar figures that follow is that the flexural capacity of the girder was exceeded prior to the ‘missing’ column load being applied at mid-span. This is logical due to the girder being designed to originally have a support at mid-span. In other words, the original span length was 28 feet compared to the analyzed span length of 56 feet.

As can be seen in Figure 4.2, the plots of the two rotations vary slightly. Using the rotation at mid-span resulted in both a larger rotation at which flexural capacity is reached, as well as a lower value of applied vertical load at the prescribed failure rotation of 0.05 radians. These differences can be attributed the curvature of a girder whose supports resist moment. The curvature is slightly less near the support compared to that at the mid-span of the girder. However, the previous research data presented in Chapter 2 quantified the rotation of the connections. For that reason, the rotation at a location 2 feet from the support is used throughout this thesis.

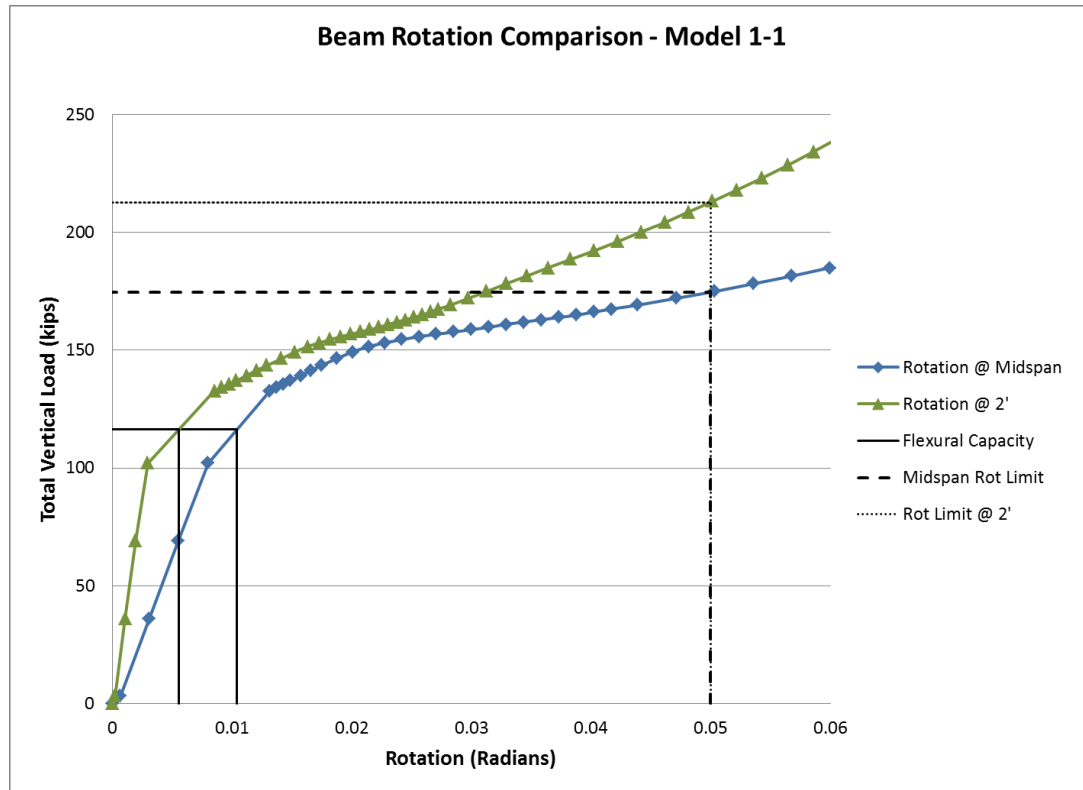


Figure 4.2. Load vs. rotation comparison for Model 1-1

Figure 4.3 shows the applied load versus connection rotation for Model 1-1, Model 1-2 and Model 1-3. As can be seen in Figure 4.3, the rotation limit for all three models was reached well after the flexural capacity of the beam was surpassed, but at a point where the girder continues to display increased load-carrying capacity. Additionally, the connection rotation behavior of all three models was very similar. The total vertical load required to reach the flexural capacity of the girder was calculated to be 116.5 kips for each model. However, the prescribed failure rotation of 0.05 radians was not reached until much larger applied loads for each model.

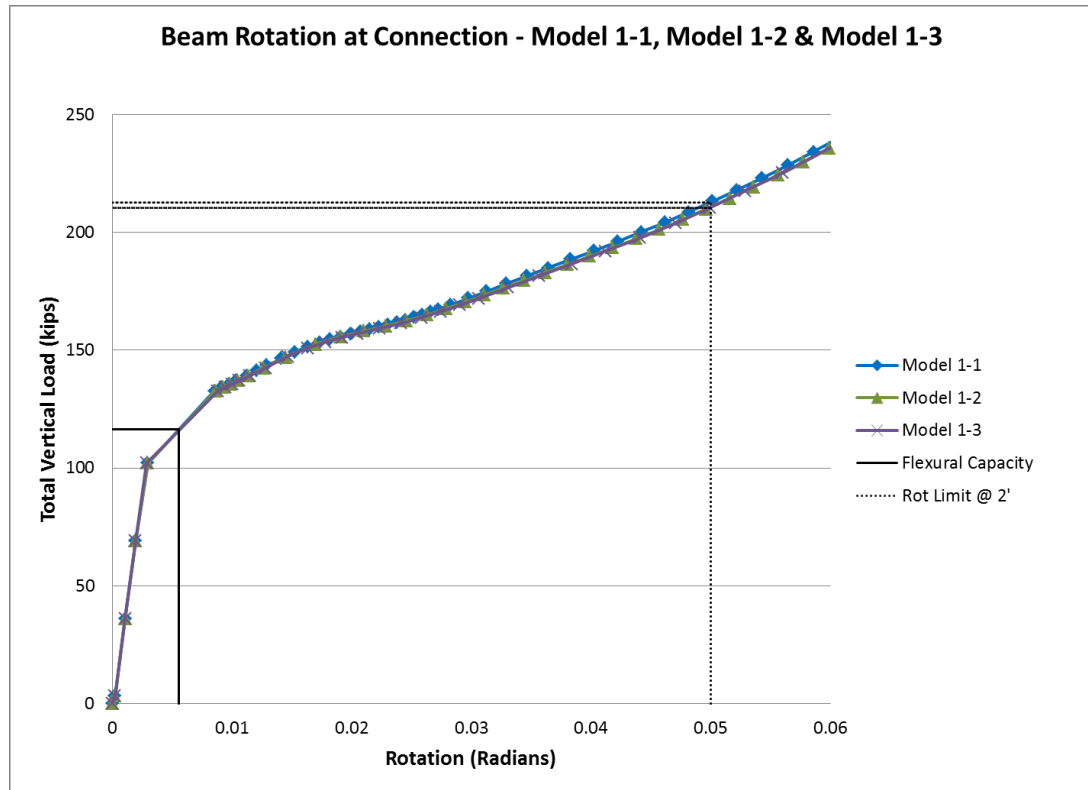


Figure 4.3. Load vs. connection rotation for Model 1-1, Model 1-2 & Model 1-3

Model 1-1 reached its flexural capacity at a connection rotation of 0.00560 radians; Model 1-2 reached its flexural capacity at a connection rotation of 0.00563 radians; and Model 1-3 reached its flexural capacity at a connection rotation of 0.005677 radians. These results show that, up to the point of flexural capacity, the three models have very similar behavior.

After the flexural capacity was surpassed for each model, the stiffness of the girder greatly decreased as the girder section began to yield at the connections due to the fixed supports as well as at the girder mid-span. Up to the prescribed connection failure rotation of 0.05 radians, the additional applied vertical load was being resisted by means other than flexural resistance of the member. Figure 4.4 shows the typical

stress contour at mid-span of the fixed support models just prior to the flexural capacity being reached, when the rotation stiffness is the highest. The higher stress concentrations at the girder connections can be seen in the figure, however the girder deflection and connection rotation is small. In comparison, Figure 4.5 shows the typical stress contour at mid-span of the fixed support models just after the flexural capacity is reached, at the initiation of the less stiff rotation behavior. Figure 4.5 shows that the stresses at mid-span of the girder are larger than in Figure 4.4 by plotting stresses at consistent contour intervals. In addition, the deflection corresponding to Figure 4.5 is also larger. It is the combination of these two behaviors that describe the noticeable change in rotation stiffness seen in Figure 4.3.

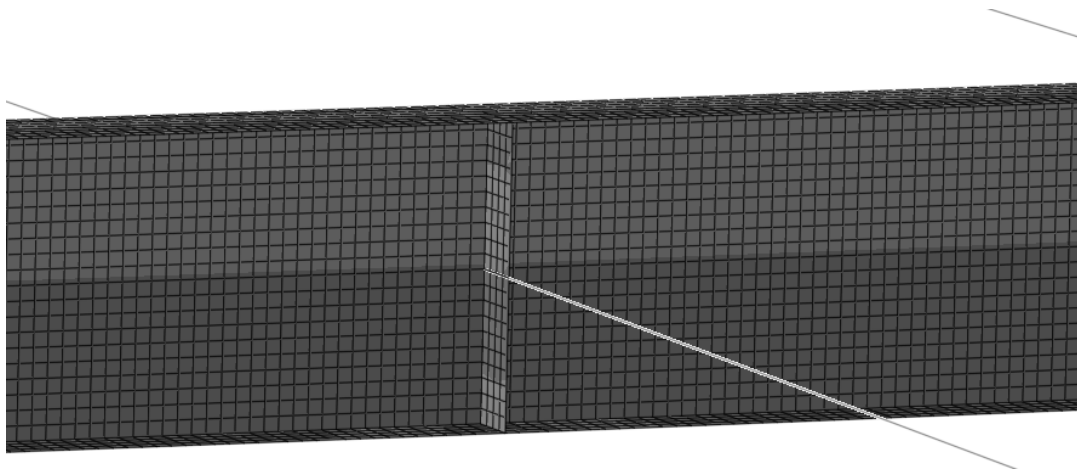


Figure 4.4. Fixed support girder prior to flexural capacity

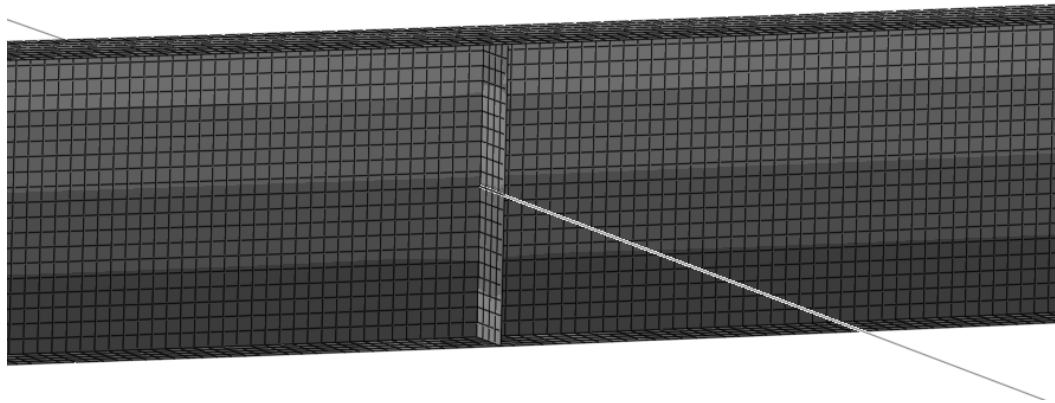


Figure 4.5. Fixed support girder after flexural capacity

The rotation limit for Model 1-1 was reached at an applied load of 212.8 kips, or 82.7% additional applied load past the flexural capacity of the girder. For Model 1-2, the rotation limit was reached at 210.8 kips, or 81.0% additional applied load. For Model 1-3, the rotation limit was reached at 210.6 kips, or 80.8% additional applied load. Looking at the maximum web stress values at a cross-section 324 inches from mid-span (12 inches from the support) at the rotation limit, Model 1-1 had a maximum stress of 76.6 ksi; Model 1-2 had a maximum stress of 75.8 ksi; and Model 1-3 had a maximum stress of 75.8 ksi. In comparison, the maximum flexural flange stress in Model 1-3 is 86.8 ksi at the rotation limit. All of these values substantially increased from the values at the flexural capacity, which were 49.8 ksi for Model 1-3. These stress values show that the model with both residual stresses and geometric imperfections had the highest maximum web stress value. These higher web stress values correlated to a larger ultimate applied load capacity. Thus, it is interesting that

the model with residual stresses and geometric imperfection displayed the highest capacity at the rotation limit.

The connection rotation versus applied load results for all three models is very similar, both prior to flexural capacity of the girder being reached and after. Model 1-1, however, had a 1.7% and 1.9% greater increase in ultimate applied load over Model 1-2 and Model 1-3, respectively. Therefore, the rotation versus applied load results for all three models show that the presence of a typical residual stress pattern and acceptable geometric imperfections does not have a significant effect on the flexural response of the steel girder nor the ultimate load at a connection rotation of 0.05 radians.

Figure 4.6 details the applied load versus connection rotation for Model 1-3 and Model 2-3. Several noticeable differences can be seen in the comparison graph shown in Figure 4.3 compared to the results observed in Figure 4.6. First, the stiffness of the two models is substantially different, both prior to and after the flexural capacity of the girders is reached. Additionally, Figure 4.6 shows that Model 1-3 is able to resist a larger percentage of applied load after its flexural capacity is reached but before its rotational capacity is reached compared to Model 2-3.

The connection stiffness of the two models was calculated for two sections of the load history: from the start of the analysis to the point when flexural capacity is reached; and from the flexural capacity to the point when the prescribed failure rotation of 0.05 radians was reached. The connection stiffness was calculated by measuring the linear slope between the two points. Up to the point when the flexural capacity of the girder is reached for Model 1-3, the connection rotation stiffness equaled 20516 kips per radian of connection rotation. For Model 2-3, the rotation

stiffness up to the point of flexural capacity equaled 2305 kips per radian of connection rotation.

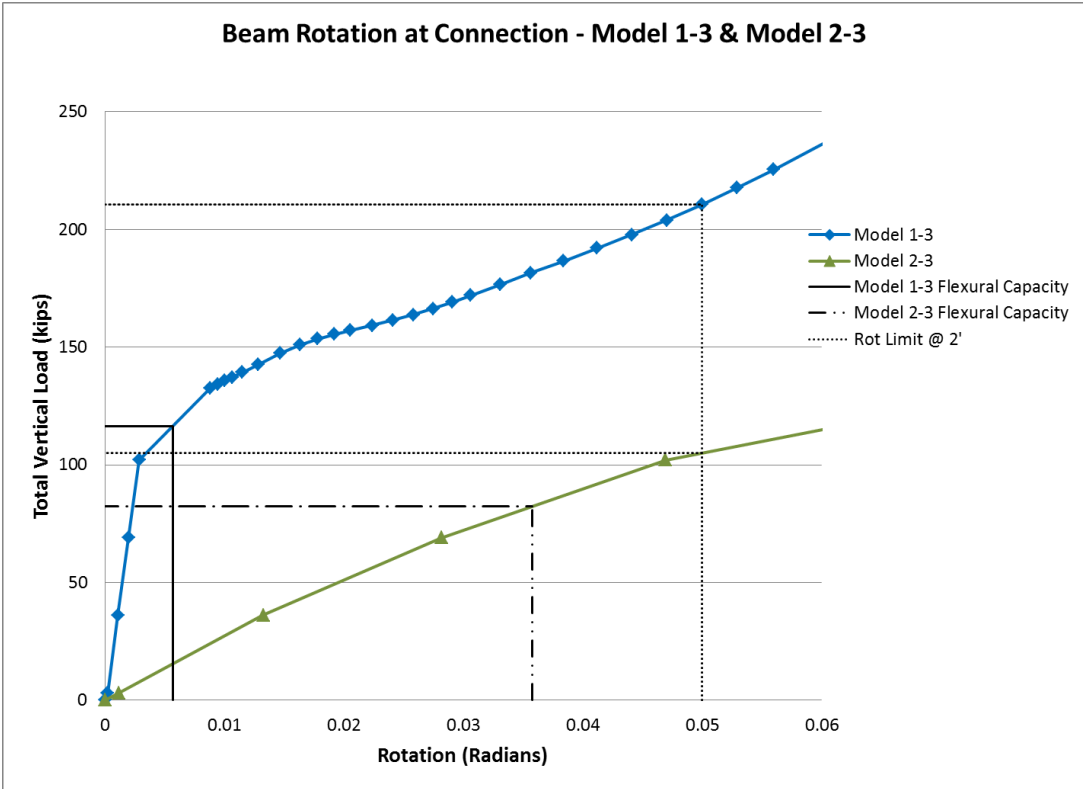


Figure 4.6. Load vs. connection rotation for Model 1-3 & Model 2-3

These results show that the fixed support model, Model 1-3, had a connection rotation stiffness 890% greater than the connection rotation stiffness for the shear connection support model, Model 2-3. This cannot be solely attributed to the difference in stiffness between fixed supports and shear supports. If the theoretical difference between a fixed support and a pinned support, representing the shear support, is taken as an extreme case, the fixed support model should have between 4

and 5 times greater stiffness depending on the loading pattern. In contrast, in the model, the results show extensive localized yielding and particularly strain at the support for Model 2-3 which leads to significantly increased vertical displacements.

After the flexural capacity of the girder is reached for Model 1-3, the connection rotation stiffness equaled 2119 kips per radian of connection rotation. For Model 2-3, the connection rotation stiffness equaled 1591 kips per radian of connection rotation. These results show that, after the flexural capacity is reached for both models, the connection stiffness becomes much more similar. This is attributed to the yielding of the cross-section in Model 1-3 at the support which then causes decreased moment resistance and greater similarity to the shear connection modeled in Model 2-3. The connection stiffness for Model 1-3 is only 33.2% greater than the connection stiffness for Model 2-3. The magnitude of the maximum tensile web stresses for these two models sheds light on the difference in slopes. At their respective flexural capacities, the maximum web stress at a cross-section at 28 inches for Model 2-3 is equal to 40.5 ksi while for Model 1-3, the maximum stress is 36.0 ksi. The higher stress value for Model 2-3 indicates that greater strain is necessitated, and thus greater deflections, at the connection compared to Model 1-3. This, in conjunction with the initially less stiff connection, is causing a smaller slope than for Model 1-3. At the rotation limit, the maximum stress at a cross-section at 28 inches for Model 2-3 is equal to 55.3 ksi while for Model 1-3, the maximum stress is 61.9 ksi. The more similar stress values for the two models at the rotation limit explains why the slopes of the graphs become similar.

Another observation that was made in comparing the load versus rotation for Model 1-3 versus Model 2-3 is that Model 2-3 eventually reached a point where the

load-carrying capacity plateaus. This occurs at an applied load of 210 kips. In contrast, Model 1-3 continues to show significant stiffness past the prescribed failure rotation of 0.05 radians.

As stated previously in this chapter, the flexural capacity for the girder in Model 1-3 is reached at an applied load of 116.5 kips. However, for Model 2-3, the flexural capacity of the girder is reached at an applied load of 82.5 kips. Model 1-3 reached its flexural capacity at a connection rotation of 0.005677 radians while Model 2-3 reached its flexural capacity at a connection rotation of .035793 radians. These results show that, up to the point of flexural capacity, the differences in connection stiffness between the two models are significant.

After the flexural capacity was surpassed for each model, the stiffness of the girder greatly decreased as quantified previously. The rotation limit for Model 1-3 was reached at 210.6 kips, or 80.8% additional applied load. While the previous research detailed in Chapter 2 dealt only with moment connections, the limiting rotation of 0.05 radians was used for Model 2-3 for comparison purposes. However, this value is likely too liberal considering the brittle failure modes that are possible to result in a simple shear connection. For Model 2-3, the rotation limit was reached at an applied load of 105.1 kips, or 27.4% additional applied load. The additional applied load resisted by Model 2-3 after its flexural capacity was reached was 53.4% less than the additional load resisted by Model 1-3. These quantitative data for the two models shows the significant post-flexural capacity strength of a fixed support girder compared to that of a shear support girder.

4.3 Percentage of Web Depth in Tension Results

In this section, the applied load versus percentage of web depth in flexural tension will be presented for the four analyzed models. The percentage of web depth in tension was calculated by dividing the number of web elements which reported any level of tensile stress by the total amount of web elements, equal to 20, for each load step and measuring the stresses in the longitudinal direction of the girder. Therefore, the values for web depth percentage in tension are in increments of 5%. The web was modeled using S4R shell elements with two through-thickness integration points. This stress output from these two integration points was averaged to determine if the web element was in tension. The cross-section locations analyzed in this thesis were labeled by their distance from the mid-span of the girder. Two of these cross-sections were located 324 inches from mid-span (12 inches from the support), and 28 inches from mid-span. These cross-sections were not located exactly at the support and mid-span due to the presence of the bearing stiffeners at those locations. Any potential distortion of results which may occur if the cross-section was taken directly at the stiffeners was desired to be avoided, although this problem was not observed in the results. The other cross-section was selected to be located near the inflection point of the girder. The location of this cross-section in terms of distance from the girder mid-span is 224 inches.

Additionally, the cross-sections were selected to be located throughout the regions of different flexural behavior for fixed support beams. Near the supports, the moment is negative with tensile stresses in the top half of the girder; while in the center of the girder, the moment is positive with tensile stresses in the bottom half of the girder. The behavior of the beam is symmetrical and therefore only one half of the beam was analyzed.

Prior to discussing the percentage of web depth in tension results, the von Mises stress distributions of the three fixed support models at the support prior to flexural capacity is reached are presented to give additional insight into the subsequent results. These distributions are shown in Figure 4.7, Figure 4.8, and Figure 4.9. The colors assigned to the contour intervals are consistent in all three figures. The flange stress values are similar for Model 1-1 and Model 1-2, however are lower for Model 1-3. This is due to the application of residual stresses in Model 1-1 and Model 1-2. In contrast, the web stress values are similar for Model 1-2 and Model 1-3, however are higher for Model 1-1. This is due to the presence of geometric imperfections in the girder for Model 1-1. As shown in the following graphs, Model 1-1 and Model 1-3 exhibit the most similar behavior while Model 1-2 tends to slightly deviate. This suggests that the presence of both geometric imperfections and residual stresses cause competing force effects that tend to cancel out one another.

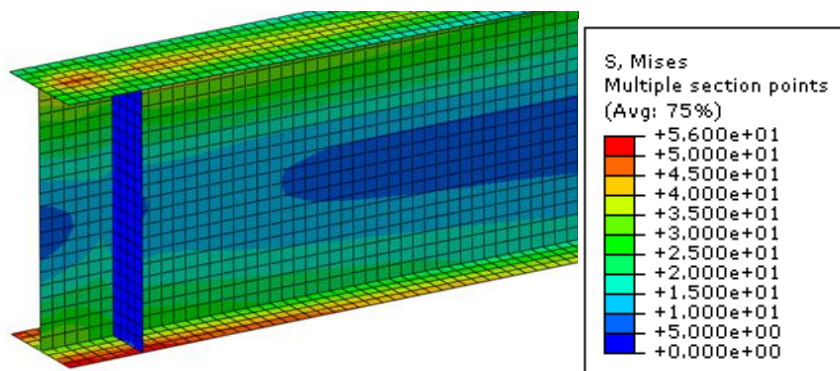


Figure 4.7. Model 1-1 stress distribution prior to flexural capacity

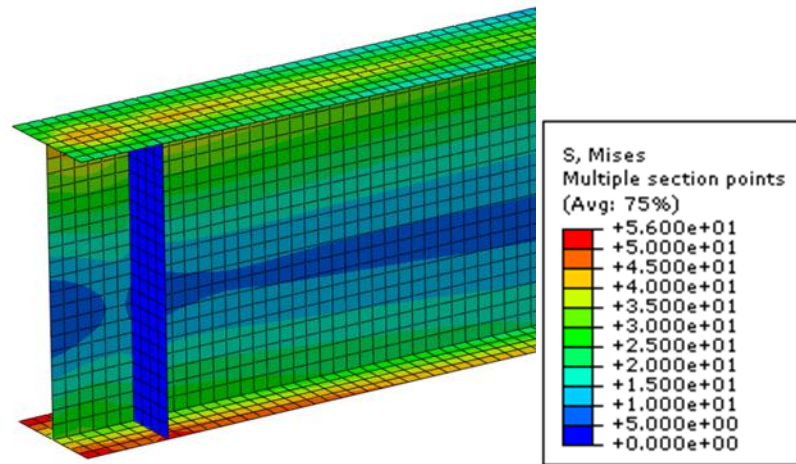


Figure 4.8. Model 1-2 stress distribution prior to flexural capacity

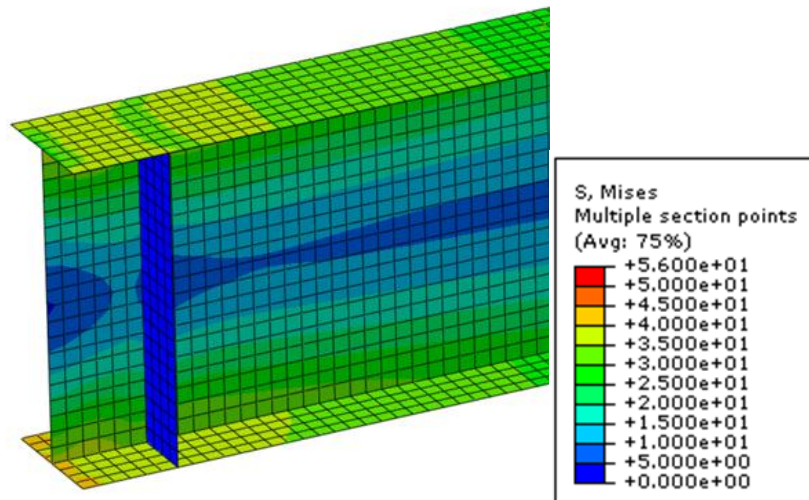


Figure 4.9. Model 1-3 stress distribution prior to flexural capacity

For the comparison graphs detailing the results of Model 1-1, Model 1-2, and Model 1-3, the three cross-sections are analyzed. The cross-sections located near the support and mid-span are analyzed due to their proximity to large applied and reaction

forces and resisting moments. The other cross-section analyzed is located at 224 inches from the end of the girder and is selected due to its proximity to the theoretical inflection point of the girders, where the moment should be approximately zero. For graphs comparing the three fixed support models, the applied load which caused a connection rotation of 0.05 radians was very similar. In order to avoid clutter in the graph and thus provide greater clarity, the average of the loads that caused a connection rotation of 0.05 radians (which vary very little from one another in these three models, as quantified in the previous section) was used for the reference point. Two graphs were created to compare the percentage web depth in tension results of Model 1-3 and Model 2-3. Since there is no inflection point for a girder with shear connection supports, the cross-section at 224 inches was not analyzed. Figure 4.10 shows the comparison of percentage web depth in tension for Model 2-3 at cross-sections located at 28 inches and 224 inches. As can be seen from Figure 4.10, the behavior is very similar and thus only the cross-section at 28 inches is analyzed further.

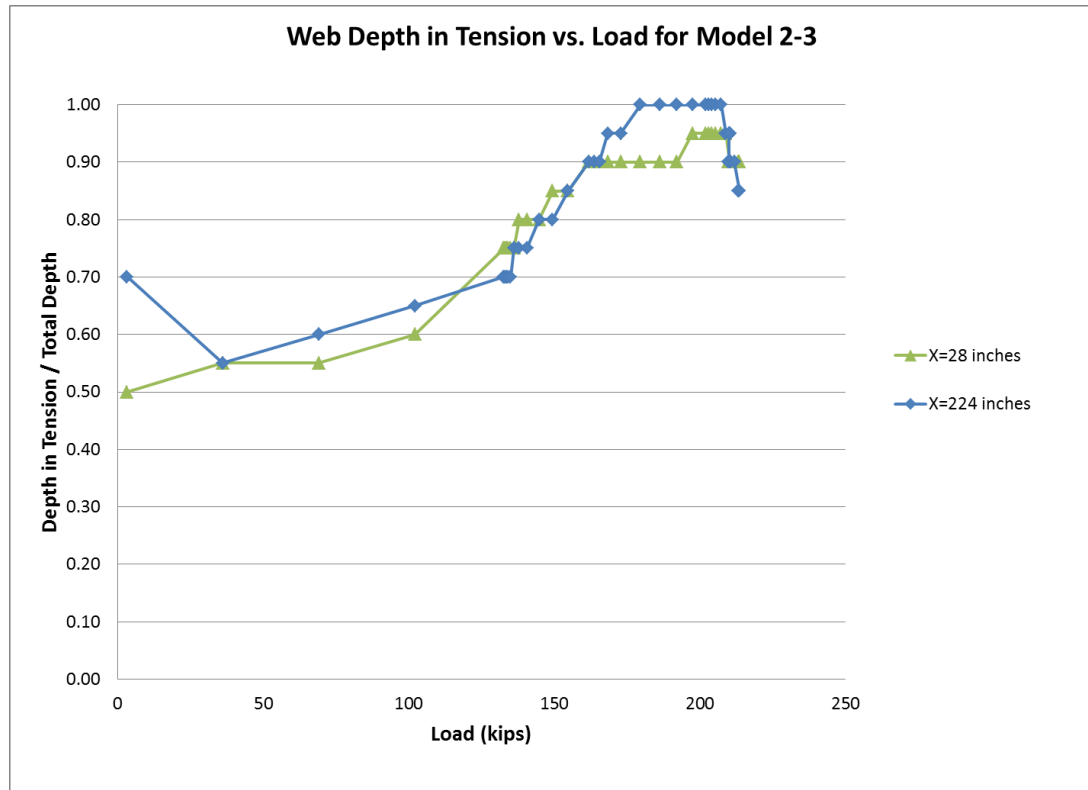


Figure 4.10. Load vs. web tension depth at 28 and 224 inches for Model 2-3

The beams which were modeled as lateral bracing supports were analyzed on a basic level to determine their stresses at the failure rotation. It was found that all of the lateral braces had between 7 ksi and 20 ksi of axial compression force at the failure rotation. These values show that the lateral bracing was clearly acting to resist the effects of lateral-torsional buckling in the girder, which was their intent.

4.3.1 Results of Cross-section at 28 Inches: Model 1-1 through Model 1-3

Figure 4.11 graphically depicts the percentage of the web depth in tension versus total applied vertical load at a cross-section 28 inches from mid-span to compare the results of Model 1-1, Model 1-2 and Model 1-3. Since Model 1-1 and

Model 1-2 utilized a residual stress pattern, the entire web depth began the analysis in uniform tension. This can be seen in Figure 4.11 with the majority of the web in tension during initial loading steps for the two models. Both Model 1-1 and Model 1-2 begin the analysis with 100% of their web depth in tension. While the entire depth of the web is initially in tension, the magnitude of this tension is relatively low, only 6.2 ksi. For Model 1-3, the lack of a residual stress pattern in the web causes the web to begin the analysis with 50% of its depth in tension, consistent with elastic flexural beam stresses.

During the initial load steps up to the point that flexural capacity is reached, the percentage of the web in tension varies for all three models but either remains at or begins to move towards an idealized flexural response of 50% of the web depth in tension. For Model 1-1 and Model 1-2, the web decreases to 60% of its depth in tension at an applied load of 132.7 kips. At the point when the flexural capacity of Model 1-1 and Model 1-2 was reached, 63% of the web was in tension. These initial results show the identical behavior of Model 1-1 and Model 1-2, and indicate that geometric imperfections have no impact on the percentage of the web depth in tension. The web depth for Model 1-3 remains consistently at 50% in tension, until the flexural capacity of the section is reached, at which point the web depth is 52% in tension based on interpolation of the available data. Since there are no residual stresses or geometric imperfections present in Model 1-3, it is logical that this value agrees well with beam flexure theory. Since the moment capacity for the girders is equal to the plastic moment of the girder, values of web depth in tension exceeding 50% are rational since the entire section is yielding at this point.

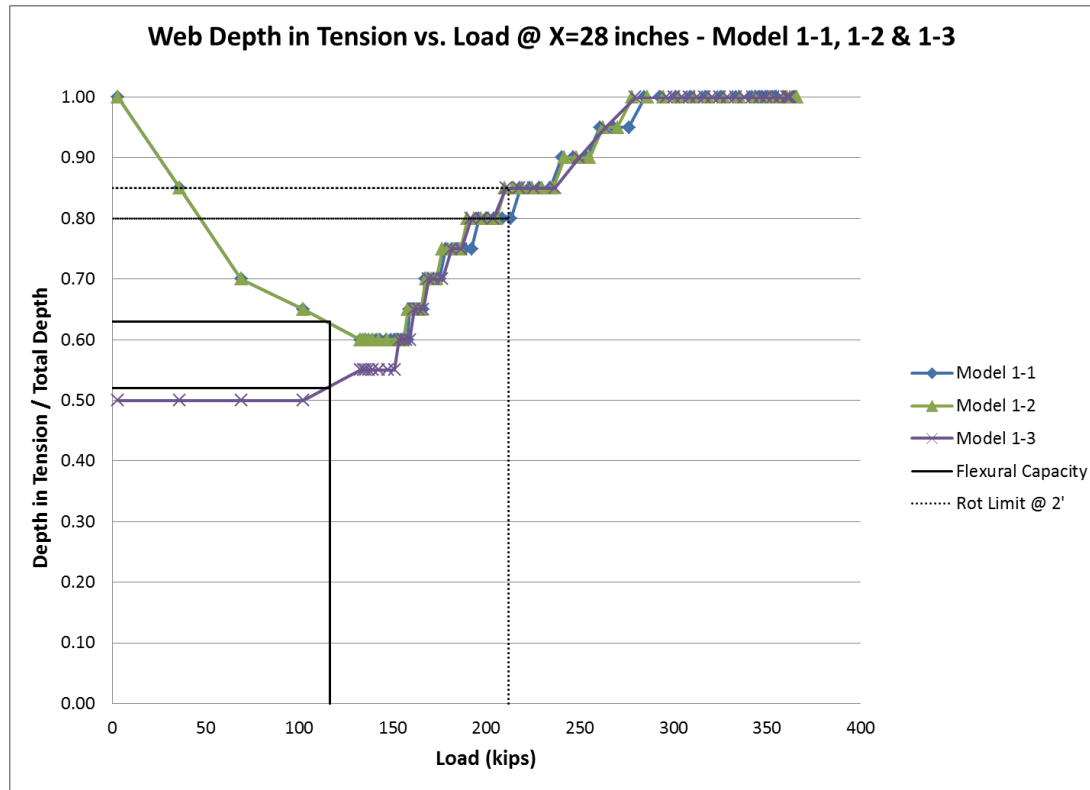


Figure 4.11. Load vs. web tension depth at 28 inches for Model 1-1, Model 1-2 & Model 1-3

After the flexural capacity of the girder was exceeded, the behavior for all three models reach a plateau and then begin to increase, demonstrating the transition to a catenary response. Between applied loads of 132.7 kips and 150.8 kips, the percentage of web depth in tension for all three models plateaued at specific, but slightly different, values. Model 1-1 and Model 1-2 plateaued at 60% web depth in tension, while Model 1-3 plateaued at 55% web depth in tension. After these plateau values, all three models exhibited very similar web depth percentage in tension values for the same applied load, up to the point when 0.05 radians of connection rotation was reached. For Model 1-1, when a rotation of 0.05 radians was reach at a point two

feet from the support, the percentage of the web in tension was 80%. For Model 1-2, when a rotation of 0.05 radians was reached at a point two feet from the support, the percentage of the web in tension was 85%, 5% greater web depth in tension than at the same failure rotation for Model 1-1.

These values for the three fixed support models at 28 inches show that the girders with no geometric imperfections utilized 5% more of its web depth in tension at the prescribed failure rotation of 0.05 radians. This may indicate that the presence of geometric imperfections, as in Model 1-1, slightly reduces the catenary behavior of a steel beam. After an applied load of 150.8 kips, the percentage of the web depth in tension for Model 1-3 drastically increased in a manner similar to the previous two analyzed models. For Model 1-3, when a rotation of 0.05 radians was reached at a point two feet from the support, the percentage of the web in tension was 85%. This is 5% greater than for the same location in Model 1-1, but is equal to the value found in Model 1-2.

Figure 4.11 shows that, for all three models with fixed supports, the girder can utilize between 80% and 85% of its web in tension near mid-span when extreme loads are applied up to a failure connection rotation of 0.05 radians. These results indicate that the girder for all three models was resisting the additional applied vertical load in a catenary manner. That is, the girder was behaving like a cable resisting the large concentrated loads after the girder's flexural capacity was exceeded. The results of these three models at a cross-section 28 inches from mid-span show the minor but noticeable increase in web depth in tension for steel girders with no geometric imperfections, as in Model 1-2 and Model 1-3. The 5% lower value of web depth in tension for Model 1-1 compared with the other two models again could likely be due

to the local instabilities caused by web out-of-planeness, causing localized buckling and compressive stresses in the web elements. However, at an applied load of 218.0 kips which corresponds to a connection rotation of 0.052 radians, the percentage of web depth in tension for Model 1-1 increases to 85% which is equal to the values for Model 1-2 and Model 1-3. The agreement in values for Model 1-2 and Model 1-3 show residual stresses have no effect on the ultimate percentage of web depth in tension values. For all three analyzed models, the results indicate that the beam was resisting the additional applied vertical load in a catenary manner. The drastic increase in percentage of web depth in tension after the beam's flexural capacity is surpassed indicates the clear initiation of catenary behavior as a load-resisting mechanism.

4.3.2 Results of Cross-section at 224 Inches: Model 1-1 through Model 1-3

Figure 4.12 graphically depicts the percentage of the web depth in tension versus total applied vertical load at a cross-section 224 inches from mid-span to compare the results of Model 1-1, Model 1-2 and Model 1-3. It can clearly be seen that the web depth in tension behavior for the three models differs at this cross-section compared to the cross-section at 28 inches. The difference between the values in Figure 4.11 and Figure 4.12 is due to differences in stress distribution between the two locations due to the proximity of the cross-section at 224 inches to an inflection point of the girder. The theoretical inflection point for girder with fixed supports and a series of equal magnitude concentrated loads is approximately 9.8 feet, or 216 inches, away from mid-span. This is only 6 inches away from the cross-section at 224 inches. The maximum magnitude of stresses for the three analyzed models at cross-

sections of 28 inches and 224 inches show that a difference in stress distribution does exist between these two locations.

Again, since Model 1-1 and Model 1-2 utilized a residual stress pattern, the entire web depth began the analysis in uniform tension. This can be seen in Figure 4.12 with the entire web in tension during initial loading steps for the two models. In fact, the behavior of Model 1-1 and Model 1-2 are identical for the entire load history at a cross-section at 224 inches. Similar to the results of Model 1-3 in Figure 4.11, the lack of a residual stress pattern in the web can be seen in Figure 4.12; as the web begins the analysis with 50% of its depth in tension, consistent with elastic flexural beam stresses.

During the initial load steps up to the point that flexural capacity is reached, the percentage of the web in tension is identical for Model 1-1 and Model 1-2, which differed from the behavior of Model 1-3. Almost the entire load history for Model 1-1 and Model 1-2 shows that the percentage web depth in tension is at 100%. However, the web depth percentage in tension fell to 95% for one load step for Model 1-1 and Model 1-2. When the flexural capacity is reached for the girder in Model 1-1 and Model 1-2, the web depth in tension is interpolated as being equal to 97% compared to the 60% at the same point in Figure 4.11. The behavior of Model 1-3, as seen in Figure 4.12, differs from that of Model 1-1 and Model 1-2 and differs from the behavior of Model 1-3 seen in Figure 4.8. The girder starts the analysis at 50% of its web depth in tension but increases to 64% in tension when the flexural capacity is reached. Again, this lower value compared to Model 1-1 and Model 1-2 is due to the lack of residual stresses in Model 1-3.



Figure 4.12. Load vs. web tension depth at 224 inches for Model 1-1, Model 1-2 & Model 1-3

After the flexural capacity of the girder was exceeded, the behavior for Model 1-1 and Model 1-2 was again identical but slightly different for Model 1-3 in that a lower percentage of the cross-section was in tension in the latter case. For Model 1-1 and Model 1-2, the percentage web depth in tension increased back to 100% at an applied load of 132.7 kips and remained at 100% for the rest of the load history. After the flexural capacity for Model 1-3 was reached, the percentage web depth in tension values drastically increased until reaching 100% at an applied load of 139.2 kips, 6.5 kips more than for Model 1-1 and Model 1-2. Again, this is due to the initial tensile residual stresses in the webs of Model 1-1 and Model 1-2. Similar to Model 1-1 and

Model 1-2, the web depth in tension values for Model 1-3 remained at 100% for the remainder of the load history after an applied load of 139.2 kips. These results show that the impact of geometric imperfections at this cross-section is again insignificant, similar to the cross-section at 28 inches. The much higher values of web depth in tension at a cross-section at 224 inches compared to 28 inches is due to the different stress distribution attributed to the proximity of this cross-section to the inflection point of the girder.

Figure 4.12 shows that, for all three models with fixed supports, the girder can utilize 100% of its web in tension near its inflection point when extreme loads are applied up to a failure connection rotation of 0.05 radians. However, this high percentage of web depth in tension is due to the proximity of the cross-section at 224 inches to the inflection point of the girder. The magnitude of tensile stresses at this cross-section is significantly lower than for the cross-section at 28 inches. However, these results still indicate that the girder for all three models was again resisting the additional applied vertical load in a catenary manner.

4.3.3 Results of Cross-section at 324 Inches: Model 1-1 through Model 1-3

Figure 4.13 graphically depicts the percentage of the web depth in tension versus total applied vertical load at a cross-section 324 inches from mid-span (12 inches from the support) to compare the results of Model 1-1, Model 1-2 and Model 1-3. The behavior of the three models at this cross-section exhibits behavior very similar to the models at a cross-section at 28 inches from mid-span.

Again, since Model 1-1 and Model 1-2 utilized a residual stress pattern, the entire web depth began the analysis in uniform tension. This can be seen in Figure 4.13 with the majority of the web in tension during initial loading steps for the two

models. The web begins the analysis at 100% in tension for both Model 1-1 and Model 1-2, identical to the behavior exhibited at a cross-section of 28 inches and a cross-section at 224 inches. Similar to the behavior at a cross-section at 28 inches, the behavior of Model 1-1 and Model 1-2 is identical to each other to the point when flexural capacity is reached. Model 1-3 exhibits identical behavior when compared to the results at a cross-section at 28 inches prior to flexural capacity being reached. Compared to Figure 4.11, the percentage web depth in tension results for Model 1-1 and Model 1-2 decrease more quickly in the initial loading stages. This is due to the cross-section at 324 inches being located near the support where the moment in a fixed support girder is highest. Similar to the results of the other two analyzed cross-sections, Figure 4.13 shows that geometric imperfections have no effect on percentage web depth in tension results.

After the initial load steps and up to the point that flexural capacity is reached, the percentage of the web in tension was again identical for Model 1-1 and Model 1-2, which differed from the behavior of Model 1-3. Similar to Figure 4.8, for Model 1-1 and Model 1-2, the web depth in tension gradually decreases until the flexural capacity is reached. When the flexural capacity is reached for Model 1-1 and Model 1-2, the web depth in tension is equal to 55% compared to 63% at the same point in Figure 4.8 and 97% in Figure 4.9. The percentage web depth in tension values for Model 1-1 and Model 1-2 when the flexural capacity is reached are identical and show that for this cross-section, the effects of geometric imperfections are insignificant. The behavior of Model 1-3, as seen in Figure 4.10, differs from that of Model 1-1 and Model 1-2 but is identical to the behavior of Model 1-3 seen in Figure 4.8 prior to the flexural capacity being reached. The girder remains at 50% of its web depth in tension until the flexural

capacity is reached, at which point 52% of the web depth is in tension. Again, this lower value compared to Model 1-1 and Model 1-2 is due to the lack of residual stresses in Model 1-3. However, this value is identical to the value of 52% for Model 1-3 at the flexural capacity at a cross-section of 28 inches but differs from the 64% value for the cross-section at 224 inches.

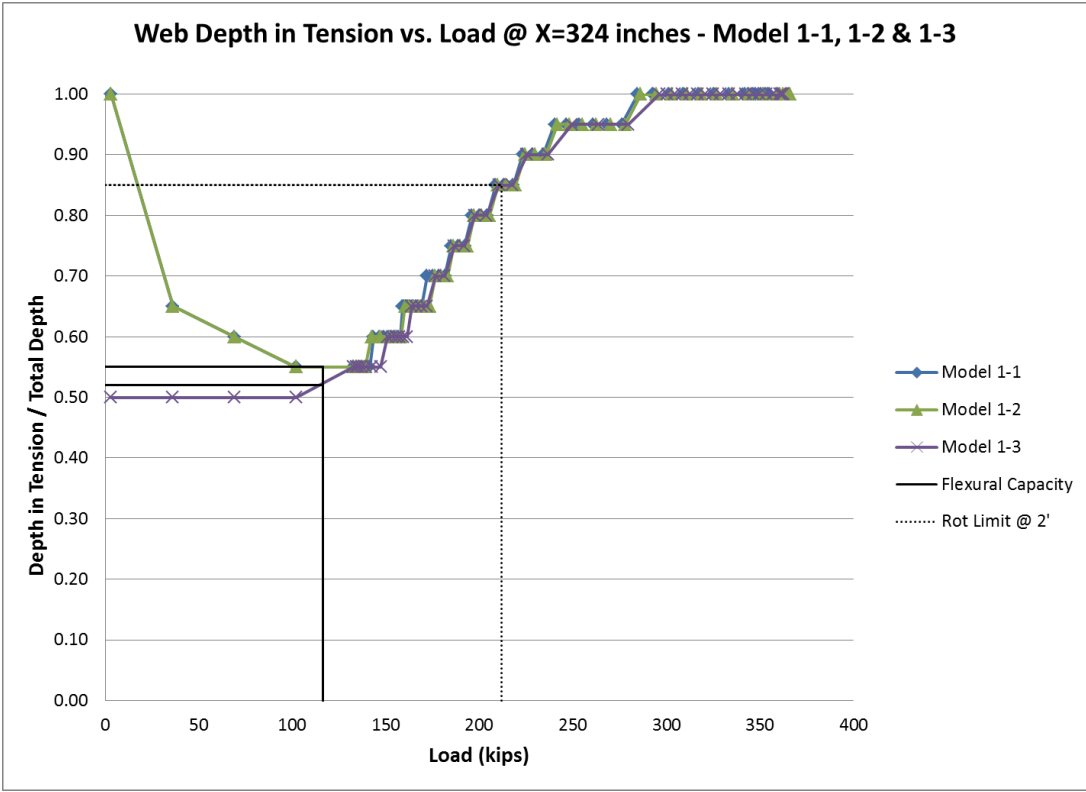


Figure 4.13. Load vs. web tension depth at 324 inches for Model 1-1, Model 1-2 & Model 1-3

After the flexural capacity of the girder was exceeded, the behavior for the three models was similar to that in Figure 4.11. However, unlike in Figure 4.11, the

values for Model 1-1 and Model 1-2 plateaued at between 55% and 60% compared to 60% seen in Figure 4.11 for applied loads between 135.7 kips and 161.3 kips. The web depth in tension values for Model 1-3 again plateaued at 55% between applied loads of 135.7 kips and 161.3 kips, similar to the cross-section at 28 inches. After an applied load of 161.3 kips, the behavior for the three models was very similar, much like that in Figure 4.11. The web depth percentage values for all three models continuously increased until the prescribed limiting connection rotation of 0.05 radians was reached. Unlike the results at a cross-section at 28 inches, but similar to the cross-section at 224 inches, all three models had the same web depth percentage in tension values when a rotation of 0.05 radians was reached at a point two from the support. For all three models, 85% of the web depth was in tension at this point. This value is 5% greater for Model 1-1 compared to the cross-section at 28 inches, but identical for Model 1-2 and Model 1-3 compared to the same cross-section. While the value of 85% for percentage web depth in tension is less than the 100% detailed at a cross-section at 224 inches, the magnitude of stresses at this analyzed cross-section is much higher.

The results of Figure 4.13 show that geometric imperfections and residual stresses have a negligible effect on the final web depth in tension values for the three models. The difference in the results of the three cross-sections for all models could be attributed to the different stress distributions at each cross-section. The cross-section at 28 inches is located in the negative moment region of the girder; the cross-section at 224 inches is located near the inflection point of the girder; and the cross-section at 324 inches is located in the positive moment region of the girder. Again, Figures 4.11 through 4.13 show that the behavior of the girder varies at different locations along the

girder, even for the same applied load. The values in Figure 4.11 through Figure 4.13 also show that the effect of residual stresses differs depending on the cross-section location, but that geometric imperfections have an insignificant effect on the percentage web depth in tension values.

Using Model 1-2 as a representative girder, the maximum tensile web stress at a cross-section at 224 inches was 12.8 ksi for the load step immediately after the flexural capacity was reached. The initial tensile residual stress pattern of 6.2 ksi contributes to the overall stress values comprising nearly 50% of the maximum tensile stress value of 12.8 ksi. In contrast, the maximum tensile web stress at a cross-section at 324 inches (12 inches from the support) was 54.8 ksi and at a cross-section at 28 inches from mid-span was 43.6 ksi at the same load step. Therefore, while the percentage web depth in tension is near 100% for the entire load history at a cross-section at 224 inches the overall stresses are much lower than near the connection and mid-span.

The results of Figure 4.13, as well as Figure 4.11 and Figure 4.12, show that, for all three models with fixed supports, the girder is utilizing catenary behavior after its flexural capacity is reached. All three graphs show that the percentage of web depth in tension initially indicates the girder is behaving in a manner consistent with flexural beam theory. After the flexural capacity is reached for each model, the web depth percentage in tension values begin to markedly increase up to the point of prescribed connection rotation failure. This consistent behavior clearly exhibits the utilization of catenary action in all three of the models analyzed in order to resist extreme loads. While the presence of residual stresses and geometric imperfections do indeed provide different values for the percentage web depth in tension, that data does

not indicate that there are any clearly defined detrimental effects due to their presence. All three of the analyzed models show the ability to resist an additional 80.8% to 82.7% of applied load after the flexural capacity of the girder is reached.

4.3.4 Results of Cross-section at 28 Inches: Model 1-3 and Model 2-3

Figure 4.14 graphically depicts the percentage of the web depth in tension versus total applied vertical load at a cross-section 28 inches from mid-span to compare the results of Model 1-3 and Model 2-3. This comparison graph was constructed to highlight the differences between a girder with fixed supports and one with shear connection supports for a cross-section located near the girder mid-span. The reference lines labeled ‘Model 1-3 Flexural Capacity’ and ‘Model 2-3 Flexural Capacity’ correspond to the load and percentage web depth in tension which causes the flexural capacity of the stated model to be reached. Similarly, the reference lines labeled ‘Model 1-3 Rot Limit @ 2’’ and ‘Model 2-3 Rot Limit @ 2’’ correspond to the load and percentage web depth in tension which causes the prescribed connection failure rotation of 0.05 radians of the stated model to be reached.

Both Model 1-3 and Model 2-3 were analyzed without geometric imperfections or a residual stress pattern. The lack of a residual stress pattern can be seen in the initial load steps for both models, as the percentage of web depth in tension begins the analysis at 50%. However, while Model 1-3 remains at 50% of its web depth in tension for several load steps, Model 2-3 increases to 55% of its web depth in tension at an applied load of 36.1 kips. When the flexural capacity of Model 2-3 is reached, at an applied of 82.5 kips, the percentage of the web depth in tension is 57%. Figure 4.15 graphically shows Model 2-3 when its flexural capacity is reached. The high stresses and stress concentrations can be seen at the location of the modeled bolts

at the end of the girder. Additionally, the stress magnitude is shown to decrease at the cross-section at 28 inches from the support. While 57% of the web depth is in tension, the average tensile stress at 28 inches is 40.5 ksi showing that the cross-section at 28 inches from mid-span has not fully yielded at this point.

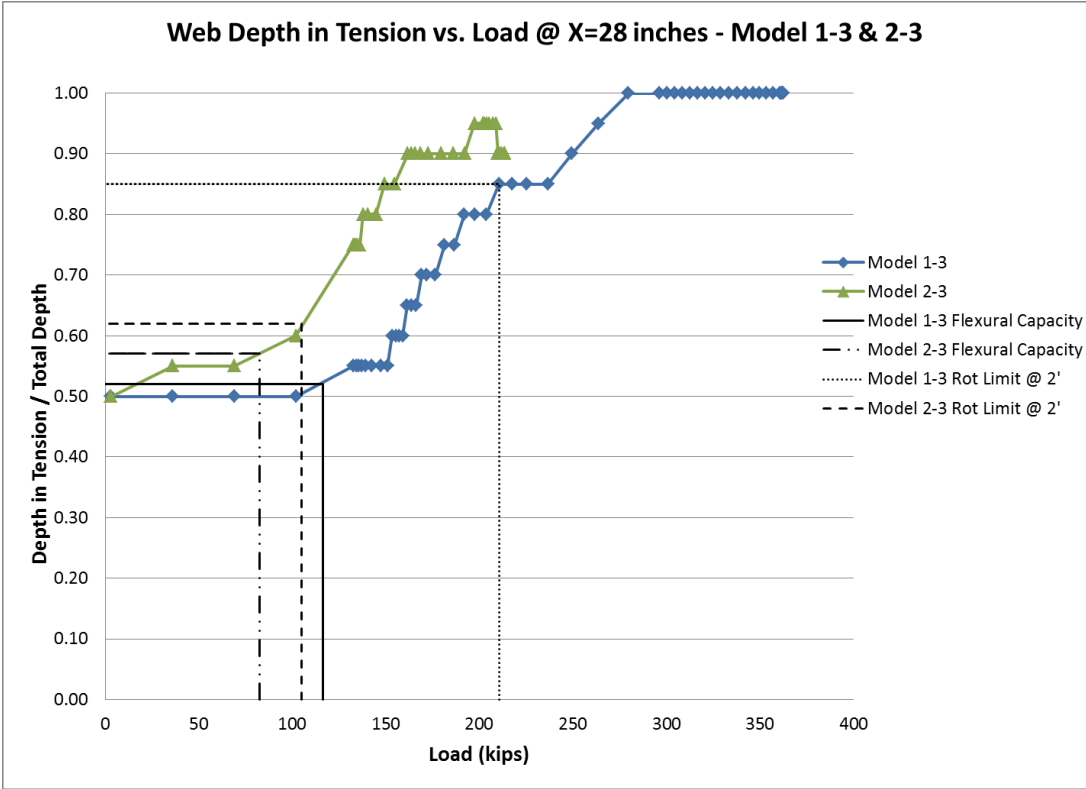


Figure 4.14. Catenary comparison of Model 1-3 and Model 2-3 at 28 inches

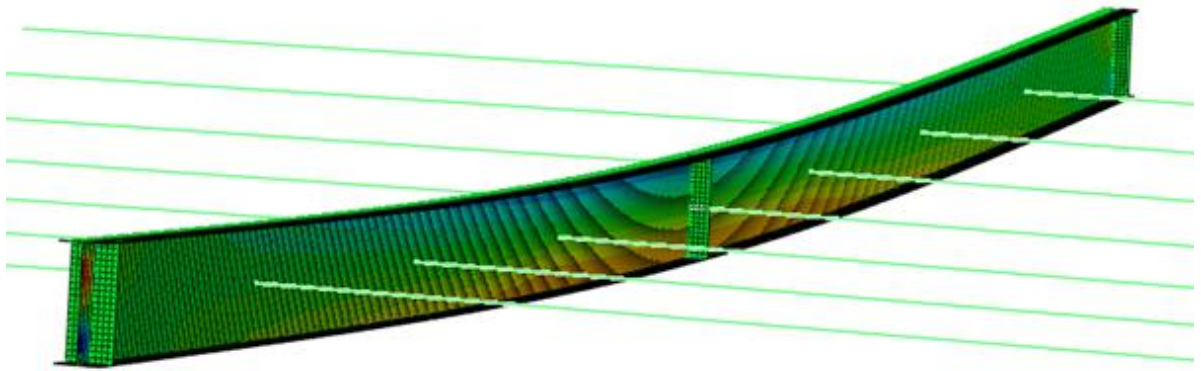


Figure 4.15. Model 2-3 at flexural capacity

When the flexural capacity of Model 1-3 is reached, at an applied load of 116.5 kips, the percentage of its web depth in tension is equal to 52%. In Section 4.2, the rotation of Model 2-3 was shown to be 0.035793 radians when flexural capacity was reached compared to 0.005677 radians for Model 1-3. This much greater connection rotation in Model 2-3 is likely causing the tensile stresses in the web to increase at an earlier load than in Model 1-3 due to localized yielding near the connection.

After the flexural capacity of the girder is reached for Model 2-3, the percentage web depth in tension increases similar to the previous results discussed for the fixed support models. However, the rotation limit is reached before significant catenary action develops. When a rotation of 0.05 radians was reached at a point two feet from the support, the percentage of the web in tension was 62%. The 62% depth of web in tension is significantly lower than for the same cross-sections in the fixed support models. The decrease in percentage web depth in tension at the end of the loading history in Figure 4.14 is due to extreme elongation and (unrealistically high) strain at the location of the modeled bolt supports in the later load history of the model. However, this behavior occurs well after the rotation limit had been

reached. In contrast, when the prescribed connection failure rotation for Model 1-3 was reached, the percentage of web depth in tension was 85%. As was detailed previously, Model 1-3 was able to resist 80.8% additional applied load after the girder's flexural capacity was reached compared to only 27.4% for Model 2-3.

4.3.5 Results of Cross-section at 324 Inches: Model 1-3 and Model 2-3

Figure 4.16 graphically depicts the percentage of the web depth in tension versus total applied vertical load at a cross-section 324 inches from mid-span (12 inches from the support) to compare the results of Model 1-3 and Model 2-3. This comparison graph was constructed to highlight the differences between a girder with fixed supports and one with shear connection supports for a cross-section located 12 inches away from the girder support.

The results of Figure 4.16 show very similar behavior for both models as detailed in Figure 4.14 for the cross-section at 28 inches. Again, the lack of a residual stress pattern can be seen in the initial load steps for both models, as the percentage of web depth in tension begins the analysis at 50%. The behavior for Model 1-3, prior to flexural capacity being reached, is identical at this cross-section as it was for the cross-section at 28 inches. However, the percentage web depth in tension for Model 2-3 increases more rapidly than in Figure 4.14. The magnitude of tensile web stresses at cross-sections at 28 inches and 324 inches show that, while a higher percentage of web elements are in tension at a cross-section at 324 inches, the maximum tensile stress value at the rotation limit is 25.5 ksi compared to 55.3 ksi for a cross-section at 28 inches at the rotation limit. When the flexural capacity of Model 2-3 is reached the percentage of the web depth in tension is 64% compared to 57% for the cross-section at 28 inches. Again, the lower connection stiffness for Model 2-3 is likely causing the

tensile stresses in the web to increase at an earlier load than in Model 1-3 due to localized yielding near the girder support.

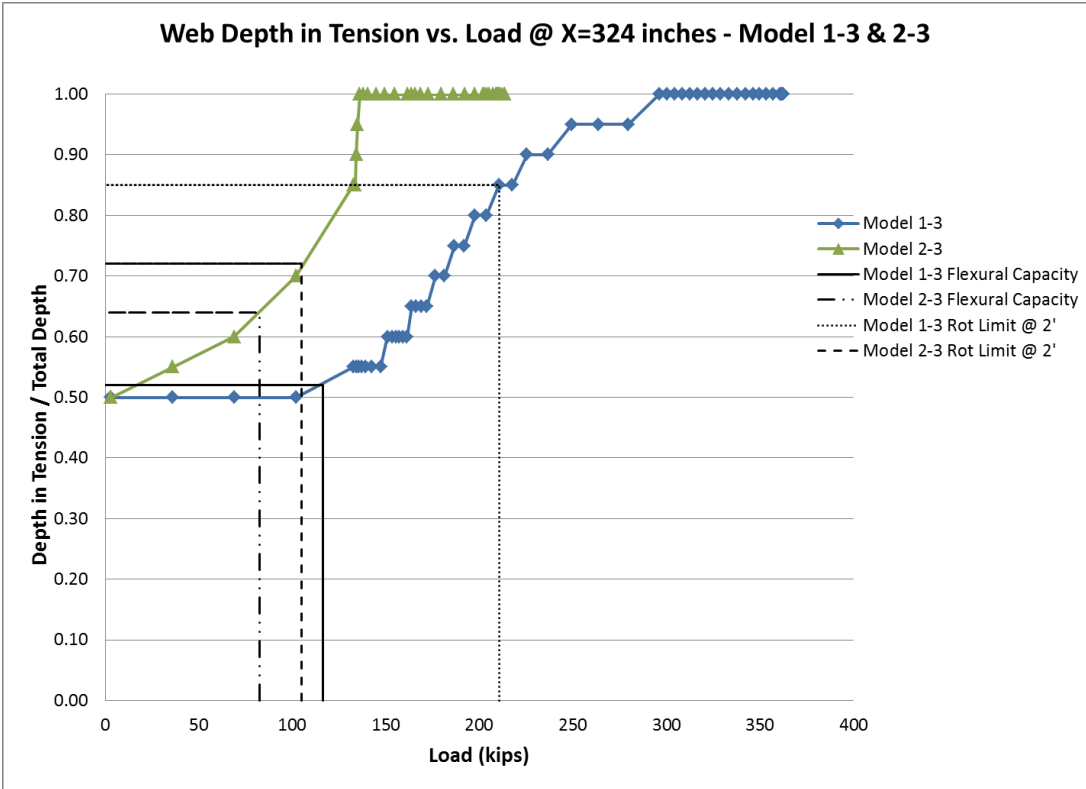


Figure 4.16. Catenary comparison of Model 1-3 and Model 2-3 at 324 inches

After the flexural capacity of the girder is reached for Model 2-3, the percentage web depth in tension increases more rapidly than seen in Figure 4.14 for the cross-section near mid-span. When a rotation of 0.05 radians was reach at a point two feet from the support for Model 2-3, the percentage of the web in tension was 72% compared to 62% for cross-section at 28 inches. This increase of 10% in percentage of web depth in tension at mid-span of the girder is likely due to the

localized yielding in the girder near the support. When the prescribed connection failure rotation for Model 1-3 was reached, the percentage of web depth in tension was 85%, identical to the value obtained for the cross-section near mid-span, previously shown in Figure 4.14.

As was detailed previously, Model 1-3 was able to resist an 80.8% increase in applied load after the girder's flexural capacity was reached compared to only 27.4% for Model 2-3. These two conclusions show that shear connections are not nearly as efficient as fixed supports to develop catenary behavior based on the connection rotation limit utilized herein. This is in part due to the additional stiffness for a fixed support girder compared to one with a shear connection support, which results in less rotation for a given level of load. Additionally, there is less redundancy of the shear connection model compared with the fixed connection model. This means that the collapse mechanism needed for a shear support girder involves the formation of one plastic hinge, while the collapse mechanism for a fixed support model requires three plastic hinges. Therefore, at least for a cross-section near the connection, a fixed support girder will develop substantially more of its web depth in tension compared to shear connection girder. The results presented herein support this theoretical behavior in that it was shown above that 72% of the web depth is in tension at the rotation limit for the simulated shear connection while 85% of the web depth is in tension at the rotation limit for the simulated fixed connection.

The results of the four models presented in this section show very clear and distinct results regarding catenary behavior. First, moment connections are vastly superior over shear connections in utilizing catenary action after flexural capacity is reached. The results showed that between 80.8% and 82.7% more applied vertical

load can be resisted by a steel beam after its flexural capacity is reached. The load versus percentage of web depth in tension graphs quantitatively showed that this increased capacity is predominantly due to catenary behavior in the beam in addition to the type of girder connection used. The ductile nature of steel, modeled using nonlinear material behavior, is also likely a contributing factor to the increased load-carrying capacity shown in the models. Figure 4.17 graphically shows the typical fixed support model at the prescribed failure rotation of 0.05 radians. As described previously, the behavior of the girder is symmetric about the mid-span and therefore only half of the girder is shown in Figure 4.17. The stress distribution change throughout the length of the girder can be clearly seen, as well as the large stress concentrations at the supports and mid-span. Specifically, at the supports and at mid-span of the girder, 80% of the web depth experiences stresses greater than 55 ksi at the failure rotation. Thus, it can be concluded that the ductility of the steel facilitates the large increase in additional load-carrying capacity after the flexural capacity is reached. In the following section, the connection forces of these supports will be quantified. This is a necessary consideration in order to design connections to resist the large axial loads generated via catenary action.

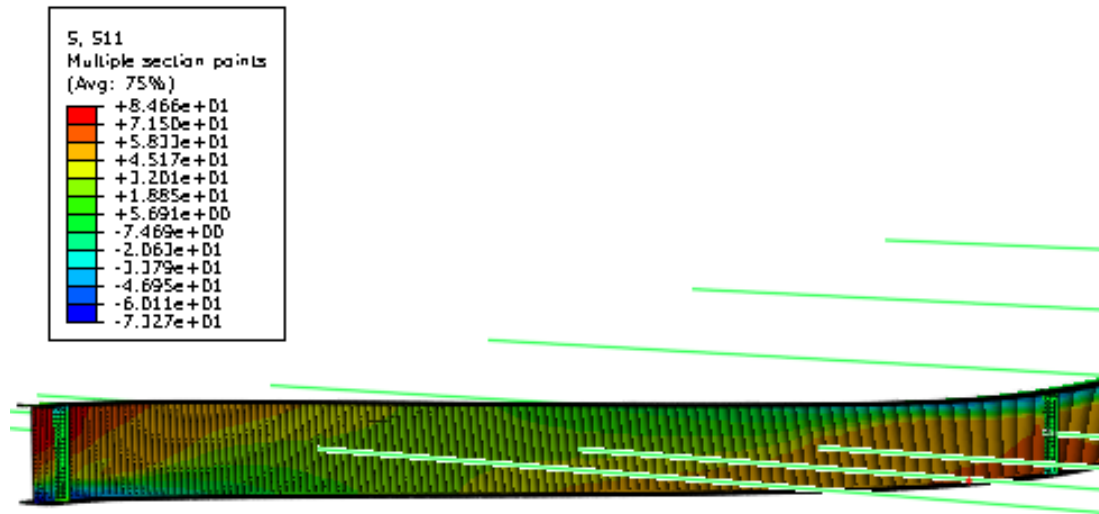


Figure 4.17. Fixed support beam at failure rotation

4.4 Connection Force Results

The previous section of this chapter provides supporting data for the potential for steel beams to resist extreme loads through the use of catenary behavior. Data was quantitatively analyzed to show the percentage of catenary action utilized in various models versus the applied vertical load. However, an equally important parameter that is needed in order to design a steel structure for the potential to use catenary behavior is the applied axial and vertical forces at the connections of the steel beams. Both the connections and the supporting columns must be robust enough to resist the resulting vertical, shear and moment forces imparted on them by the steel beam.

In this section, the connection force results of the models previously discussed will be presented. For each analyzed model, a graph was created of the axial force at the support versus the connection rotation, based on the rotation over a length of 24 inches from the support as well as a graph of the axial force at the support versus total applied vertical load. The axial force at the connection is obtained by summing the

total reaction forces of the support nodes in the longitudinal direction of the girder. Similar to the graphs presented in Section 4.3, several reference points were plotted on the graphs. For each graph, the flexural capacity of the steel girder was plotted as well as the vertical load which caused a rotation of 0.05 radians 2 feet from the support. These reference points were used to graphically display the additional capacity of the member after its flexural capacity is reached.

4.4.1 Connection Force Results: Model 1-1 through Model 1-3

Figure 4.18 details the girder rotation at two feet versus axial connection force for Model 1-1, Model 1-2 and Model 1-3. Several initial observations are apparent in Figure 4.18. As can be seen, there is a substantial increase in axial connection force between the two reference points: flexural capacity of the beam; and rotation limit at a location two feet from the support. This result shows that connection design for flexural capacity of a girder would not be adequate to resist the very large axial connection forces at the prescribed failure rotation of 0.05 radians. Also, the graph shows that the slope of the plot for each of the three models varies during the loading history, increasing more rapidly as catenary action and rotation increase. Lastly, the behavior of the all three fixed support models is very similar throughout the loading history, but Model 1-1 results in the greatest axial force in the girder.

For the three models, the initial slopes of the plots are all similar until a rotation of 0.003 radians is reached. After a rotation of 0.003 radians, the slopes of the models slightly level off. Figure 4.4 and Figure 4.5 respectively show the behavior of the fixed support girders just prior to and after a rotation of 0.003 radians reached, the last load step before the flexural capacity is exceeded. The difference in magnitude of stress between the two figures is apparent. The increase in proportion of stresses at

mid-span indicates that the girder has yielded at the support, causing a redistribution of load towards mid-span. This yielding results in the leveling off seen in Figure 4.18 between rotations of 0.005 and 0.015 radians, similar to that seen in Figure 4.3. After several load steps, the slopes of the plots all begin to increase and eventually become linear prior to the prescribed failure rotation of 0.05 radians being reached. Specifically, between a rotation of 0.025 and 0.05 radians, the average R-squared value for the three data series shown in Figure 4.18 is 0.9995. This is likely due to the catenary behavior of the girders being utilized, resulting in increased kips of axial connection force per radian of rotation.

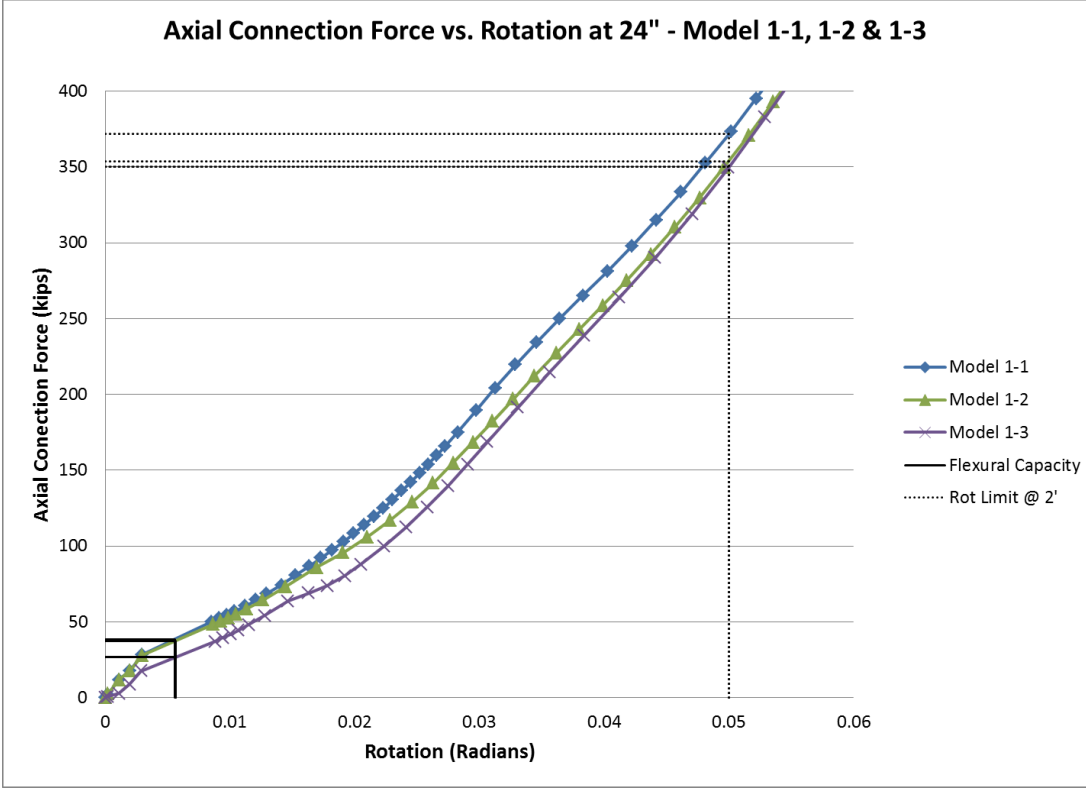


Figure 4.18. Axial connection force vs. rotation comparison of Model 1-1, Model 1-2 & Model 1-3

For Model 1-1, when the flexural capacity of the girder is reached, the rotation at two feet from the support is 0.00560 radians with a corresponding axial connection force of 38.5 kips. For Model 1-2, when the flexural capacity of the girder is reached, the rotation at two feet from the support is 0.00563 radians with a corresponding axial connection force of 37.4 kips. When the flexural capacity of the girder is reached for Model 1-3, the rotation at two feet from the support is 0.005677 radians with a corresponding axial connection force of 26.6 kips. These results show that the model with residual stresses and geometric imperfections imposed 2.9% more axial connection force than the model with only residual stresses but no geometric imperfections; and 44.7% more axial connection force than the model with no residual stresses and no geometric imperfections. This suggests that at flexural load levels, residual stresses significantly increase the axial force, and geometric imperfections slightly increase the axial force. Furthermore, while these magnitudes are not insignificant forces, axial load on connections is typically not considered in building design practices for beams and girders under gravity load.

At the prescribed connection failure rotation of 0.05 radians, the axial connection force in Model 1-1 was 371.6 kips. This constitutes a 965% increase in axial connection force over the connection force at the flexural capacity of the member. For Model 1-2, at the connection rotation limit of 0.05 radians, the axial connection force is 353.8 kips. This constitutes a 946% increase in axial connection force over the connection force at the flexural capacity of the member. Compared to Model 1-1, Model 1-2 develops 17.8 kips, or 4.8%, less in axial connection force at the prescribed failure rotation. For Model 1-3, at the connection rotation limit of 0.05 radians, the axial connection force is 350.1 kips. This constitutes a 1316% increase in

axial connection force over the axial connection force at the flexural capacity of the member. Model 1-3 develops 21.5 kips, or 5.8%, less in axial connection force compared to Model 1-1 and 3.8 kips, or 1.1%, less in axial connection force compared with Model 1-2 at the failure rotation. The axial connection force values for Model 1-2 and Model 1-3 are very similar, only 1.1% apart from each other, which indicates that the presence of a residual stress pattern does not have a significant effect on the magnitude of connection forces at the prescribed failure rotation of 0.05 radians. However, the model with geometric imperfections, Model 1-1, has between a 4.8% and 5.8% larger connection force at the failure rotation compared to the other two models. While this is small, geometric imperfections in the girder appear to be the primary cause of a slightly larger axial connection force at the failure rotation. It is interesting that this is in contrast to the differences in response of the different models at flexural load levels that were discussed above.

Figure 4.19 plots the results of the axial connection force versus the total applied load for Model 1-1, Model 1-2 and Model 1-3. Similar to the results shown in Figure 4.18, all three models exhibit very similar results throughout their loading history. Figure 4.19 provides a good visual of how drastically the connection forces begin to increase soon after the flexural capacity of the girders is reached in all three models. This drastic and almost immediate increase in the axial connection forces is directly tied to the percentage web depth in tension results for all three models. In those figures, detailed in Section 4.3, the percentage web depth in tension for all three models began to increase after the flexural capacity of the girders was reached. Those results, coupled with the results presented in Figure 4.19, clearly show the initiation

and utilization of catenary action as a load-resisting mechanism in steel girders after flexural capacity is exceeded.

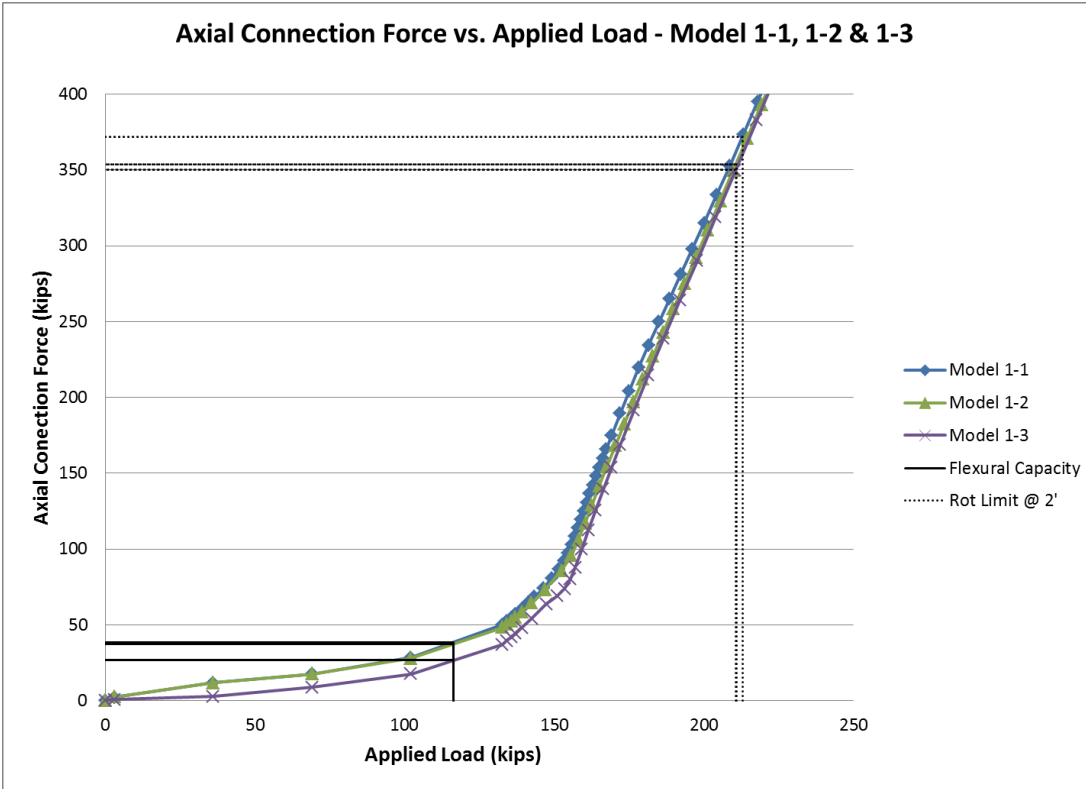


Figure 4.19. Axial connection force vs. applied load comparison of Model 1-1, Model 1-2 & Model 1-3

For all three fixed support models, the axial connection force is extremely large, between 946% and 1316% greater, compared with the axial force at the flexural capacity of the steel beam. These extremely large axial loads, in conjunction with half of the applied vertical load, must be taken into consideration for both connection design as well as column design. While previous data discussed in this chapter

indicates that the steel beam is able to resist large loads through catenary action, great care must be taken to ensure that the load path is adequately designed to transfer the loads to the foundations. Since beam-to-column connections for gravity systems are not typically designed for axial load, additional design criteria must be developed and implemented if catenary behavior is to be utilized. Building columns would also need to be significantly larger and stronger to resist the bending moment and shear which these axial connection forces would impart. These substantial forces would likely require larger column sections than those designed to typical building code criteria. The large connection forces not only apply a substantial shear force to the column, but also induce a large moment in the column. These substantial forces are non-existent for typical design, but must be accounted for if a structure is designed for a ‘missing’ column scenario. Additionally, the beam-to-column connections would need to be much stronger than traditional design necessitates. The large axial loads, in addition to the theoretically calculated shear loads, would necessitate that the number of bolts in the beam web connection increase (possibly 5 times the amount of bolts compared to traditional design). The beam flange-to-column connections would also require larger weld sizes and thicker connecting sections, such as WT or angle sections.

4.4.2 Connection Force Results: Model 1-3 and Model 2-3

Figure 4.20 graphically depicts the axial connection force data for Model 1-3 and Model 2-3 to determine the effects of support conditions on connection force behavior. Section 4.3.5 detailed the large differences in percentage web depth in tension results for models with fixed supports compared to those with shear connection supports. The purpose of Figure 4.20 is to detail the effects of support conditions on two models with no geometric imperfections or residual stress patterns.

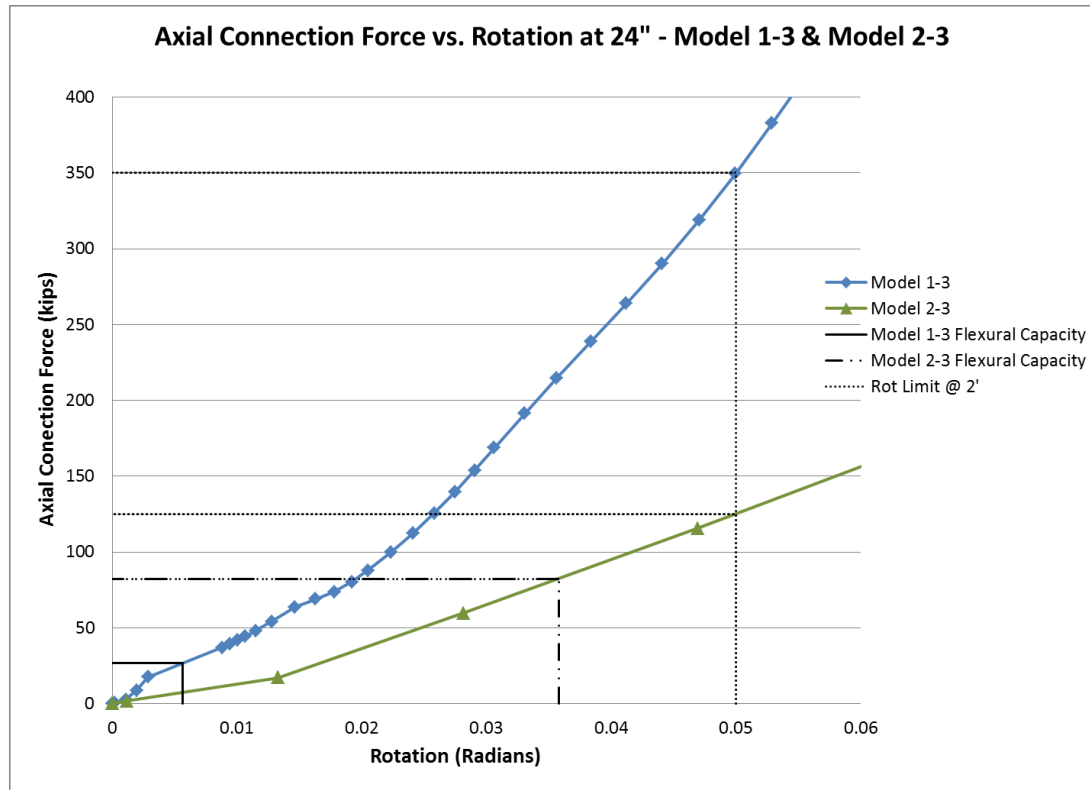


Figure 4.20. Axial connection force vs. rotation comparison of Model 1-3 & Model 2-3

Figure 4.20 shows a much different girder behavior when compared with the previous three models, all of which had fixed supports. For Model 2-3, the discrepancy between axial connection force at the flexural and rotation limits is much less than the previous models. This is likely due to the fact that the simply supported beam analyzed in Model 2-3 does not utilize catenary behavior to the extent of the fixed support beams, as shown in Section 4.3.5. The slopes of the two plots in Figure 4.20 are much different than those with identical boundary conditions in Figure 4.18. For Model 1-3, the slope of the plot from the beginning of the analysis until the failure rotation at 0.05 radians, is equal to 7000 kips of axial connection force per radian of

rotation. For Model 2-3, the same slope is equal to 2500 kips of axial connection force per radian of rotation. These results show that Model 1-3 applies 280% more axial connection force per radian of rotation throughout the loading history compared to Model 2-3. These results make sense in light of the data presented in Figure 4.14 and Figure 4.16. Those graphs showed that Model 1-3 utilized more of its web depth in tension and resisted more applied load than Model 2-3. Comparing the percentage web tension depth results to the axial connection force results, it is clear that the increase in utilization of catenary action results in significantly larger axial connection forces.

When the flexural capacity of the girder is reached for Model 1-3, the rotation at two feet from the support is 0.005677 radians with a corresponding axial connection force of 26.6 kips. For Model 2-3, when the flexural capacity of the girder is reached, the rotation at two feet from the support is 0.035793 radians with a corresponding axial connection force of 82.3 kips. For Model 2-3, the axial connection force at the flexural capacity of the girder is 309.4% greater than the axial connection force in Model 1-3. As can be seen in Figure 4.20, this corresponds to the much higher rotation of 0.035793 radians at which the flexural capacity is reached in Model 2-3 compared to the rotation of 0.005677 radians at which the flexural capacity is reached in Model 1-3. The percentage web depth in tension results for all models analyzed in this chapter show that increasing rotations lead to an increase in the percentage of the web depth in tension. This phenomenon explains the increased axial connection force in Model 2-3 compared to that of Model 1-3 at their respective flexural capacities.

At the prescribed connection failure rotation of 0.05 radians, the axial connection force in Model 1-3 was 350.1 kips; which constituted a 1316% increase in

axial connection force over the connection force at the flexural capacity of the member. For Model 2-3, at the connection rotation limit of 0.05 radians, the axial connection force was 125.1 kips. This only constitutes a 52% increase in axial connection force over the connection force at the flexural capacity of the member, which is still a significant increase but much less than the corresponding increase for the fixed connection models. Compared to Model 2-3, this increase is 1264% less. This is due to the smaller post-flexural capacity strength of Model 2-3 with only shear connection supports compared to Model 1-3 with its fixed supports. Since the fixed support beam is able to utilize catenary action to a much greater degree than the shear connection beam, the connection forces which must be resisted are necessarily larger. Model 2-3 undergoes significantly larger rotation at a location two feet from the support due to the lack of a moment-resisting connection which is found in Model 1-3.

Figure 4.21 plots the results of the axial connection force versus the total applied load for Model 1-3 and Model 2-3. Similar to Figure 4.20, the slopes of the two plots in Figure 4.21 are much different than those with identical boundary conditions in Figure 4.19. However, two distinct slopes can be seen for each model throughout the loading history. For Model 1-3, the slope of the plot from the beginning of the analysis until flexural capacity is reached, is equal to 0.998 kips of axial connection force per kips of applied load. From the point when flexural capacity is reached until the rotation limit of 0.05 radians is reached, the slope is equal to 1.190 kips of axial connection force per kips of applied load. While this change is not drastic, it equates to an increase of 19.2% in the slope of the graph after the flexural capacity is reached. For Model 2-3, the slope of the plot from the beginning of the analysis until flexural capacity is reached, is equal to 0.228 kips of axial connection

force per kips of applied load. This is the 77.5% less than for the same load history in Model 1-3. From the point when flexural capacity is reached until the rotation limit of 0.05 radians is reached, the slope is equal to 1.662 kips of axial connection force per kips of applied load. This is 39.7% larger than for the same load history in Model 1-3. The slopes of the graphs for the two detailed load histories indicates that, prior to flexural capacity being reached, a fixed support girder will develop far less connection forces than a shear support girder. This is due to the higher rotations for a shear support girder at its flexural capacity, which has been shown to relate to larger connection forces. However, after the flexural capacity of the girders is reached, the fixed support model actually shows a larger increase in axial connection forces than a shear support model. Again, this corresponds well with the data in Figure 4.11, Figure 4.12 and Figure 4.13 which shows that fixed supports lead to more of the web depth in tension causing larger connection forces.

These results correspond well with previous results which show that fixed supports, or moment connections, are ideal for most efficiently utilizing catenary behavior in steel beams, as shown in Section 4.3. However, the data still shows that a girder with shear connection supports is still able to achieve some level of catenary action which corresponds to very large axial connection forces. Therefore, if designers are relying on catenary behavior in such a supported beam, the connections and columns must still be carefully detailed to resist the applied loads.

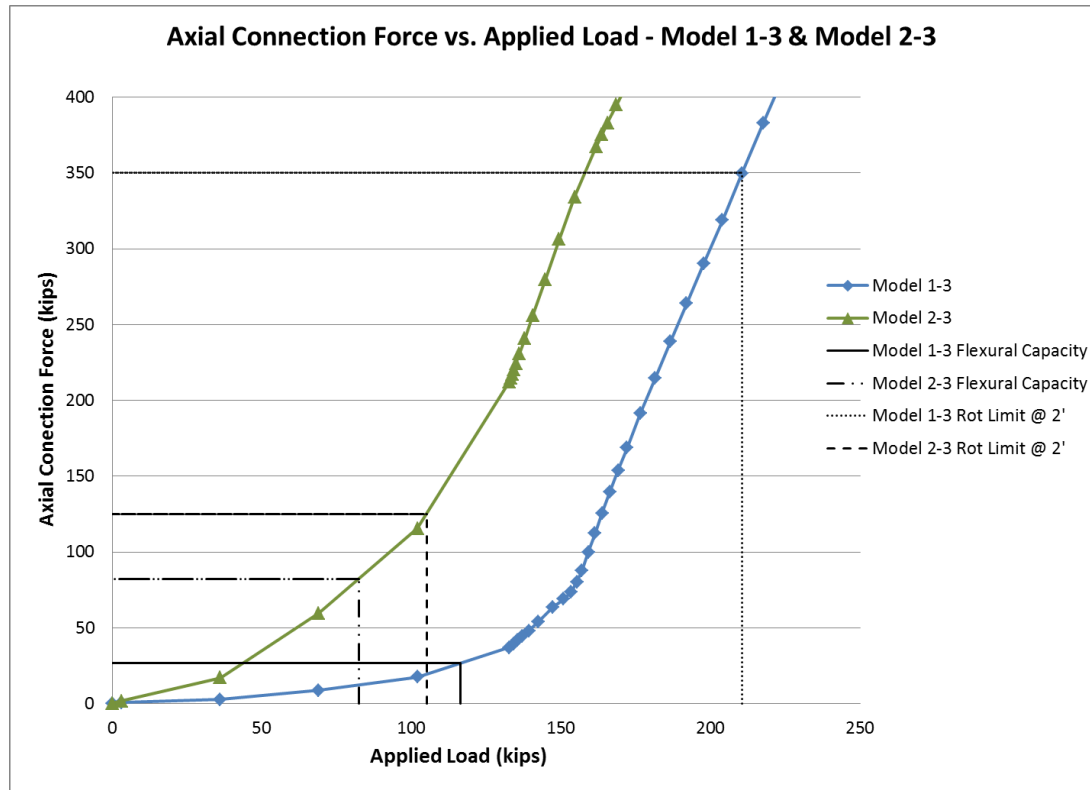


Figure 4.21. Axial connection force vs. applied load comparison of Model 1-3 & Model 2-3

The total shear force at the girder connections for the models presented in this thesis was not quantified. However, since the lateral bracing beam supports have no vertical support, all vertical force must be taken by the girder connections to satisfy equilibrium. The theoretical shear force for Model 1-1 is used as an example to calculate the magnitude of the shear force which would need to be designed for if the structure was to meet a ‘missing’ column design scenario. For Model 1-1, the rotation limit of 0.05 radians was reached at a total applied vertical load of 212.8 kips. Half of this value is equal to 106.4 kips, which is the shear force which the connection would need to be designed for in a ‘missing’ column scenario. The bolts in a web connection

would need to be designed for 106.4 kips of shear in conjunction with the 371.6 kips of axial tension force calculated in Section 4.4.1. These large values would likely necessitate several rows of bolts in the web connection, compared to one row of bolts typically used in a bolted web connection for a building designed using traditional codes.

4.5 Summary

The models presented in this chapter reveal a variety of important results related to the catenary behavior of steel beams under extreme loads. All models were assumed to represent a system in which a center supporting column was removed and the two originally independent beams were then acting as one continuous beam. The parameters varied in this thesis were: geometric imperfections; residual stresses; and support conditions. These parameters are described in greater detail in Chapter 3 of this thesis.

The results of this chapter showed that geometric imperfections and residual stresses had a small effect on the behavior of steel beams using catenary action to resist applied loads. The percentage of web depth in tension versus applied load graphs for Model 1-1, Model 1-2, and Model 1-3 were all very similar especially at the prescribed failure rotation of 0.05 radians, as shown in Table 4.2. These graphs, detailed in Section 4.3.4, were used to quantify the extent to which catenary action could be utilized in the analyzed girders up to the physical limits of typical modern connections. Larger values of percentage of web depth in tension would correlate to a greater use of catenary behavior in the girders. The graphs showed that after the flexural capacity of the beam was surpassed, the percentage of web depth in tension began to increase up to the limiting connection rotation, 0.05 radians. This rotation

value was used after analyzing several previous experimental and theoretical studies, presented in Chapter 2.

Table 4.2. Summary of model results

| SUMMARY OF MODEL RESULTS | | | | |
|---------------------------------|-----------------------------|--------------------------------|-----------------------|--|
| Model | Load (kips) @ Mp | Load @ 0.05 radians | | Load (kips) @ 100% Catenary |
| | | Value (kips) | % Increase | |
| Model 1-1 | 116.5 | 212.8 | 82.7% | 284.5 |
| Model 1-2 | 116.5 | 210.8 | 80.9% | 286.3 |
| Model 1-3 | 116.5 | 210.6 | 80.8% | 296.2 |
| Model 2-3 | 82.5 | 105.1 | 27.4% | N/A |

The results indicated that the steel beams analyzed in this work with fixed supports are able to resist an additional 80.8% to 82.7% of additional applied vertical load after flexural capacity is reached depending on whether geometric imperfections and residual stresses are applied. These results show that after the girder's flexural capacity is surpassed, the additional load is resisted through a combination of flexural behavior and increasingly dominant catenary behavior. The percentage web depth in tension was between 80% and 100% when the rotation limit of 0.05 radians was reached at a location two feet from the support for the three fixed support models. The results for Model 2-3, which analyzed a steel beam with shear connection supports, indicate that shear connections are much less efficient than moment connection for utilizing catenary behavior. Model 2-3 was only able to resist an additional 27.4% of applied load after the flexural capacity was reached, compared with between 80.8% and 82.7% for the fixed support models. Only between 62% and 72% of the web

depth was in tension when the rotation limit of 0.05 radians was reached, based on measuring rotation over a two feet length from the support. This shows that steel beams with shear connections utilize much less catenary behavior when their ultimate capacity is reached.

The axial yield force of the analyzed beam is 891.0 kips if the yield stress of the beam is assumed to be 55 ksi. For the three models with fixed supports, the ultimate axial force at the connection was between 350.1 kips and 371.6 kips; this force is equal to the tensile axial force in the beam when 0.05 radians of rotation is reached near the support. This ultimate axial force corresponds to between 39.3% and 41.7% of the axial yield force of the cross-section. As presented in Table 2.1 of Chapter 2, several previous finite element analyses (FEA) measured the ratio of actual axial force to axial yield force at specified rotations. Specifically, Khandelwal and El-Tawil (2007) measured 42% of axial yield force achieved at a rotation of 0.06 radians. Lee et al. (2009) measured 20% of axial yield force achieved at a rotation of 0.06 radians for a girder with a span-to-depth ratio of 15 (the value most comparable to the L/D of 16.1 for the girder in this thesis). Additionally, Kim and An (2008) measured 25-30% of axial yield force achieved at a rotation of 0.06 radians. Although the analysis in this thesis is limited to rotations less than 0.05 radians, data for the behavior of the models was collected for rotation values greater than 0.05 radians. Using Model 1-1 as an example, the connection force at a rotation of 0.06 radians was calculated to equal 484.9 kips. This value corresponds to 54.4% of the axial yield force percentage at a rotation of 0.06 radians. Comparing the results of this thesis and the previous data, it is suggested that the results are most similar to Khandelwal and

El-Tawil (2007), but variables such as girder depth, span length, connection type may affect the axial force at high rotations.

The utilization of catenary behavior requires that large axial forces be resisted by the connections and supporting columns. Section 4.4 of this thesis quantified the forces present during the loading history for the four analyzed models. The three fixed support models developed axial connection forces of between 350.1 kips and 371.6 kips when the rotation limit of 0.05 radians was reached at the connection. These values are between 946% and 1316% greater than the axial forces developed when the flexural capacity is reached. Therefore, in order for a steel framing system to develop catenary action, great attention must be paid to the design and detailing of the connections and associated supporting columns.

Chapter 5

CONCLUSION

Throughout the last few decades, several high-profile progressive collapse events have occurred. These include the partial building collapses of the Ronan Point Apartments, Alfred P. Murrah Federal Building, and the twin towers of the World Trade Center. These progressive collapses occurred when a localized load-bearing member, such as a column, was destroyed or damaged and unable to resist load. The result is the partial or total collapse of the structure as a result of the removal of one structural member.

The goal of the research presented in this thesis was to study the behavior of a steel beam during a ‘missing’ column event. This scenario is the loading event required to be resisted in current structural codes, such as UFC 4-023-03 *Design of Buildings to Resist Progressive Collapse* (DoD 2010) and General Services Administration *Progressive Collapse Analysis and Design Guidelines* (GSA 2003). The intent of the research was to investigate the ability of a steel beam to utilize catenary behavior after it has surpassed its flexural capacity while considering the limitations of current typical connections. Catenary action is the ability of a beam or girder to resist applied vertical loads through axial tensile force once the member’s flexural capacity has been surpassed. Because of this, research into the catenary behavior of beams has great potential to be incorporated into future design of structures to resist progressive collapse.

5.1 Summary of Results

Four analytical models were run using the finite element analysis (FEA) program, ABAQUS. Each of the four analyses modeled the steel girders in two adjacent bays with their shared column removed, causing an extreme loading event. Consistent with current progressive collapse design guidelines (DoD 2010, GSA 2003), a perfect connection between these two members is assumed via modeling the girder as a single continuous member. Each of the four models considered the same member size, lateral bracing size and spacing, and applied load. Three parameters were varied in these four models: geometric imperfections; a residual stress pattern; and support conditions. The geometric imperfections were obtained from the AISC (2005) and the residual stress pattern was taken from research performed by Galambos and Ketter (1959). Two end support conditions were modeled: fully fixed and bolted web shear connection. A constant AISC steel wide flange beam, W21x55, was used for all four models.

The primary analysis results considered were: rotation versus applied load; percentage of web depth in tension versus applied load; and axial connection force versus beam rotation at connection. Due to extensive previous research from many different authors, a maximum rotation value of 0.05 radians was adopted as a benchmark at which it was assumed that the connection performance terminates the load-carrying capacity of the beam. Limiting the girder to a maximum allowable steel strain was also considered, but was found to not govern for typical fracture strains for steel. Additionally, the research presented in Chapter 2 dealt specifically with maximum rotation of steel beams. Therefore, using a prescribed failure rotation of 0.05 radians was utilized in the results of this thesis, as it had substantial research behind it. The load which caused a rotation of 0.05 radians was compared to the loads

which caused the girder to reach its flexural and axial capacities and results of this comparison showed that the beams with fixed supports considered in this work could exceed their flexural capacity by 80.8% to 82.7% but only achieve 39.3% and 41.7% of their uniaxial tension capacity.

The results of the percentage of web depth in tension versus applied load for the four models showed that, for the majority of the cross-sections analyzed for each fixed support model, between 80% and 90% of the web depth at the most heavily stressed cross-sections, near mid-span and the girder supports, was in tension at a connection rotation of 0.05 radians. Up to 100% of the web depth was in tension at the cross-section located near the theoretical inflection point of the girder, however the maximum stress was much smaller compared to cross-sections at the support and mid-span. Specifically, for Model 1-2, the maximum tensile web stress was 12.8 ksi near the inflection point, 43.6 ksi near mid-span and 54.8 ksi near the support for the load step immediately after the flexural capacity was reached. The graphs showed that after the flexural capacity of the girder was reached, the percentage of web depth in tension began to drastically increase until the point of failure.

These results showed that for steel girders, including those with geometric imperfections and residual stresses, catenary action was being utilized after the flexural capacity of the member was surpassed. Additionally, the models with fixed supports were shown to have superior load-resisting and catenary behavior performance over the model with shear connection supports. Model 1-3, a fixed support girder with no residual stresses and no geometric imperfections, was able to resist 80.8% of additional load. However Model 2-3, a shear support girder with no residual stresses and no geometric imperfections, was only able to resist 27.4% of

additional load. Geometric imperfections and residual stresses were shown to have a negligible effect on the catenary behavior of the girders. Model 1-1, with both residual stresses and geometric imperfections, was able to resist 82.7% additional load and Model 1-3, with no residual stresses and no geometric imperfections, was able to resist an additional 80.8% of additional load. This difference of only 2.3% reveals the negligible effect on post-flexural load-carry capacity of residual stresses and geometric imperfections. Additionally, at a cross-section 324 inches from the girder mid-span (12 inches from the support), Model 1-1, Model 1-2 and Model 1-3 all utilized 85% of their web depth in tension at the prescribed failure rotation of 0.05 radians. Again, this highlights the negligible impact of residual stresses and geometric imperfections on the percentage of the girder cross-section in tension at the failure load.

The results of this thesis showed the ability of steel girders to resist substantial amounts of additional applied load after flexural capacity. However, design and detailing of the beam-to-column connections may be the most integral part of the entire system. The connection must be strong and ductile enough to resist the substantial rotations, shear forces, and axial loads inherent to catenary action of steel beams. Because of this, the connection forces were quantitatively analyzed and plotted versus the connection rotation. The results of the analyses showed that when a rotation of 0.05 radians was reached, the axial force at the connection was massive. The analyses showed that at the point the flexural capacity of the girder was reached, there was between 26.6 and 38.5 kips of axial tensile force at the connection for models with fixed supports. However, at the ultimate connection rotation of 0.05 radians, between 350.1 and 371.6 kips of axial tensile force existed at the connections.

This resulted in between a 946% and 1316% greater increase in tensile axial force which the connection must be designed to resist. These forces corresponded to between 39.3% and 41.7% of the axial yield capacity of the W21x55 girder. In addition to these substantial axial forces, the connection must also be designed to resist the applied vertical loads. Simple statics show that half of the total applied vertical load would be transferred to each connection. Therefore, the maximum force which the connections would have to resist would be the axial force values quantified in this thesis plus the vertical force component, which is easily solved for. These results compared well with those of Khandelwal and El-Tawil (2007), which showed that at a rotation of 0.06 radians, the axial tensile forces in a steel girder were 42% of its axial yield capacity.

The models analyzed in this thesis yielded three very important results: First, quantitative data of catenary behavior in steel girders was detailed, which showed that steel girders have the ability to resist a substantial portion of additional applied load after their flexural capacity was exceeded; Secondly, catenary behavior produces extremely large axial tensile forces at the connections; Third, the effects of geometric imperfections and residual stresses were shown to be negligible regarding the catenary behavior and axial connection forces in steel beams. The effects of a residual stress pattern and geometric imperfections on the behavior of steel beams under extreme loads had not been previously investigated. The results of this thesis provide unique variables, residual stresses and geometric imperfections, which contribute to previous research in this area. In order for the full benefit of catenary behavior to be utilized, the connections must be extremely robust and strong. However, if great attention is paid to the design and detailing of these critical components, catenary behavior can

allow steel beams to resist more than 80% additional applied load to aid in mitigating progressive collapse.

The results of this thesis highlight the similarities and differences compared to previous research. None of the previous research presented in Chapter 2 investigated the effects of residual stresses or geometric imperfections on the catenary behavior or axial connection forces in steel beams. Therefore, the data presented in this thesis adds to the previous data since the effect of residual stresses and geometric imperfections were investigated and shown to have a negligible impact on the girder's behavior. Additionally, the previous research presented in Chapter 2 of this thesis did not investigate the percentage of the girder web depth in tension versus the applied vertical load. The results of this thesis showed that, for all fixed support models, the web depth percentage in tension linearly increased after the flexural capacity of the girder was reached. This shows that the girder is resisting the additional applied load in a catenary manner, through axial tension of the girder. However, the results of Khandelwal and El-Tawil (2007) showed agreement to the results of axial forces presented in this thesis. Their analysis showed that the axial forces in a steel beam reached 42% of its axial yield capacity at a rotation of 0.06 radians, while the results of this thesis showed a value of between 39.3% and 41.7% at rotation of 0.05 radians.

5.2 Need for Further Research

While the results presented in this thesis revealed several extremely beneficial results, the scope of the research was fairly narrow. While the effects of geometric imperfections and residual stresses were investigated, several other parameters were not. Moving forward, there are several areas which should be explored in order to

further the understanding of catenary behavior in structures. The most pertinent areas of future research are presented below.

The research presented in this thesis focused on one steel girder size, a W21x55 section. There are many other shapes and sizes of standard rolled steel beams, and the effects of varying girder sizes on the post-flexural capacity behavior of steel girders should be investigated. Based on previous research by Lee et al. (2009), the span-to-depth ratio of steel beams has a significant impact on the catenary behavior of steel beams. In particular, steel beams with larger span-to-depth ratios are able to resist more applied load than beams with smaller span-to-depth ratios. Therefore, if a shallower beam was used for the models in this thesis, the data may have showed additional load-carry capacity coupled with larger axial connection forces. Future research should be performed to quantify the catenary behavior of beams with larger span-to-depth ratios than used in this thesis. Additionally, concrete beams with various steel reinforcing details should be investigated as to their potential for utilizing catenary behavior in extreme loading events.

The supports for the girder modeled and analyzed in this thesis consisted of simple restraints on the nodes at the ends of the girder. However, real life moment and shear connections are extremely complex and must therefore be investigated as to their behavior during catenary action in a girder. The connections modeled in this thesis were idealized representations of commonly used fully-restrained moment connections and web shear connections. The effects of connection material fracture, bolt slip, bolt yielding, and local deformations of connection components are behaviors which could impact the results presented in this thesis. Deformation and yielding of connection components would result in increased connection rotations

which could possibly lead to less additional applied load which can be resisted the beam after its flexural capacity is reached. Future research should be performed to analyze the effects of these types of connection limit states on the quantitative effect on catenary action and axial connection forces. It may also be appropriate to investigate the effects of a true pinned connection on the catenary behavior of steel beams and connection axial forces. In this thesis, a realistic ‘pinned’ shear connection was modeled to represent a shear connection used in common construction practice. However, this type of connection still has some level of rigidity compared to a true pinned connection. Therefore, a connection with no ability to resist rotation should be investigated to form a lower bound to the data presented in this thesis. More detailed connection models would have possibly revealed different results to those given in this thesis. The effects of the previously mentioned connection limit states may have shown that the steel girders reached the prescribed failure rotation of 0.05 radians at a lower applied load than that presented in Chapter 4. This would have also likely lead to decreased axial connection forces at the ultimate load of the steel girder. The quantitative effects on percentage web depth in tension and axial connection forces of these more detailed connections should be investigated in future research.

To be certain, there are other areas of research which must be investigated in order to provide a full picture of catenary behavior. Much research is left to be done in order to provide quantitative design parameters for the utilization of catenary behavior in actual structures. However, the results of this thesis have yielded one important initial step: Catenary action, at least in steel girders, is a viable method for resisting the extreme loads which are present during the catastrophic event of a ‘missing’ column. Additionally, the results of this thesis show that the effects of a

residual stress pattern and geometric imperfections are negligible, and may be omitted in future analyses. If utilized properly, catenary behavior may very well prove cost-effective means to mitigating progressive collapse and saving lives.

REFERENCES

- American Institute of Steel Construction. (2005). *Steel Construction Manual, 13th Edition* (AISC 360-05).
- American Society of Civil Engineers. (2007). *Minimum Design Loads for Buildings and Other Structures* (ASCE 7-05).
- American Society of Civil Engineers. (2006). *Seismic Rehabilitation of Existing Buildings* (ASCE 41-06).
- An, Dawoon, and Kim, Jinkoo. (2009). "Evaluation of progressive collapse potential of steel moment frames considering catenary action." *The Structural Design of Tall and Special Buildings*, 18(4), 455-465.
- Astaneh-Asl, Abolhassan, and Nader, M. N. (1989). "Experimental studies of single story steel structure with fixed, semi-rigid and simple connections." *Report No. UCB/EERC-89/15*, University of California, Berkeley.
- Bao, Yihai, Lew, H. S., Main, Joseph A., and Sadek, Fahim. (2011). "Testing and Analysis of Steel and Concrete Beam-Column Assemblies under a Column Removal Scenario." Vol. 137 *Special Issue: Commemorating 10 Years of Research since 9/11*, 881-892.
- Barth, K. E., White, D. W., Righman, J. E., and Yang, L. (2005). "Evaluation of Web Compactness Limits for Singly and Doubly Symmetric Steel I-Girders", *Journal of Constructional Steel Research*, 61(10), 1411-1434.
- Burnett, E., and Leyendecker, E.V. (1976). "The incidence of abnormal loading in residential buildings." *Building Science Series No. 89*.
- Byfield, Mike P. (2006). "Behavior and Design of Commercial Multistory Buildings Subjected to Blast." *Journal of Performance of Constructed Facilities*, 20(4), 324-329.
- Byfield, Mike P. (2004). "Design of steel framed buildings at risk from terrorist attack." *Structural Engineer*, 82(22), 31-38.

- Byfield, Mike P., and Paramasivam, Sakthivel. (2007). "Catenary action in steel-framed buildings." *Proceedings of the Institution of Civil Engineers: Structures and Buildings*. Vol. 160, 247-257.
- Dassault Systemes. (2011). "Abaqus 6.11."
- Davidson, Buick, Tyas, Andy, and Munoz-Garcia, Enrique. (2005). "Structural integrity of steel connections subjected to rapid rates of loading." *Proceedings of the Structures Congress and Exposition*. 2199-2210.
- Department of Defense Unified Facilities Criteria. (2010). *Design of Buildings to Resist Progressive Collapse* (UFC-4-023-03).
- Davidson, B., Liu, R., and Tyas A. (2005). "A Study of Progressive Collapse in Multi-Storey Steel Frames." *Proceedings of the Structures Congress*. Vol. 1, 1-9.
- Ellingwood, Bruce R., and Xu, Guoqing. (2011). "Probabilistic Robustness Assessment of Pre-Northridge Steel Moment Resisting Frames." *Journal of Structural Engineering*, 137(9), 925-934.
- El-Tawil, S., and Khandelwal, K. (2007). "Collapse Behavior of Steel Special Moment Resisting Frame Connections." *Journal of Structural Engineering*, 133(5), 646-655.
- Fahnestock, Larry A., and Hoffman, Seth T. (2011). "Behavior of multi-story steel buildings under dynamic column loss scenarios." *Steel and Composite Structures*, 11(2), 149-168.
- Federal Emergency Management Agency. (2000). *State of the Art Report on Connection Performance* (FEMA-355D).
- Fenves, G. L., Mazzoni, S., McKenna, F., and Scott, M. H. (2006). *Open System for Earthquake Engineering Simulation User Command-Language Manual – OpenSees Version 1.7.3*. Pacific Earthquake Engineering Research Center, University of California, Berkeley.
- Galambos, Theodore V., and Ketter, Robert L. (1959). "Columns under combined bending and thrust." *Journal of the Engineering Mechanics Division*, 85(2), 1-30.
- General Services Administration. (2003). "Progressive Collapse Analysis and Guidelines."

- Hamburger, Ronald O. (2006). "Prequalified Connections for Special and Intermediate Steel Moment Frames for Seismic Applications, ANSI/AISC 358-05." ASCE Proceedings of Structures Congress. Vol. 1, 41-48.
- Han, Kyu-Hong, Kim, Seonwoong, Lee, Cheol-Ho, and Lee Kungkoo. (2009). "Simplified nonlinear progressive collapse analysis of welded steel moment frames." Journal of Constructional Steel Research, 65(5), 1130-1137.
- Hong, J., Houghton, D., Karns, J., and Kim, J. (2009). "Behavior of Varied Steel Framed Connection Types Subjected to Air Blast, Debris Impact, and/or Post-Blast Progressive Collapse Load Conditions." Proceedings of the Structures Congress. Vol. 1, 1-10.
- Kaliakin, Victor. *Introduction to Approximate Solution Techniques, Numerical Modeling, and Finite Element Methods*. New York, NY: Marcel Dekker, Inc, 2001. Print.
- Kim, Jinkoo, and Kim, Taewan. (2009). "Collapse analysis of steel moment frames with various seismic connections." Journal of Constructional Steel Research, 65(6), 1316-1322.
- Leon, R. T., Smallidge, J. M., and Swanson, J. A. (1999). *SAC Steel Project – Subtask 7.03: Results and Data CD*, Georgia Institute of Technology.
- Liu, Chuangng, and Mei, Zuoyun. (2012). "Analytical Investigation of Progressive Collapse Resistance Mechanism in Steel Moment Frame with Fiber Model." Applied Mechanics and Materials, Vols. 166-169, 1848-1853.
- Liu, Min. (2011). "Progressive collapse design of seismic steel frames using structural optimization." Journal of Constructional Steel Research, 67(3), 322-332.
- Papp, Ferenc, and Szalai, Jozsef. (2005). "A new residual stress distribution for hot-rolled I-shaped sections." Journal of Constructional Steel Research, 61(6), 845-861.
- Pirmoz, Akbar. (2009). "Performance of bolted angle connections in progressive collapse of steel frames." The Structural Design of Tall and Special Buildings, 20(3), 349-370.
- Popov, Egor P., and Takhiro, Shakhzod M. (2002). "Bolted large seismic steel beam-to-column connections Part 1: experimental study." Engineering Structures, 24(12), 1523-1534.

- Popov, Egor P., and Takhirov, Shakhzod M. (2002). "Bolted large seismic steel beam-to-column connections Part 2: numerical nonlinear analysis." *Engineering Structures*, 24(12), 1535-1545.
- Popov, Egor P., and Tsai, K. C. (1989). "Performance of Large Seismic Steel Moment Connections under Cyclic Loads." *Engineering Journal*, 26(2), 51-60.
- Righman, J. (2005). "Rotation Compatibility Approach to Moment Redistribution for Design and Rating of Steel I-Girders", Doctoral Dissertation, West Virginia University, Morgantown, WV.
- Roeder, Charles W. (2002). "Connection Performance for Seismic Design of Steel Moment Frames." *Journal of Structural Engineering*, 128(4), 517-525.
- Schneider, Stephen P., and Teeraparbong, Itthinun. (2002). "Inelastic Behavior of Bolted Flange Plate Connections." *Journal of Structural Engineering*, Vol. 128 *Special Issue: Steel Moment Frames After Northridge-Part II*, 492-500.
- Tan, Kang Hai, and Yang, Bo. (2012). "Numerical analyses of steel beam-column joints subjected to catenary action." *Journal of Constructional Steel Research*, 70(1), 1-11.
- Yang, L., Righman, J., and Barth, K. (2005). Personal communication.

Appendix

REPRINT PERMISSION LETTERS

Reprint permission for Figure 3.1, Figure 3.6 and Figure 3.7



LIMITED CONSENT AGREEMENT FOR COMMERCIAL REPRINTING OF PROTECTED WORKS

Note to Author(s): Please complete all information in Part I and sign and date this agreement in Part III.

Mail to: AISC, One East Wacker Drive, Suite 700, Chicago, IL 60601-1802, Attn: Janet Cummins. Or fax to: 312-896-9022, Attn: Janet Cummins. Or e-mail to: cummins@aisc.org.

Date: 4/17/2013

PART I: [to be completed by the Author]

The American Institute of Steel Construction ("AISC"), hereby grants a limited, non-transferable, non-exclusive consent to:

Thomas J. Cotter
[name(s) of Author(s)]

thomasj.cotter@gmail.com
[address/e-mail/fax number for corresponding author]

(the "Author") to reprint the following copyrighted publications (the "Reprinted Material") titled:

Steel Construction Manual - 13th Edition
[name of the AISC publication from which the Reprinted Material is to be taken]

The portions to be copied are as follows:

Table 1-22 ASTM A6 Tolerances for W Shapes and HP Shapes page 1-117
[list of pages and/or portions thereof that make up the Reprinted Material]

Table 3-2 W Shapes - Selection by Z_x page 3-11

This limited consent is expressly subject to the following terms and conditions:

1. Limited Use.

The Reprinted Material is to appear unchanged in text in a publication or standard, password-protected internet-based course, or online posting entitled:

Catenary Behavior of Steel Beams under Progressive Collapse-Type Leads
[name of Publication in which the Reprinted Material will appear; if internet-based course or online posting, please also provide URL.]

(the "Publication"), to be published and distributed by:

University of Delaware (Thesis Paper)
[name of Publisher]

and may not be used or reprinted for any other purpose. This Consent does not authorize any other use beyond the terms of this agreement.

2. Publication.

The approximate publication date is:

June 1, 2013
[date of Publication]

(the "Publication Date"), and the probable selling price to the public is:

\$0.00
[selling price of Publication in U.S. Dollars per copy]

Reprint permission for Figure 3.1, Figure 3.6 and Figure 3.7

PART II: [to be completed by AISC]

3. Reproduction Fee.

In consideration of the rights granted herein to reproduce the Reprinted Materials, the Author agrees to pay to AISC

\$0 as a one time fee, payable in advance.

\$0 per copy, payable quarterly.

Royalty of 0% of sale price of each copy, payable quarterly.

4. Author's Covenants.

The Author agrees (i) to give full credit to AISC, in the form specified in Section 5 below; (ii) to restrict the use of the Reprinted Material to the Publication; (iii) to make available at its expense one copy/version of the Publication to AISC; and (iv) if at any time a new edition of the Publication is contemplated, to secure further permission from AISC to use the Reprinted Material therein.

5. Attribution of Ownership.

The Author shall cause an appropriate notice of the AISC's copyright in the Reprinted Material and the following form of credit to be printed on the copyright page of every copy of the Publication or on each page in which a quotation from the Reprinted Material appears:

"Copyright © American Institute of Steel Construction
Reprinted with permission. All rights reserved."

6. Duration of Limited Consent.

Failure to keep the Publication in print/posted on the internet shall result in the reversion of this right and termination of this limited consent without notice.

PART III: [to be completed by the Author and AISC]

Signed:

Shawn A. Cott 4/17/2013
[enter name (last, first, initial) of Author(s)] [enter date (m-d-y), day, year]
Janet Cummins 4/17/13
American Institute of Steel Construction

Reprint permission for Figure 2.57



May 2, 2013

Tom Cotter
University of Delaware

Re: Reproduction Permission Letter

Dear Tom:

Thank you for reaching out to us to obtain written permission to publish an image of a SidePlate® moment connection. Based on the image you provided us (see below), it is acceptable to SidePlate Systems, Inc. to include the image for your master's thesis in structural engineering at the University of Delaware. For added clarification to your audience, I think it would be prudent to add to your column call out "or wide flange section". As you may be aware, the use of steel tube or box columns filled with concrete actually have limited practical application for widespread use in steel buildings because of the limited selection of HSS sections available, the higher cost of built-up box columns and the inherent limited stiffness that HSS columns have to control building drift, which the design of moment frames are typically controlled by.

If you have any further questions or stand in need of any additional graphics, please feel free to contact us again.

Best regards,

A handwritten signature in blue ink, appearing to read "Henry Gallart", is written over a horizontal line.

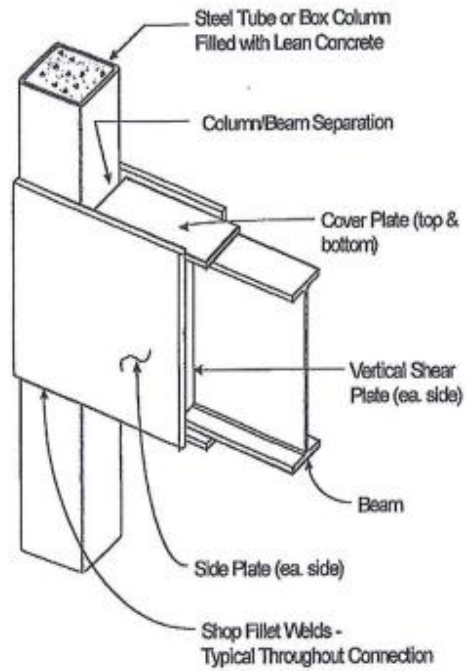
Henry Gallart, S.E.
President

HG/th

Enclosure Image of SidePlate® moment connection

SIDEPLATE SYSTEMS, INC.
A subsidiary of MITek, a Berkshire Hathaway Company
23332 Mill Creek Drive, Suite 225, Laguna Hills, CA 92653 Tel: 800-475-2077 Fax: 949-305-6395

Reprint permission for Figure 2.57



SIDEPLATE SYSTEMS, INC.
A subsidiary of MiTek, a Berkshire Hathaway Company
23332 Mill Creek Drive, Suite 225, Laguna Hills, CA 92653 Tel: 800-475-2077 Fax: 949-305-6395